INFORMATION TO USERS

This manuscript has been reproduced from the microfilm master. UMI films the text directly from the original or copy submitted. Thus, some thesis and dissertation copies are in typewriter face, while others may be from any type of computer printer.

The quality of this reproduction is dependent upon the quality of the copy submitted. Broken or indistinct print, colored or poor quality illustrations and photographs, print bleedthrough, substandard margins, and improper alignment can adversely affect reproduction.

In the unlikely event that the author did not send UMI a complete manuscript and there are missing pages, these will be noted. Also, if unauthorized copyright material had to be removed, a note will indicate the deletion.

Oversize materials (e.g., maps, drawings, charts) are reproduced by sectioning the original, beginning at the upper left-hand corner and continuing from left to right in equal sections with small overlaps. Each original is also photographed in one exposure and is included in reduced form at the back of the book.

Photographs included in the original manuscript have been reproduced xerographically in this copy. Higher quality 6" x 9" black and white photographic prints are available for any photographs or illustrations appearing in this copy for an additional charge. Contact UMI directly to order.

UMI

A Bell & Howell Information Company
300 North Zeeb Road, Ann Arbor MI 48106-1346 USA
313/761-4700 800/521-0600

ELECTROSPRAY AS A NEW SAMPLE INTRODUCTION TECHNIQUE FOR THE FLAME PHOTOMETRIC DETECTOR

by

Taghi Khayamian

Submitted in partial fulfilment of the requirements
for the degree of Doctor of Philosophy

at

Dalhousie University
Halifax, Nova Scotia
January, 1997

DALHOUSIE UNIVERSITY

FACULTY OF GRADUATE STUDIES

The undersigned hereby certify that they have read and recommend to the Faculty of Graduate Studies for acceptance a thesis entitled "Electrospray as a New Sample Introduction Technique for the Flame Photometric Detector (FPD)"

by Taghi Khayamian

in partial fulfillment of the requirements for the degree of Doctor of Philosophy.

Dated: November 1, 1996

External Examiner

Research Supervisor

Examining Committee

DALHOUSIE UNIVERSITY

DATE: February 13, 1997

AUTHOR: Taghi Khayamian

TITLE: Electrospray as a New Sample Introduction Technique for the Flame Photometric Detector.

DEPARTMENT OR SCHOOL: Chemistry

DEGREE: Ph.D. CONVOCATION: May YEAR: 1997

Permission is herewith granted to Dalhousie University to circulate and to have copied for non-commercial purposes, at its discretion, the above title upon the request of individuals or institutions.

[redacted]
Signature of Author

ABSTRACT

In atomic and molecular flame spectroscopy, with combustion flames and plasma, the quality of analytical results for liquid samples is limited by the means of sample introduction, especially when sample flow rates are small. In this project, electrospray was examined as a method to introduce small liquid flows (typically 10 μL/min) into a flame photometric detector (FPD). This method was used to introduce ionic and nonionic sulphur and phosphorus compounds as well as ionic metal compounds into the FPD. Atomic lines or molecular band spectra from a variety of elements (K, Sr, Sc, S, P, Mn, Mg, Ni, Cu, B, Se, As) were recorded. To demonstrate the potential of electrospray as a new sample introduction technique for the FPD, mass detection limits of selected elements were measured. Detection limits varied from 0.6 ng Cu/s to 18 ng In/s. The dynamic range for Cu was about two and half decades. The application of the electrospray-FPD for phosphorus and sulphur analysis in biological samples was confirmed by obtaining the phosphorus spectra for adenosine 5'-monophosphate (AMP), DNA, lecithin, and sulphur spectrum for glutathione. The phosphorus dynamic range (AMP) was more than two and half orders of magnitude while a quadratic response with two decades for sulphur (glutathione) was obtained. The detection limit for sulphur was 1 ng S/s. The signal to noise ratio for P and Cu increased at lower flow rates, suggesting that detection limits could be improved with lower flows.

The noise power spectrum was used as a diagnostic tool to obtain the limiting noise on the signal. Flicker noise and interference noise appeared to dominate and could be reduced by about a factor of two by using an internal standard in dual channel mode. It was also found that, at high voltages, the noise on the electrical current had a correlation coefficient of 0.806 with the optical noise, indicating that the electrical signal may be an interesting field for further investigation. At high voltages (ca. 5000 V) corona discharges caused strong emission of the nitrogen second positive system in the flame. This observation suggested that metastable nitrogen species in a flame may provide additional excitation pathways for the analyte.

TABLE OF CONTENTS

Chapter 6. CONCLUSIONS AND FUTURE WORK

LIST OF FIGURES

LIST OF TABLES

ABBREVIATIONS

AMP	Adenosine 5'-monophosphate
CZE	Capillary zone electrophoresis
DC	Direct current
DIN	Direct injection nebulizer
DNA	Deoxyribonucleic acid
ECD	Electron capture detector
ESI	Electrospray ionization
ETV	Electrothermal vaporization
FAAS	Flame atomic absorption spectrometry
FID	Flame ionization detector
FPD	Flame photometric detector
GC	Gas chromatography
GFAAS	Graphite furnace atomic absorption spectrometry
HAB	Hexadecyltrimethyl ammonium bromide
HEN	High efficiency nebulizer
HPLC	High performance liquid chromatography
i.d.	Internal diameter
ICP	Inductively coupled plasma
IET	Ion evaporation theory

kV	Kilovolts
LC	Liquid chromatography
MΩ	Megaohms
mA	Milliampere
MS	Mass spectrometry
MW	Molecular weight
nA	Nanoampere
NPS	Noise power spectrum
NSP	Nitrogen second positive
o.d.	Outer diameter
p-p	Peak to peak
PMT	Photomultiplier tube
ppm	Part per million
PTFE	Polytetrafluoroethylene
PVA	Polyvinyl alcohol
RNA	Ribonucleic acid
S/N	Signal to noise ratio
SDS	Sodium dodecyl sulphate
SIDT	Single ion droplet theory
TEP	Triethyl phosphate
THG	Thermochemical hydride generation
WB	Wide band

ACKNOWLEDGEMENTS

I acknowledge my supervisor Dr. W. A. Aue for his patience, encouragement and guidance throughout the project. I would like to also acknowledge my committee members Dr. R. D. Guy, Dr. L. Ramaley and Dr. P. D. Wentzell for their corrections and suggestions pertaining to the dissertation. I am especially grateful for the help of Dr. Wentzell who spent much time for corrections to the thesis. I express my sincere thanks to Dr. A. Montaser for his thorough corrections on the thesis and for his comments about experiments that are important for introducing a new sample introduction system. I would like to thank Isfahan University of Technology for my scholarship and the Department of Chemistry (Dalhousie University) for financial support. I would like to thank Mr. C. G. Eisener for machining the detector. Finally, I thank fellow graduate students Z. Lin, N. Lowery, K. Thurbide, and especially H. Singh for their assistance.

Dedicated to my teachers and my family

Chapter 1

INTRODUCTION

1.1 INTRODUCTION

Gas chromatography (GC) is a method employed in the physical separation of volatile compounds, while nonvolatile organic or inorganic compounds can be separated by liquid chromatography (LC) which is complementary to GC. The physical separation of the compounds constitutes only one aspect of the GC and LC. For the quantitative and qualitative determination of the separated compounds, a detector is required.

Flame ionization detectors (FID) and thermal conductivity detectors (TCD) are the most common "universal" (non-selective) detectors in GC. Many selective detectors of elements or molecules are available. These include electron capture detectors (ECD), flame photometric detectors (FPD), thermionic detectors (TID), photoionization detectors (PID), and microwave induced plasmas (MIP). According to Scott [1], the rapid development of GC was a consequence of the availability of many sensitive detectors.

Common liquid chromatographic detectors are based on ultraviolet absorption (UV), refractive index measurement (RI), fluorescence spectrometry, electrochemistry, atomic spectroscopies (such as inductively coupled plasma (ICP), flame atomic absorption spectrometry (FAAS), and graphite furnace atomic absorption spectrometry (GFAAS)), chemiluminescent flames (FPD), and mass

spectroscopy. Although several detectors are available, at present there is no universal detector comparable to flame ionization detector in GC [2].

Small, chemical flame-based detectors are very successful in GC but they are much less successful in LC for two reasons. First, the introduction of a relatively large flow of mobile phase (mL/min) into the flame disrupts the delicate balance of chemical and physical processes that occur there [3]. The second reason is the lack of satisfactory methods for the introduction of samples into the flame. The first problem was solved by the development of miniaturized high performance liquid chromatography (HPLC) columns operating at μL/min. The second problem is a general limitation. In LC, the sample introduction technique defines the success or failure of the coupling to FPD or to any other chemical flame or plasma. Although many interfaces exist for introducing liquid samples into the flame or plasma, researchers are still working to address the drawbacks of these methods. The small sample flow rates that are used with micro-LC and other micro techniques require a sample introduction device that can handle small sample flow rates with good nebulization and transport efficiencies.

The aim of this research is to find a new sample introduction technique which will eliminate many of the previously encountered difficulties with the FPD. It is, therefore, worthwhile to briefly review first the different sample introduction techniques used for flames or plasmas, evaluate each system, and then examine the sample introduction techniques used specifically in the FPD. Finally, a new method will be introduced for injection of μL/min samples into the FPD.

1.2 SAMPLE INTRODUCTION TECHNIQUES

A variety of methods exists for introducing a sample into a flame or plasma [4,5]. In most cases, the interfacing of LC to a flame or plasma is performed by the direct transfer of the effluent from the column to pneumatic nebulizers, either cross flow or concentric types [6]. Pneumatic nebulizers are simple and inexpensive, but the precise microscopic processes by which pneumatic nebulizers operate are not well understood, though some general principles are known. In simple terms, a liquid jet is shattered by interaction with a high velocity gas jet, and successive thin surface films of liquid are removed by the gas flow. The films then spontaneously collapse under surface tension forces to produce aerosol droplets [7,8]. The Babington nebulizer is another type of pneumatic nebulizer. In this method, the liquid flows freely over a surface having a gas orifice. Because the liquid does not pass through a narrow orifice, a blockage does not occur when solutions that have a relatively high level of dissolved solid matrix are nebulized. The v-groove nebulizer is the most commonly used version of the Babington nebulizer. The conspray nebulizer, another type of Babington nebulizer, was constructed by Sharp [7] and may be a preferable alternative to the v-groove nebulizer as a high dissolved solid nebulizer. The conspray nebulizer was made by press-fitting sapphire inserts into endcaps made from Polytrifluorochloroethylene (Kel-f). A precise gas orifice and polished internal surface were made for the sapphire inserts. The conspray can be used as a general purpose nebulizer which can replace both the cross-flow and v-groove nebulizers when sample consumption

rate is not the major concern [9]. Pneumatic nebulizers suffer from short term noise, long term drift, and sample transport inefficiency. A wide range of droplet sizes is produced by these nebulizers. Because the larger droplets are lost in transport, this results in inefficient sample delivery [4,5,10].

Ultrasonic nebulization is different in its principle of aerosol production from pneumatic nebulization. In the ultrasonic nebulizer, surface instability is generated in a pool of liquid by a focused or unfocused ultrasonic beam. The beam is generated by a piezoelectric transducer [8]. Because the ultrasonic nebulizer offers better detection limits than pneumatic nebulizers, much fundamental research has been conducted to better understand it [11,12,13,14]. Browner and associates [11] reported that the droplet size distribution for ultrasonic nebulizer is broader than the commonly used concentric pneumatic nebulizers. Transport efficiencies are from 10 to 30 % by using 0.5 to 2 mL/min sample flows and a desolvation process, while transport efficiencies of pneumatic nebulizers (used for ICP) are 0.5 to 2 %. [15]. Ultrasonic nebulizers are often used with a desolvating process to prevent overloading the plasma [8] or the FPD [16]. Ultrasonic nebulizers can handle flow rates down to 150 µL/min [17], however Browner and associates [18] designed a microflow ultrasonic nebulizer that can handle sample flows as low as 5 µL/min. An micro-ultrasonic nebulizer in comparison with typical ultrasonic nebulizers, offers narrower droplet size distribution and smaller mean droplet size. The ultrasonic nebulizer is more complex and expensive than pneumatic nebulizers [10,11].

Another nebulizer, designated as "frit-type", has been shown to be highly efficient: up to 94% of the sample is transported to the flame or plasma in an unusually fine sample mist. The device is simple to make and operate, but it does experience clogging problems and suffers from memory effect. It is constructed using a porous glass frit (pore size of 4-8 μm) for nebulizing the liquid [10]. This nebulizer is, however, suitable for small-sample flow rates and has been used in LC [19].

Another method is electrothermal vaporization (ETV), which can be used as an on-line or off-line interface for HPLC introduction to an ICP. In on-line ETV, sample treatment is followed by introduction into the ICP. In the off-line approach, a peak fraction is collected for separate introduction to the ETV stage and introduction to the ICP [20]. The advantages of this method are micro-sampling capabilities, low detection limits, ability to analyse samples in a variety of physical forms, and ability to separate the element of interest from the sample matrix. The principal disadvantages of this method are complexity, cost, and relatively poor short-term reproducibility, as relative standard deviation values of approximately +/- 10% are typical [21].

Hydride generation has been developed as a primary-vapor generation sample introduction method. A number of elements (As, Bi, Ge, Sb, Pb Se, Sn and Te) form volatile covalent hydrides. This increases sensitivity by a factor of 10 to 100. Unfortunately the method is limited to a small number of metals [22].

Total consumption nebulizers offer 100% analyte transport efficiency into

flame or plasma [23]. The direct injection nebulizer (DIN), a micro-concentric nebulizer mounted inside the ICP torch, has been interfaced to the HPLC for ICP atomic emission spectrometry. Although this method offers high transport efficiency, it does not improve detection limits based on the total sample volume introduced into the plasma. Because of the high linear velocity of the nebulizing gas, a considerable fraction of the sample is suspected to traverse the plasma without generating a signal. Nebulized aerosol leaves the DIN at a velocity of 120 m/s [24]. When a 1% salt solution is fed for about 5 minutes into the DIN, the central channel of the plasma begins to skew, presumably because of salt build-up on the tip of the DIN [24]. In addition, excessive solvent loading and vapor interaction in the plasma may cause changes in plasma characteristics which affect atomic emission [25].

Recently a new pneumatic nebulizer for small sample flow rates, called a high efficiency nebulizer (HEN), was introduced into the market (J. E. Meinhard, Santa Ana, CA, USA) for ICP [26]. The HEN is a concentric pneumatic nebulizer with a small capillary (i.d. 79 µm) and operates at a solution uptake rate between 10 to 150 µL/min [27,28,29]. Olesik [27] compared common pneumatic nebulizers (Perkin Elmer cross flow and Meinhard TR-30-A3) which use sample slow uptake rates of 0.5-3 mL/min with a HEN which was operated at 0.05 mL/min. Detection limits for the HEN were very similar to those for the two nebulizers using a 1 mL/min uptake rate. Transport efficiencies of the cross flow, TR-30 and HEN nebulizers were 1.5%, 2% and 20% respectively. Montaser and coworkers [28]

used two phase Doppler instruments (a two-beam and a four-beam laser light scattering interferometer) for the diagnostic studies of the aerosol produced by the HEN. The investigators showed that the Sauter mean diameter of the tertiary aerosol generated by the HEN is approximately 2-3 μm smaller than that of a conventional pneumatic nebulizer over a wide range of uptake rates (10-120 μL/min). High transport efficiency and high responsivity (analyte emission intensity/amount of analyte entering the plasma) of the HEN result in an excellent detection limit with a smaller sample flow rate [27]. The HEN was used for coupling microbore-HPLC-ICP-MS for the determination of arsenic compounds, and absolute detection limits in the femtogram range were obtained [29].

Thermospray has been a highly successful approach for interfacing LC and mass spectrometry. The effluent is introduced into a stainless steel capillary vaporizer. In "indirect" electrical heating, the liquid is forced through an electrically heated stainless steel capillary [30]. Indirect heating has been replaced by "direct" electrical heating in which the necessary power to vaporize the liquid is obtained by passing an electrical current through the capillary tube. The thermospray vaporizer is powered by a feedback controlled triac power supply. At the inlet end, the flowing water is heated until vaporization begins. From this point, the temperature remains constant until vaporization is complete. At the point corresponding to complete vaporization the temperature again rises rapidly since input heat is only consumed for heating of the vapour [31]. Thermospray nebulizers can be clogged by high concentrations of dissolved solids; however, Koropchak

[32] claimed they have solved this problem.

There are other sample introduction devices such as high pressure nebulization [33,34], oscillating capillary nebulization [35], monodisperse dried microparticulate injection [36,37] which are used in atomic spectrometry.

The techniques described above are the most common methods for introducing samples into plasmas or flames for spectral purposes. Most of them have been used as an interface between LC and chemical flames or ICP. In LC-FPD, a few of these methods have been used; however, phosphorus and sulphur were the only elements so examined.

1.3 MOLECULAR EMISSION SPECTROMETRY IN THE RELATIVELY HOT OXY-HYDROGEN FLAME

Sulphur and phosphorus have their principal atomic resonance lines in the far ultraviolet region of the spectrum and, because of the almost total absorption of these lines by air and flame gases, the direct determination of these elements by atomic spectrometry with chemical flames is not useful. However, atomic spectrometry with plasma or spark can be used for the measurement of these lines. Indirect methods of flame photometry for phosphorus determination are based on the suppression action of phosphorus upon the emission intensity of other elements [38,39,40]. Sulphur and phosphorus can also be determined directly by molecular spectroscopy in chemical flames. In earlier work [41,42,43], i.e., before the FPD had been introduced as a detector for GC, phosphorus was determined based on measurement of the PO molecular band emission of

phosphorus, in a hot oxy-hydrogen air flame or other type of flame such as the air acetylene flame. Measurement of phosphorus in only an air oxy-hydrogen flame will be discussed.

Barite [41] described a direct method for the determination of phosphorus in organophosphorus compounds in alcohol or kerosene. The detection limit was 3 ppm. He measured the emission from the continuous spectrum obtained with an oxy-hydrogen total consumption flame at 540 nm. Sodium and calcium caused positive spectral interference. Nitrogen, sulphur, iodine and chlorine did not interfere at concentrations equivalent to that of phosphorus.

Davis and co-workers [42] also used an oxy-hydrogen turbulent flow flame for the photometric determination of phosphorus in different solvents based on the continuum centered at 540 nm. They found that inorganic and organic compounds of various structural types all yielded the same emissivity based on phosphorus content. In their experiments, a wide spectral slit width was used in order to gather sufficient energy from the continuum for maximum precision. With wide slits, however, almost all emissive metallic elements interfered strongly. To avoid this, an acid ion exchange resin was used to remove metallic cations. The detection limit in aqueous solution was 8 ppm. These researchers also found that only solvents which did not give highly luminous flames could be used in the analysis. The use of organic solvents caused high background emissions which had to be subtracted from the phosphorus emission.

1.4 MOLECULAR EMISSION SPECTROMETRY IN THE COOL FLAME

Another method for the determination of phosphorus in organic compounds involves the measurement of the emission from the HPO species, a method first used by Brody and Chaney [44] as a detector for GC. In this method, organic vapors leave the GC column with nitrogen as the carrier gas. The vapors are then mixed with a volume of oxygen to give the same nitrogen to oxygen ratio as in air. This mixture is fed to the burner where hydrogen is brought directly to the flame photometer burner and is not premixed with the oxygen-nitrogen mixture. The use of narrow bandpass interference filters and a photomultiplier results in a very sensitive and selective elemental detector for sulphur, phosphorus and some main-group and transition elements [45-47]. The limit of detection for phosphorus at 526 nm is 0.006 ppm, and for sulphur at 394 nm 0.6 ppm. This method is applicable to those compounds which can be handled directly by GC. Thus far, all studies on the determination of phosphorus by flame photometry in cool hydrogen flames have been based on the measurement of the emission from the HPO species at 526 nm. Syty and Dean [48] assumed that the phosphorus compounds decompose to PO and then form HPO according to the following reaction:

$$PO + H + M \longrightarrow HPO^{*} + M$$

where M was a third body. In contrast, Gilbert [49], suggested an alternative mechanism:

$$PO + OH + H_2 \longrightarrow HPO^{*} + H_2O$$

Phosphorus is more sensitive than sulphur in cool, hydrogen-rich flames.

Therefore, phosphorus compounds have been selected to evaluate different sample introduction techniques were used for FPD.

West and co-workers [50] were the first to use HPO emission in a cool flame for determining phosphorus initially introduced in liquid form into the flame. The intense green emission of HPO at 526 nm, observed after nebulizing orthophosphoric acid solution into a cool, nitrogen-hydrogen diffusion flame, was particularly prominent in the cool inner regions of the diffusion flame (about 350° C). The intensity of the emission at 526 nm was linear over the range of 0.2-500 ppm of phosphorus. The detection limit was 0.1 ppm of phosphorus. The presence of 10 percent (V/V) of organic solvents miscible with water decreased the signal up to 85%. This decrease was attributed by West and associates [50] to the quenching action of such radicals as CH and CHO. These investigators measured the gas temperature of the flame and confirmed that the decrease in the signal was not caused by any increase in the temperature of the flame. They also noted that most cations depressed the signal. These cationic interferences could generally be overcome by removal on a cation-exchange resin in its hydrogen form. The authors also explained that a total consumption nitrogen-hydrogen flame gave negligible HPO emission, probably because the turbulent nature of the flame caused considerable entrainment of air and hence produced a much hotter flame. The air-hydrogen flame produced a similar spectrum for phosphorus, but, because of comparatively large background emission, sensitivity decreased.

In 1970, West and co-workers [51] described the determination of

phosphorus and sulphur in organic and aqueous solutions by photometry, using a cool nitrogen-hydrogen flame. An interference filter was used instead of the monochromator because sensitivity was lost when radiation was recorded over a narrow spectral region (about 0.2 nm) by using a monochromator. Some modification, such as a heated nebulizer chamber for sample volumes greater than about 1 mL/min, was also done to the pneumatic nebulizer in order to increase transport efficiency (percentage of analyte mass reaching the atomizer compared with that aspirated). They suggested that, in a cool, nonturbulent flame, a nebulizer must produce fine aerosols for the chemical process to proceed faster. The limit of detection in aqueous solution by using conventional nebulizing techniques with a heated chamber was 0.08 ppm for sulphur and 0.07 ppm for phosphorus. Matrix effects in the cool flame were also serious, and all metal cations interfered to the same extent, usually depressing the emission. Again, the depression caused by metal ions was removed by using a cation exchange resin in its hydrogen form. Organic solvents completely quenched the emission by interfering with the chemiluminescent reaction process in the flame. This technique has been used for the determination of phosphorus in detergents [52] and lubricating oils [53].

1.5 FLAME PHOTOMETRY AS A DETECTOR IN LIQUID CHROMATOGRAPHY

The FPD is a flame-based GC detector. The effluent is introduced into a cool, hydrogen-rich flame to produce an excited molecular or atomic species of

analyte by means of chemiluminescent reactions. The FPD is commonly used for the analysis of sulphur and phosphorus, but has also shown good sensitivity and high selectivity for some volatile organometallic compounds of main-group elements and transition metals [45-47]. LC-FPD needs special sample introduction devices and the interfaces that have been used in HPLC-FPD can be divided, based on the HPLC column, into two categories: (1) conventional column, and (2) microcolumn. In the following survey they will be discussed separately.

1.5.1 Conventional column

Mass transport systems such as moving wire, porous belts or rotating disks [54,55] are interfaces used to eliminate mobile phases, as an organic mobile phase in the flame can quench the analyte and produce extraneous signal and soot [56]. One of the limitations of these techniques is "off line" application. Nebulizers are another type of interface that can be used in LC-FPD.

Kirkland and co-workers [56] were the first group that interfaced HPLC and FPD for the determination of phosphorus and sulphur compounds. A flame emission detector for HPLC, which included a crossflow pneumatic nebulizer and a laboratory constructed burner head assembly with a 1.5 cm diameter containing thirty-eight 1.5 mm holes. In this detector, a large fraction (25%) of the solution was aspirated into a cool hydrogen-rich diffusion flame. Phosphorus and sulphur compounds were selectively detected by monitoring the optical emission of the HPO (526 nm) and S_2 (384 nm) species. With a premixed gas supply, phosphorus

and sulphur could be detected at 0.02 and 0.2 ppm, respectively. Usually in flame photometry, the flow rates of the gases producing the flame are significantly related to both the flame temperature and the resultant emission intensity. Here, however, air flow rates from 11-28 L/min had little effect on the emission of a dilute organic phosphate solution. Also, a constant signal to noise level was obtained at hydrogen flow rates of 4.6-6.8 L/min. The optimum flow rate for nitrogen was 12 L/min. Lower nitrogen flow rates resulted in decreased emission and higher flow rates increased noise. Organic solvents caused the quenching of HPO, the chemiluminescent species. For example, when changing from water to water plus 1% methanol at an aspiration rate of 2.4 mL/min, the phosphorus response dropped to 50%; hence, application of this detector was limited to pure aqueous systems. The effect of decreasing emission response did not appear to be due to changes in flame temperature. The high flow-rate of gases in the flame tended to stabilize the temperature of the flame even when combustible organic materials were present.

Metal cations also had a significant effect on the signal. Phosphorus emission intensity usually decreased. However, copper gave a positive interference because the CuH and CuCl bands overlapped the HPO emission. Because of the limitation in the nature of the mobile phase, this detector could be used only for ion exchange and, perhaps, reversed phase liquid chromatography.

In the preceding experiments, it was noted that the FPD analyte signal suffered from quenching caused by coeluting hydrocarbons [56]. To solve this

problem, one must investigate the effects the shape of the flame and the type of the flame (normal or inverse) has on quenching. In a "normal" flame, hydrogen is introduced in the center tube and burns in atmosphere. For HPLC applications, coeluting organic materials reduce sensitivity and enhance interferences, thus limiting the selection of a solvent system and separation modes. Chester [57,58] proposed the use of an "inverse" flame to minimize interferences by many organic solvents, metal ions and buffers . In an inverted air-hydrogen diffusion flame, air is used for nebulization at a flow rate of 7 L/min. Hydrogen is introduced through the sheath attachment to the burner head at a flow rate of 6 L/min. Chester used a solution uptake rate of 6 mL/min [57,58]. Note that the detection limits obtained with this modified FPD were not significantly improved, with 0.01 ppm phosphorus being detected with continuous sample introduction. In order to compare the chemical interference of different solvents in normal and inverse flames, argon was used for nebulization at a flow rate of 7 L/min, instead of the air used in the inverse hydrogen diffusion flame. Hydrogen was burned at a flow rate of 6 L/min in entrained room air. With this detector, spectral interference was generally three times smaller than that in the normal flame. Chemical interferences were significantly lower with the inverse flame compared to the normal flame. A 10% solution of acetone in water caused the complete quenching of HPO with the normal flame solution. In the inverted flame, a 20% solution of acetone produced essentially no quenching. The reason for the decreased chemical interference in the inverse flame was attributed to flame geometry. In the normal flame, HPO is

formed on the inner side of the primary reaction zone. When organic materials are introduced into the flame, they pass through the HPO formation region with minimum contact with the hotter outer region where decomposition of organic materials chiefly occurs. These organic materials quench reactions. In the inverse flame, the HPO is formed on the exterior of the primary reaction zone and any organic material is almost completely decomposed prior to reaching the HPO formation region. In other words, organic constituents in the sample are exposed to oxidizing conditions prior to reaching the HPO formation region. Patterson and associates [59,60] also proposed a similar mechanism for the application of an inverse flame in a dual flame FPD for GC. This group speculated that when samples are mixed with air and enter the hydrogen diffusion flame, they are exposed to a flame region, characterized by an abundance of O and OH radicals, where decomposition takes place. The secondary flame could be described as consisting of a central core region rich in H atoms for the formation of HPO.

Recently Blais and coworkers [61] used thermochemical hydride generation (THG) to determine sulphur species such as methylthiophene, carbon disulphide and ethanesulphonic sulphonate in 100% methanolic effluent. In this technique the methanol decomposes in a pyrolysis process before it enters into the flame. This method of hydride generation was introduced initially to determine certain arsenic compounds that could not be reduced by borohydride [62,63]. The method involved four processes: (a) thermovaporization of the HPLC methanolic eluent (thermospray); (b) pyrolysis of analytes in a kinetic methanol-oxygen flame; (c)

thermochemical hydride generation mediated by hydrogen radicals formed in a reducing post-combustion stage fuelled by hydrogen; and (d) transport of the volatilized analytes to the hydrogen radical rich surroundings of an inverted hydrogen oxygen diffusion flame. The detection limits for 2-methylthiophene and CS_2 were 1.5 ng/s and 2.25 ng/s respectively. The detection of phosphorus was not a quantitative technique because of deposition of phosphorus on the surface of the transporting tube.

1.5.2 Microcolumn

Applications of microbore columns in HPLC are rapidly gaining recognition in modern separation science because of their very high efficiency and reduced consumption of sample and solvent [64]. The advantages of microcolumns [65] are: (1) high efficiencies; (2) decreased detection limits, primarily with mass flow detectors; (3) decreased solvent consumption and cost; and (4) compatibility with on-line detectors such as the mass spectrometer. An effective use of flame-based detectors combines the unique attributes of micro-columns with the mobile phase flows of a few µL/min. An extremely valuable feature of the flame-based detectors is their extremely small dead volume.

The use of a FPD in micro-column LC was first described by McGuffin and Novotny [3]. While, flame-based detectors have not been successful in conventional HPLC, the microcolumn LC has been found to be particularly well suited to the selective flame-based detectors. The microcolumn effluent can be

nebulized by a concentric nebulizer directly into a cool, hydrogen-rich diffusion flame, i.e. the total column effluent is introduced into the flame with much lower dead volume because the end of the capillary column can be simply inserted into the flame. One disadvantage of the approach is the low nebulization efficiency.

A glass capillary with 10 cm length (i.d. 50 µm, o.d. 0.6 mm) is typically connected to the micro capillary HPLC column with shrinkable PTFE tubing and is inserted through the baffle, burner base and flame jet. The capillary extends approximately 1 mm above the top of the jet. McGuffin and Novotny observed no decrease in HPO emission for moderate concentrations of acetone and alcohols for the introduction of trimethyl phosphate plus methanol as a test solute (with concentrations ranging from zero to 50%) to the aqueous mobile phase. However, small increases in detector response were observed at certain concentrations of these solvents. An alteration of the physical properties of the effluent was primarily responsible for the enhancement of the phosphorus emission in the presence of acetone or alcohols. The enhanced response does not indicate the absence of quenching in the miniaturized FPD. The detection limit obtained with this system was 70 pg P/s.

Kientz and co-workers [66] introduced another method for interfacing a micro-column to the FPD. In this method, the column effluent was evaporated and subsequently introduced into the detector, allowing volatile organophosphates to be detected. The authors suggested that insufficient evaporation due to the relatively high boiling points of the compounds in the interface area caused peak

broadening, and peak asymmetry, thus reducing the detector sensitivity for tributyl phosphate. With this interface, non-volatile analytes such as organophosphorus acids and high molecular weight compounds could not be detected. The detection of such compounds by using either LC (with UV) or GC is not possible without derivatization. Kientz and co-workers [67] detected a series of organophosphorus acids (representing nonvolatile compounds) by introducing the LC effluent into the detector by means of a fused silica capillary, while helium was passed as a nebulizer gas (40 mL/min) through the wider coaxial fused silica capillary. A hydrogen flow of 650 mL/min was passed through a stainless steel tube into the burner just below the tips of the two fused silica capillaries. The air flow was 350 mL/min. To obtain maximum stability detector response, the tip of the fused silica capillary was positioned at 1.4 mm above the outlet of the hydrogen flow. The hydrogen flow was relatively high in comparison with conditions in GC. At lower hydrogen flow rates, the tip of the capillary started to glow, and nonvolatile compounds blocked the fused silica capillary. The authors obtained a detection limit of 20 pg P/s when aqueous ammonium acetate or nitric acid solution was used as the eluent. The addition of methanol or acetonitrile to the eluent quenched the detector response. When dimethyl phosphoric acid was used as a test compound a mass flux of 0.1 mmole of methanol or 1.2 milligrams of oxidizable carbon per second caused a 20% loss in the detector signal.

Karnicky and co-workers [16] were the first group that used an ultrasonic micronebulizer for introducing liquid samples into the FPD. In this approach, (Fig.

1.1) the HPLC effluent was introduced through a stainless steel tube onto the surface of a 0.76 mm thick glass diaphragm which was vibrating at high frequency due to the focused ultrasonic excitation produced by a piezoelectric crystal. The micronebulizer was designed for effective nebulization at 2-20 µL/min. A uniform distribution of droplets with diameters of less than 10 µm was formed at this solution uptake rate. These were swept out of the nebulizing chamber and transported by the air supply to the FPD. Water was circulated through the transducer chamber in order to cool it and provide a medium for focusing the ultrasonic waves. In the transport tube, the droplets were desolvated in an attempt to prevent overloading of the flame. The aerosol was passed through a condenser cooled to a temperature just above the solvent's freezing point before introduction into the FPD. Most of the evaporated solvent was condensed and drained from the transport tube. Karnicky and co-workers [16] suggested that in the desolvation process possibly 50% of the particles containing the sample were also lost. The flame processes that led to HPO emission were the same for the nebulized nonvolatile samples in water and for the gas phase samples. Water did not show any quenching effect. The best detectable limit, 50 pg P/s, was obtained using water as solvent. Application of an organic solvent as the mobile phase decreased sensitivity and the largest part of this reduced sensitivity was due to quenching of the HPO emission by the presence of large amounts of organic material in the flame. Quenching is a well-known phenomenon in the FPD [68].

A dual-channel approach was used to minimize noise that resulted from

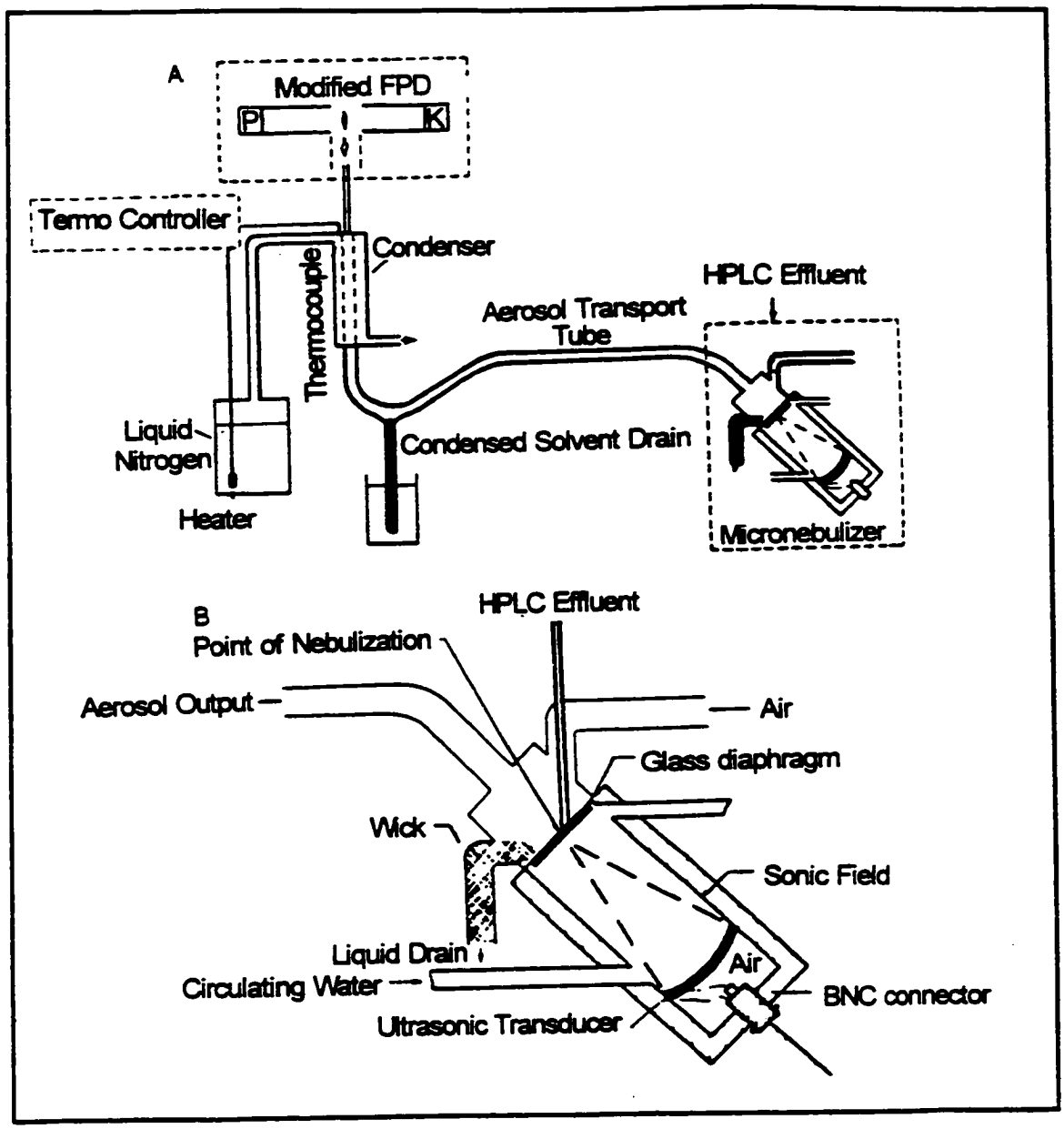

Figure 1.1 Schematic of the ultrasonic micronebulizer with the FPD.

(from reference 16 with permission).

fluctuations in nebulizing efficiency caused by the buffer salts and ion pairing [16]. Because the high salt concentrations of the mobile phase caused instability of the flame and incomplete evaporation of the salts which consequently cause spikes and enhanced background noise. A reference signal was created by adding a few millimoles of potassium salt to the mobile phase. The potassium emission signal at 767 nm acted as an internal standard signal, thereby improving the signal-to-noise ratio by a factor of 5.

1.6 CAPILLARY ZONE ELECTROPHORESIS

Capillary zone electrophoresis (CZE) is a unique separation technique that offers an extremely high separation efficiency without a need for a stationary phase. Several million theoretical plates can be obtained after optimization [69].

Brinkman and co-workers [70] coupled the CZE to the FPD and analyzed a mixture of three organophosphorus compounds. Because the sample flow rate in the CZE ranged from 0.1 to 1 µL/min, a make-up water flow was mixed into the grounded outlet capillary to feed a sample flow of 10 µL/min into the flame. The outlet capillary was grounded by using a modified PTFE tube. The investigators explained that the coupling was successful and detection limit of 1-2 ng methylphosphonic acid could be obtained.

In Chapter 3 of this thesis it will be explained that it is possible to use nanoelectrospray for very small sample flows. Therefore it may be possible to use the electrospray-FPD as a detector in CZE without necessarily using a sheath flow.

1.7 SUMMARY

Although there are a variety of liquid sample introduction techniques, LC-FPD has been used with only few of these systems. For conventional HPLC, pneumatic nebulizers have been used. In the absence of a mobile organic phase, this nebulizer has been used with a normal flame. In the presence of an organic phase, it has been used with an inverse flame to reduce the quenching of the analyte by the organic phase. A total consumption nebulizer and an ultrasonic nebulizer have been used for micro-LC. Total consumption nebulizers have 100% transport efficiency, but nebulization efficiency is low. The ultrasonic nebulizer offers better nebulization efficiency but it is an expensive and sophisticated nebulizer. In the following chapters, liquid film and electrospray as new sample introduction techniques will be introduced. The advantages and limitations of each system will be discussed.

Chapter 2

LIQUID FILM AS A NEW SAMPLE INTRODUCTION TECHNIQUE

2.1 INTRODUCTION

The objective of this research was to introduce liquid samples as a continuous and even liquid film into a small, low-background and hydrogen rich-flame. If liquid could be introduced continuously as a film with a thickness of about a few nanometers it should evaporate smoothly in the flame. In other words, it would not be subject to typical nebulization problems such as large droplet formation and wide particle size distribution, which produce incomplete evaporation of analyte and flicker noise in the flame.

Work was initiated by designing a special capillary depicted in Figure 2.1. A syringe pump (model 355, Sage Instruments Division of Orion Research, Incorporated) with a 50 μL Hamilton syringe was used to deliver a constant liquid flow of 4 μL/min of the test sample into the capillary. Compressed air was used as a carrier gas to form and transport liquid film on the capillary wall. The drive gas was humidified by bubbling it through distilled water (for use in the aqueous solutions) to saturate it with water vapour. The place at which liquid and gas met in the capillary, hereafter named the interface area, was the crucial part of the capillary, often determining the success or failure of liquid film formation. The liquid samples selected for experiment included high viscosity fluids such as glycerine,

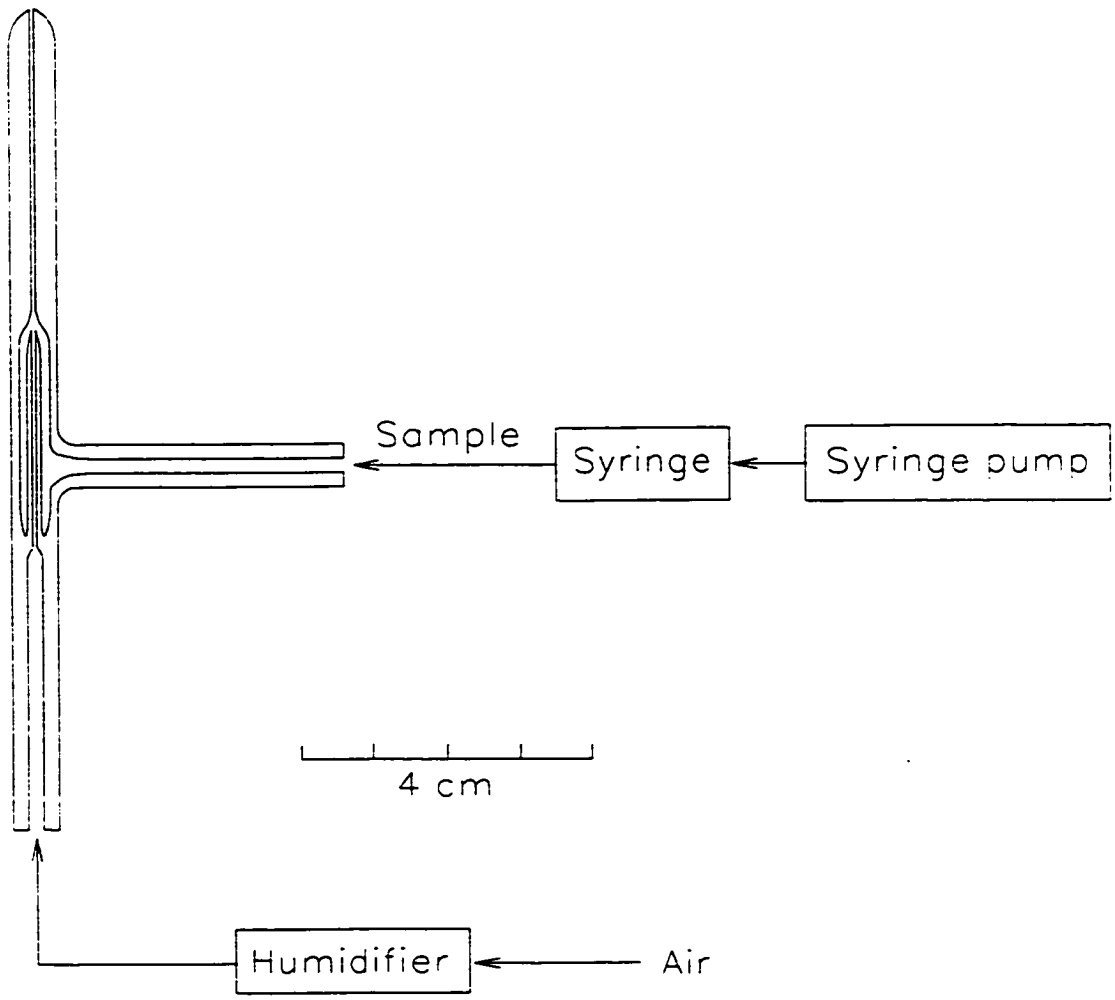

Figure 2.1 Burner assembly.

polyvinyl alcohol (PVA) (75% mole hydrolysed, MW 3000) (20% w/v) solutions and polyethylene glycol (approximate MW 600). These liquids could not produce a continuous and even liquid film at air flow rates varying from 40 mL/min to 60 mL/min. At a high air flow rate, nebulization occurred, while at a low air flow rate, the film-forming process is not continuous.

To solve the problem, capillaries with differing shapes and interface areas were designed and constructed. The following overall results were obtained:

a. A smaller "interface area" - the cross-sectional area over which sample liquid first meets the driven air flow - produced a better liquid film. For example, a metal needle (i.d. 0.3 mm) for sample introduction gave better results, since the interface area was decreased.
b. Increasing the liquid flow into the capillary enhanced the interruptive effects. In other words capillaries cannot produce good films at high sample flow rates.
c. Increasing the gas flow rate decreased bubble production in the liquid film.
e. When the concentration of polyvinyl alcohol in aqueous solution was decreased to 1% w/v, the interruptions in the liquid film also diminished.

These preliminary experiments were concentrated to design a new capillary which is shown in Figure 2.2 to investigate the ability of different carrier gases to form and transport liquid film.

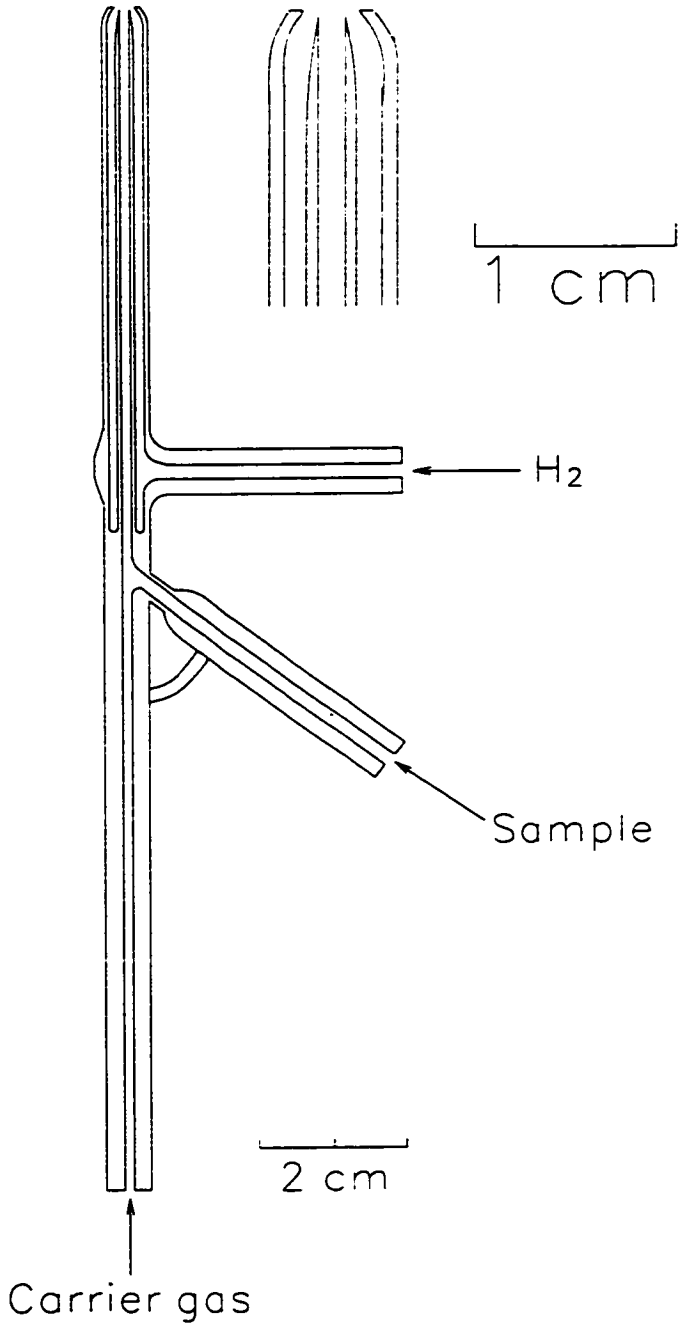

Figure 2.2 Glass capillary burner.

2.2 CARRIER GASES

Polyvinyl alcohol liquid solution (1%) was fed into the inner tube of the capillary at a rate of 4 µl/min.

2.2.1 Air

An air flow of 120 mL/min was used to examine film making and liquid film transport. Hydrogen was passed through the outer tube of the capillary at 200 mL/min. The flame was a combinations of normal and reverse flames and the capillary tip was hot enough to deposit carbon inside the inner tube. Consequently the air flow could not pass through the capillary at a constant flow and in turn, gas pressure increased in the humidifier (Erlenmeyer flask) which ultimately pushed up the rubber stopper of the Erlenmeyer. This experiment showed that air is not a suitable carrier gas for producing films.

2.2.2 Nitrogen

The following procedure was used for introducing aqueous PVA solution into the flame when nitrogen was used.

a. Hydrogen was introduced into the outer tube of the capillary at a flow rate of 20 mL/min and the flame was ignited.
b. Nitrogen was introduced into the inner tube at a flow rate of 300 mL/min and then sample delivering started.

c. Hydrogen flow rate was decreased to 13 mL/min.

Under these conditions the flame was very small and stable. Nitrogen was a good choice as a carrier gas, and also, because of its thermal conductivity, it can cool the flame.

2.2.3 Nitrogen and air

Air and nitrogen were mixed at flow rates of 26 mL/min and 300 mL/min respectively. When the sample solution was delivered into the capillary, carbon was deposited inside the inner tube of the capillary.

2.2.4 Nitrogen and hydrogen

Hydrogen was mixed with nitrogen at high flow rates. The increase in the hydrogen flow rate was necessary to prevent the flame from being extinguished. At a high-flow rate of 300 mL/min nitrogen, the hydrogen flow was 150 mL/min. The shape of the flame was cylindrical, different from a typical flame. No deposit was formed at the tip of the capillary because of the cool introduction of the sample into the flame. Hydrogen removed most of the heat from the capillary tip because of its thermal conductivity, and consequently little light was emitted by the tip of the capillary. Unfortunately, this flame was not stable. The end result of this experiment was the selection of nitrogen as a carrier gas for the film-making process.

2.3 AN IMPROVED CAPILLARY

In order to decrease the interface area and enhance the carrier gas speed at the capillary tip to introduce sample into the flame, a variety of capillaries were designed and constructed. The best one is shown in Figure 2.3 and had the following characteristics:

a. An inner tube (i.d. 0.5 mm) was used for the sample introduction.
b. Glass drilling instead of glass blowing was used to make the hole for connecting the two inner tubes to each other.
c. To increase the gas speed and decrease the film thickness, the upper part of the capillary was pulled into a fine tip.

No interruption in film formation was noticed when polyvinyl alcohol (1%) and formic acid solutions were introduced with this capillary at a high nitrogen flow rate (200 mL/min). The only serious problem was carbon deposition inside the sample tube and at the capillary tip, which could destroy the whole film making process. In order to solve this problem, different methods were examined such as doping nitrogen with chlorine, adding hydrogen peroxide to the solution, mixing different gases such as hydrogen, nitrogen and air. Finally it was discovered that mixing nitrogen (240 mL/min) with hydrogen cooled the capillary tip adequately to solve the problem. This methodology will be described later for cooling a needle tip in the electrospray approach. The next step was to mix analyte with the PVA

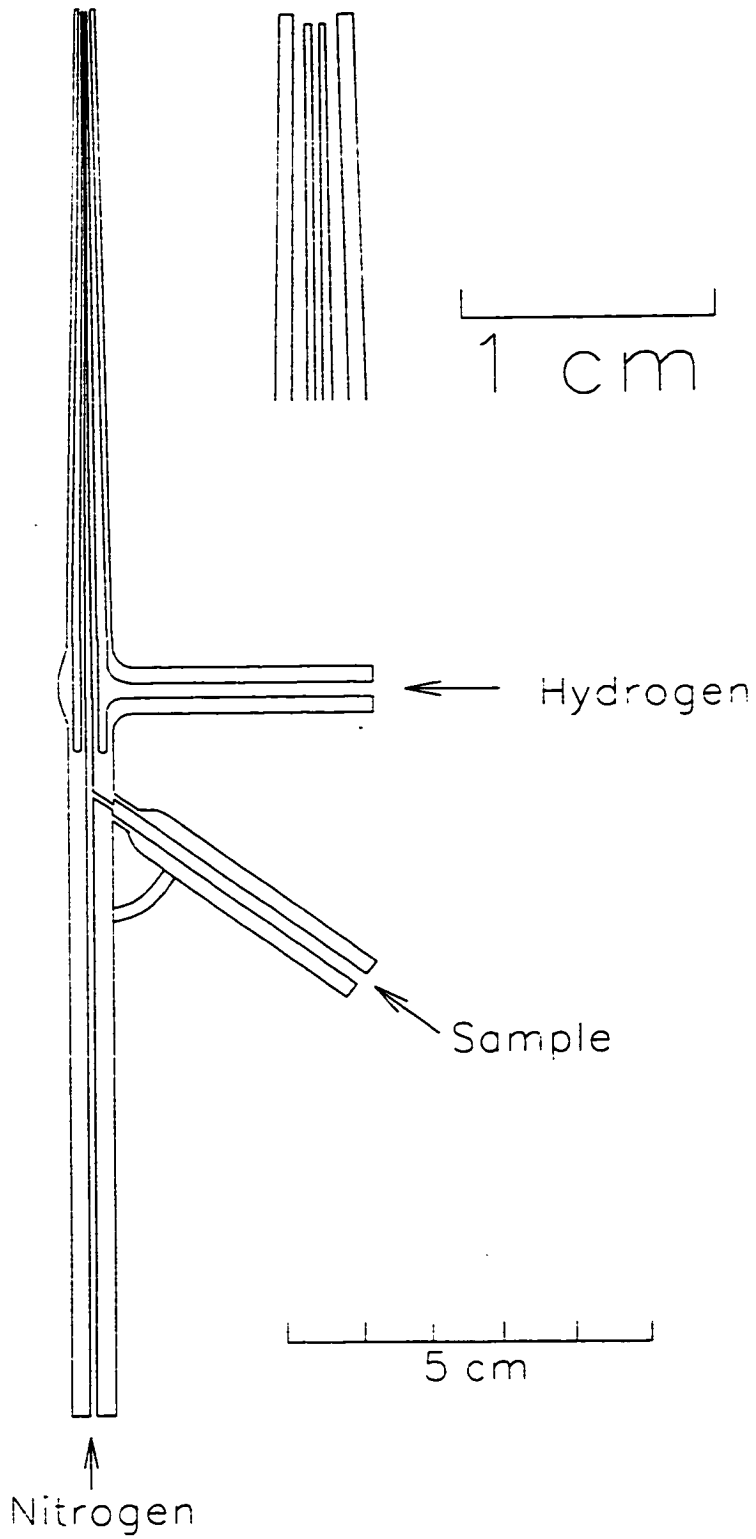

Figure 2.3 Improved capillary burner.

or formic acid solution and to measure the signal and the noise. A four-channel detector system was designed and constructed for these measurements.

2.4 FOUR-CHANNEL DETECTOR

The design of the four-channel detector system constructed for this work is shown in Figures 2.4 and 2.5. The detector was made from aluminum and consisted of a block body, four channels and lower and upper insert ports. The block body was made from an aluminum block of dimensions 6.3 x 6.3 X 6.3 cm^3. All surfaces of the block body were covered with a heat insulator (asbestos) and painted black. Two cartridge heaters in a parallel circuit were connected to a Variac (variable auto-transformer) to heat the block body to approximately 200° C. Four aluminum channels with equal internal diameters of 40 millimeters were screwed to the aluminum block body . Two channels were cooled by circulating water around the channels designed to hold the PMT housings. The other two channels were not used for optical measurements. By using a heat insulator and water cooling system, the temperature of the channels was dropped to room temperature (to prevent PMT damage and decrease dark current). The two aluminum ports were secured by inserting Swagelok fittings into the lower and upper port of the block. The lower port was used for connecting the burner to the block. It was found that the high-thermal-conductivity connection between the capillary and lower insert port caused evaporation of the solvent and deposition of the analyte inside the inner tube. Two modifications were made to cool the lower

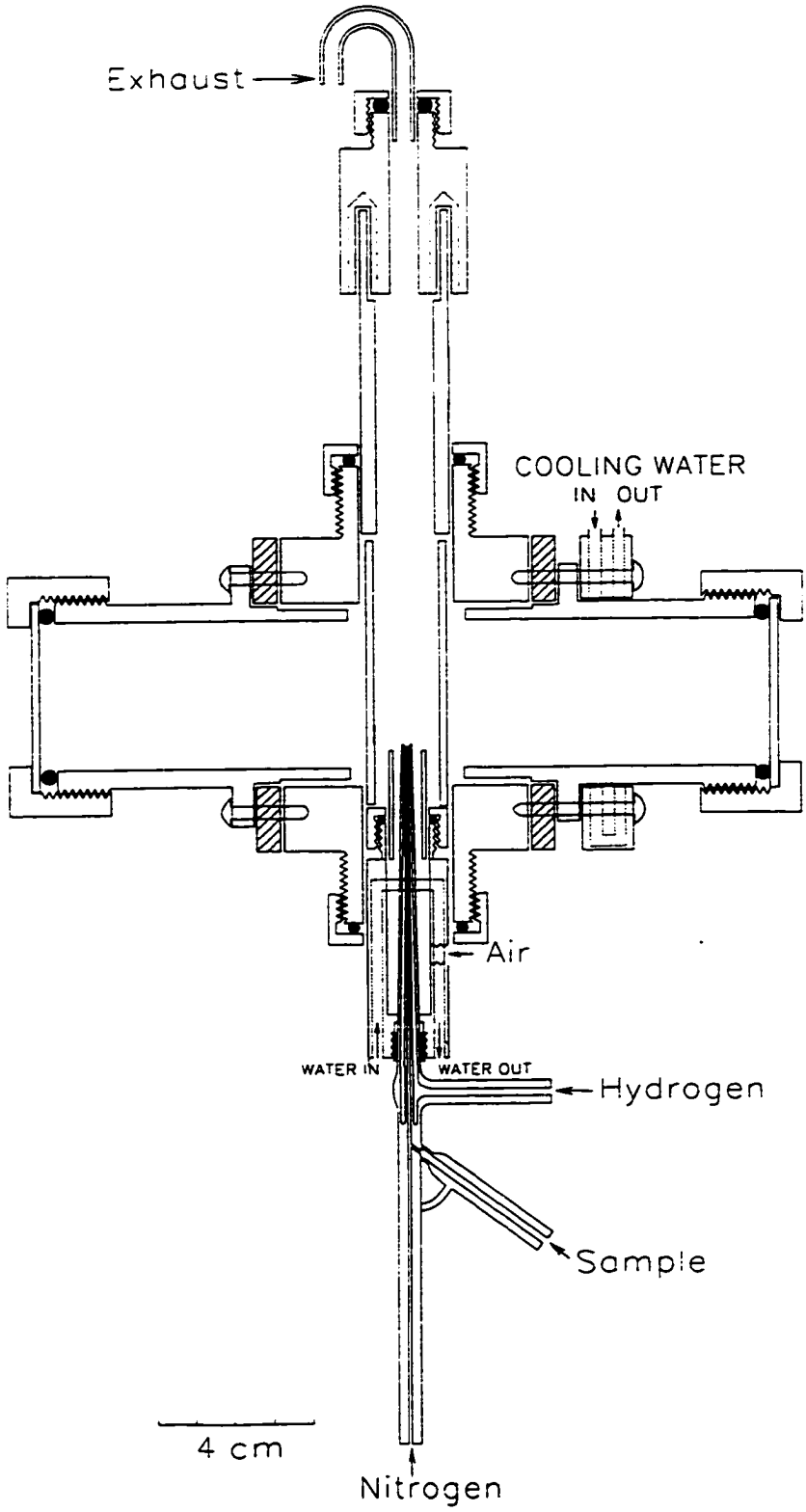

Figure 2.4 Four-channel detector assembly (side view).

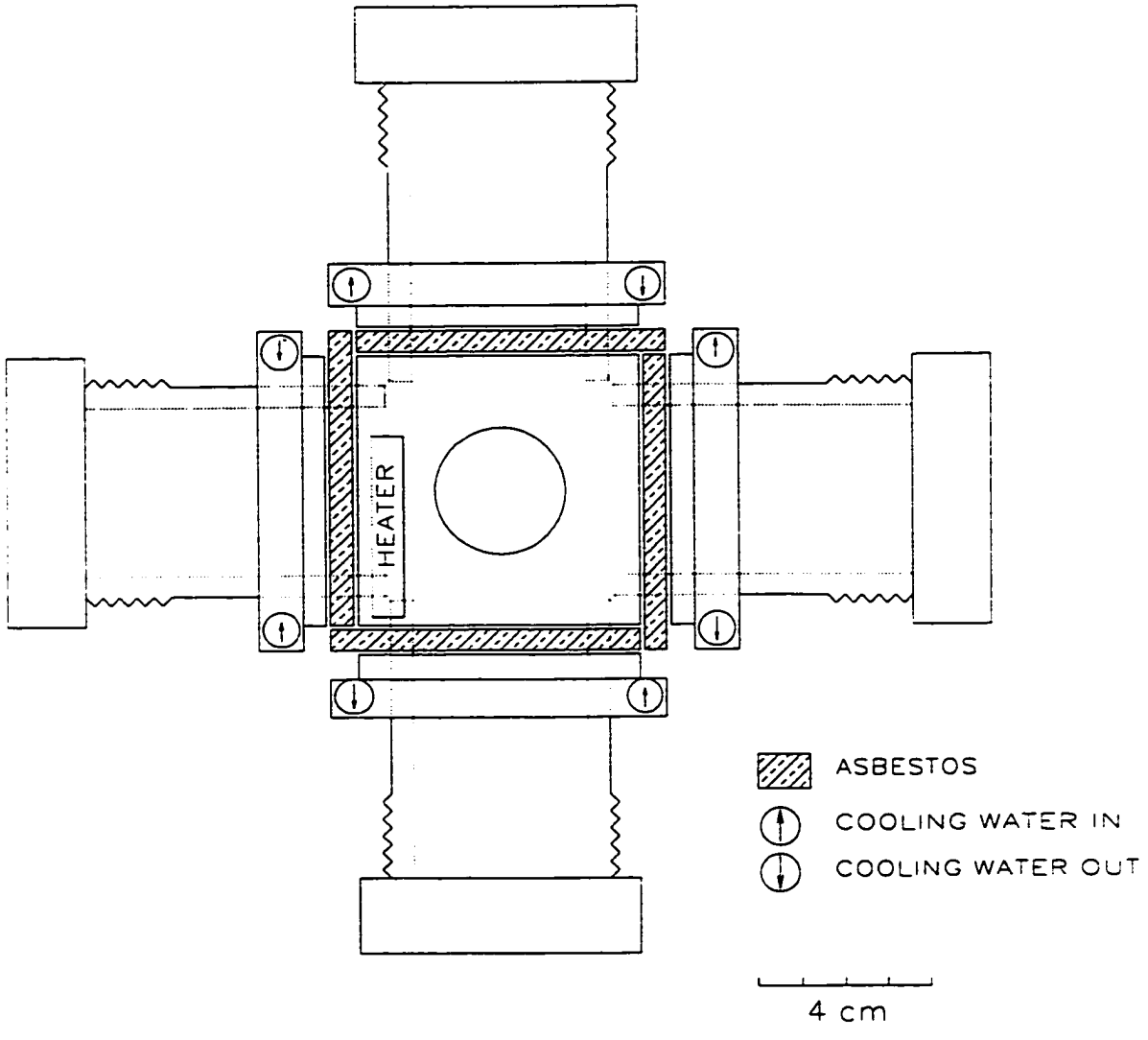

Figure 2.5 Four-channel detector (top view).

insert port. First, the outer wall of the lower insert port was machined to decrease its diameter and to prevent direct contact between the lower insert port and the aluminum block body. Second, a copper tube (o.d. 1.58 mm) was imbedded into the lower insert port for water circulation. These changes cooled the lower insert port to approximately room temperature. A Teflon tube was also placed into the lower insert port to align the burner in the center. Exhaust gases were directed to the upper port, with its cap so designed as to prevent light leak. A chimney (i.d. 2 0 mm) was used to prevent diffusion of the gases and water vapor to the PMT's. The burner was connected to the lower insert port by a Teflon connector.

2.5 NORMAL, REVERSE AND PREMIXED FLAME

Four flames were explored for liquid film introduction: Hydrogen in inner and air in outer port of the flame (normal flame), air in inner and hydrogen in outer port of the flame (reverse flame), a premixed flame, and a combination of normal and reverse flames. Tetrahydrothiophene was used as a test compound using a head space procedure. The intensity of the blue sulphur emission at 394 nm was used as a criterion to evaluate the flames. Two flames, depicted in Figure 2.6, could tolerate a high nitrogen flow rate in the inner tube (film making required a high nitrogen flow rate) without the flames being extinguished. The following sections summarize the results of these flame studies.

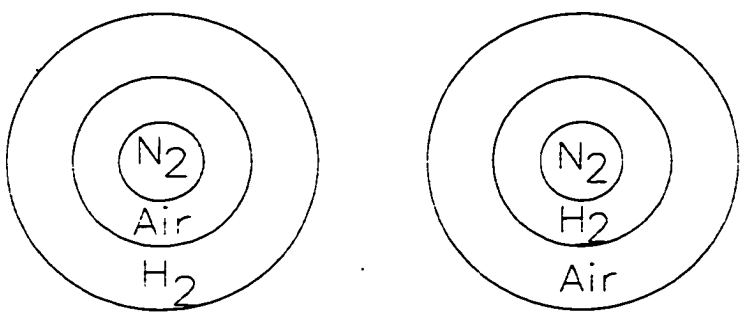

Figure 2.6 Cross sections of the burner.

2.5.1 LIQUID INTRODUCTION INTO THE AIR ATMOSPHERE (REVERSE FLAME).

A capillary with an inner tube (i.d. 0.4 mm) for sample and nitrogen, an outer tube (i.d. 3 mm) for air, and a third tube (i.d. 8 mm) for hydrogen were used. The experimental conditions were: Hydrogen: 150 mL/min; Air: 140 mL/min; Nitrogen: 100 mL/min; Sample flow rate: 24 ng P/s (from triethyl phosphate). The following overall results were obtained. Triethyl phosphate (TEP) in formic acid or PVA (1%) solution showed a green color due to phosphorus emission. However, semi-volatile or non-volatile compounds such as triphenyl phosphate (TPP) and phosphoric acid in formic acid (120 ng P/s) did not produce a signal, or a green emission signal was observed accompanied by a reddish orange deposit at the capillary tip. The same results were obtained when diglyme and ethylene glycol were used as film-making liquids. The above observations can be explained as follows. When formic acid is used to carry phosphoric acid it could evaporate inside the inner tube as a result of the high nitrogen flow rates, because the boiling point of the formic acid is about 100° C. Consequently, phosphoric acid is left behind. If any amount of phosphoric acid reaches the capillary tip-perhaps not as a liquid film but as a droplet-depending on the temperature of the capillary tip, it overflows into the hydrogen tube or deposits inside and at the tip of the capillary, and a green color is observed. Diglyme and ethylene glycol, because of their higher boiling points, could carry the phosphoric acid. However, near the capillary tip, where the temperature is relatively high, diglyme evaporates, leaving behind the

phosphoric acid. Therefore, the temperature of the capillary tip (and below the capillary) should be low to prevent solvent evaporation and analyte deposition for sample introduction into the flame. Note that the flame must be hot enough for evaporation and dissociation to occur without disrupting chemiluminescence. These opposing trends prevent the attainment of a reasonable compromise condition. In addition to the problems outlined above, formic acid also introduces a significant amount of carbon into the flame. Carbon appears to quench the phosphorus chemiluminescence by interfering with the chemiluminescent reactions or by collisional deactivation of HPO* [71].

In order to overcome some of these problems, a normal flame instead of a reverse flame was explored.

2.5.2 LIQUID INTRODUCTION INTO THE HYDROGEN ATMOSPHERE (NORMAL FLAME)

The glow from the capillary tip was less intense in normal flame. Note that the capillary tip in the normal flame is cooled by hydrogen, which has a large thermal conductivity. According to Chester et al. [57,58], the reaction zones of normal flames occur at regions away from the burner, and thus the capillary tip is exposed to a lower temperature. For this reason, the normal flame was used for subsequent experiments with liquid film and electrospray sample introduction.

Because of the properties of water as a solvent, phosphorus and other element emissions were investigated more extensively in an aqueous solution.

Water alone was not able to produce liquid films. However, liquid films were produced from water solutions of surfactants such as 8.1x 10^{-3} M hexadecyltrimethyl ammonium bromide (HAB), 0.1% Thorowet RL (a surfactant that does not foam) and 0.1% CF-32. The green emission from phosphorus introduced as TEP was observed in both normal and reverse flames. The capillary tip in normal flame has a lower temperature, as indicated by the smaller glow. Sodium chloride (100 ng Na/s) in 8.3 x 10^{-3} M HAB was fed into the flame but no response was observed. A white deposit was noticed inside the capillary. The sample flow rate was then increased to approximately 20 µL/min (with the same analyte mass flow rate or 100 ng Na/s). A response was observed but the liquid film was interrupted at the interface area and an analyte deposition was observed in the inner tube of the capillary and in the hydrogen tube. Similar observations were made for lithium hydroxide. Thus, the higher sample flow rates interrupted film formation, caused incomplete evaporation of the analyte in the flame, and led to analyte deposition inside the inner tube. To decrease analyte deposition, three experiments were conducted:

a. Polyacrylic acid solution, 10 to 1000 ppm, was used to bind Li^+ to $-COO^-$, but, a polyacrylate salt deposited inside the inner tube.
b. A 0.1M glycerine solution was used and found to help carry the analyte to the capillary tip because glycerine has a higher boiling point than water.
c. A variety of combinations of tube heights and caps were tested for the capillary,

i.e., positions where the inner tube was above, at the same level, or below the level of the cap or outer tube (without a cap) were examined. The best case seemed to be a capillary with a cap, where the inner tube reached about 2 millimeters above the cap.

The changes in b and c helped to solve the deposition problem but could not eliminate interruption in film formation at the interface area because of the relatively high sample flow rates. A number of experiments were designed to overcome this particular problem.

1. Different metal burners were explored using different inner and outer tubes for relatively high sample and hydrogen flow rates, but continuous signal emission could not be produced.
2. A hypodermic needle (hypodermic syringe needle tubing) was inserted into the inner tube of the capillary (i.d. 0.5 mm) liquid was fed around the hypodermic needle while nitrogen gas was flowing through the needle to decrease the thickness of the liquid. While vibrations in liquid were noted, some liquid was splashed onto the wall of the inner tube, and the gas flow rate could not be increased past a certain limit.
3. To decrease the thickness of the film, a stainless steel wire (o.d. 0.12 mm) was inserted inside the inner tube. The interruption of the liquid, and consequently the pulsation of the lithium emission was decreased. This change

is attribute to the decrease in the thickness of the film. The best results were obtained when the wire was about one millimeter above the inner tube. This method decreased fluctuation in lithium emission but it was still too noisy.

4. A setup was assembled to apply high voltage to the wire to force positive ions toward the flame. At 3000 V, the shape of lithium emission was changed from a pear shape to a sharp and discontinuous emission. It was thought that if voltage is applied to the liquid in a capillary with a small i.d., the flow discontinuity problem could be solved. Therefore a new burner was designed and constructed.
5. A 25-cm quartz tube (i.d. 0.3 mm) was used for samples. A high voltage was applied to liquid samples while a Teflon tube was used to prevent direct contact with the block body of the detector. A pulsed emission signal was produced. Subsequently the sample was fed into the quartz tube but, no flame was ignited. Droplet pulses were observed, suggesting that nebulization did not occur at the quartz tip and a better nebulization technique was required.

The idea of using high voltage combined with better nebulization led us to investigate the use of electrospray, an established technique that uses high voltages to nebulize liquid samples. In the next chapter, the experimental results of applying electrospray as a new sample introduction technique for FPD will be discussed.

2.6 CONCLUSIONS

The liquid film sample introduction technique is a very interesting idea because transport efficiency is 100 % and a sample with a few nanometer thickness can evaporate smoothly in the flame. There are several parameters in the film making process which determine the success or failure of the technique. The interface area is the most important; the composition of the solution, the gas flow, and the sample flow are others. In the following, an equation relating gas flow, sample flow and the minimum thickness of the film is presented. In the calculations, it is assumed that the liquid film speed is equal to the linear speed of the gas inside the capillary. In reality the thickness of the film is larger than the calculated value because the liquid speed profile in the tube is parabolic. The linear speed of the gas is:

$$V_g = r^2 \pi v_g$$

where V_g: gas flow rate; v_g: linear speed of the gas; r: radius of the inner tube. The thickness of the of the film is:

$$V_L = Sh = 2\pi r v_g h$$

where V_L: sample flow rate; S: surface area; h: thickness of the liquid film. By substituting the v_g from the previous equation:

$$V_L = 2 \pi r V_g / (r^2 \pi) h$$

$$h = V_L r / 2 V_g$$

For example, if the V_L, r and V_g are 4 µL/min, 0.2 mm and 100 mL/min respectively, the thickness of the film is:

$$h = 4x10^{-3}x\ 0.2 \times 10^{-1}/(2 \times 100) = 4 \times 10^{-7}\ cm$$

Based on the last equation, lower sample flows, smaller capillary i.d. and higher gas flow decrease film thickness. There are some other factors which affect the film making process which are not included in the formula. For example a higher gas flow enhances solvent evaporation and it can evaporate the solvent completely. Consequently there would be no any liquid film. If the analyte also evaporates, the whole of the sample will be introduced into the flame in the gas phase. Otherwise, analyte is left behind and, if it reaches the flame, it will not be introduced as a liquid film. Also, in a lower sample flow, the probability of complete solvent evaporation increases. Another parameter is the capillary tip temperature. If the temperature is hot, the solvent can start to evaporate inside the capillary a few millimeters below the capillary tip. Therefore, the whole film making process will be disturbed. If the capillary tip temperature is low, the sample can reach the tip of the capillary and it might overflow into the hydrogen tube, not being introduced into the flame, or be introduced into the flame without evaporating smoothly. There is no doubt that the capillary tip temperature must be cool and also the flame temperature should be hot enough to evaporate the sample and cool enough to favour chemiluminescent reactions. Compromised conditions where the sample could evaporate smoothly in the flame were not obtained. However, experimental work involving sample introduction as a liquid film had some positive results. Overall they can be summarized as follows:

1. A four-channel detector was designed, constructed and modified to improve its

applications.

2. It became clear that a sample introduction into a hydrogen atmosphere (normal flame) had some advantages relative to the reverse flame. This type of flame was used in the electrospray technique.
3. Mixing nitrogen with hydrogen cooled the capillary tip, a successful technique which was later used to cool the needle tip of an electrospray interface.
4. Formic acid, because of its low boiling point and evaporation inside the capillary, was not considered a good solvent for the liquid-film introduction technique. However, it was the original solvent tried in the electrospray approach, and there proved to be one of the best solvents.
5. Experience was acquired in the application of different surfactants. Because of their properties of wetting and decreasing the surface tension of the aqueous solutions, these surfactants were used extensively for the electrospray method as well.

Chapter 3

ELECTROSPRAY AS A NEW SAMPLE INTRODUCTION TECHNIQUE

3.1 INTRODUCTION

In the previous chapter, the liquid film was introduced as a new sample introduction method. The final modification in the device was to apply voltage for better nebulization, which led to the exploration of the electrospray as an alternative sample introduction technique.

Electrospray is an atmospheric pressure soft-ionization technique used in mass spectrometry (MS). It occurs through a process whereby a liquid surface, in the presence of a strong electric field, is sheared into a spray of fine, highly charged droplets [72]. The original study of this phenomenon is credited to G. M. Bose [73] who in 1745 discovered the formation of water threads by an electric field. Zeleny [74] in 1914 "rediscovered" this phenomenon while Drozin [75] reported a quantitative explanation of electrospray ionization (ESI). Dole and co-workers [76,77] in 1960 used electrospray in MS with a Faraday cup as a detector, while Yamashita and Fenn [78,79] designed and applied ESI with quadrupole mass spectrometers as a novel means of delivering nonvolatile analytes into the gas phase for mass analysis [80].

Nebulization is produced by the application of a strong electric field to a

small flow of liquid (generally 1-10 μL/min) from a capillary tube. A high voltage from 3 to 6 kilovolts is applied between the capillary and a counter electrode with an inter-electrode distance between 3 and 20 millimeters. The electric field results in charge accumulation on the liquid surface at the capillary terminus. The strong electric field disrupts the liquid surface, and highly charged liquid droplets are formed [81]. A simple view of the droplet as a conducting medium suggests that the excess charges reside at the surface. As the solvent evaporates, the electric field at the surface of the droplet increases due to the decreasing radius [82]. The charge density on the surface increases until droplet instability occurs, which is manifested in a coulomb explosion or droplet fission event [83]. This tears the droplet apart, producing charged smaller droplets that also evaporate. This process continues until an extremely small charged droplet (radius 1 nm), which contains only one ion is produced and, by solvent evaporation from this droplet, a gas phase ion is produced [84]. This theory was first suggested by Dole [76], and Kebarle named it single ion in droplet theory (SIDT). Another theory for the gas phase ion production from the small charged droplet was proposed by Iribarne and Thomson [85,86]. The sequence of coulomb explosion repeats until the radius of curvature of a derivative droplet becomes sufficiently small so that the field due to the surface charge density is strong enough to desorb ions from the droplet into the gas phase [87]. Based on this theory, production of a very small charged droplet (R = 1 nm) that has only one ion is not necessary [84]. This theory was named ion evaporation theory (IET). The rate of ion evaporation depends on the

solvation energies of the individual ions; thus, one type of ion may preferentially evaporate if it has lower solvation energy [82]. Rollgen [88,89] criticized IET and argued that the electric field for ion evaporation is larger than Rayleigh fission.

Gas phase ions are produced from very small droplets by either the single ion droplet theory or the ion evaporation theory. It is unclear whether ions escape from droplets (IET) or solvent evaporates to leave ions (SIDT) [83]. In this project, electrospray of metal and nonmetal ionic solutions, are explored; therefore information about the chemical compositions of the gas phase ions originating from metal ionic solutions is useful. Kebarle and associates [84,90-93] conducted experimental and theoretical investigations about electrospray of metal ionic solutions. For example they investigated the hypothesis that metal ions evaporate as a cluster, and go to the gas phase instead of evaporation of naked ions. Evaporation of sodium as sodium ion solvent clusters [$Na(H_2O)_7$] requires 56.5 Kcal/mole energy, while, 98.2 Kcal/mole is needed for evaporation of naked sodium ions. Horlick and associates [94-98] investigated the potential of ES-MS as a new analytical tool for qualitative and quantitative elemental analysis. In their earlier report [94], the authors observed declustered single positive ions (M^+) from different elements such as Na, Li, Mn, Cu, Cd, Ni, and Ag in both aqueous and organic phases such as methanol. In another report [96], Horlick and co-workers investigated how the type of the spectrum changes with experimental conditions. Three different positive modes were defined: (1) the ion cluster mode; (2) the intermediate mode, and (3) the bare metal ion mode. In the ion cluster mode, ion

solvent clusters with a different number of solvent molecules are produced. In the bare metal ion mode, the metal ion is declustered and also reduced to single positive ions. In this mode, by declustering of a multiple positive metal ion and loss of solvent, at some point charge reductions compete with the desolvation process because desolvation can no longer stabilize the charge on the metal ion [91]. This declustering and reduction continue until single positive ions are produced. The intermediate mode is the intermediate between those two positive modes.

3.2 ELECTROSPRAY AS A NEBULIZER

In all nebulizers, sufficient energy is needed to overcome the surface tension of the solution. In pneumatic nebulizers the energy is the high gas velocity that shears droplets from the liquid stream. In ultrasonic nebulizers, the energy is sonic. In electrospray, an electric field is used to overcome the surface tension of a liquid sample, causing it to disperse into fine droplets.

3.3 WHY ELECTROSPRAY ?

Separation techniques such as capillary zone electrophoresis, micro-LC and nanoscale-LC have a special advantage when a sample amount is limited [99]. Other advantages of microscale separation methods are: a higher separation efficiency, a lower detection limit, less solvent consumption, lower separation time and waste reduction [100-103]. The coupling of these separation devices with chemical flames such as FPD and needs sample introduction systems with good

transport and nebulization efficiencies. Now an important question is how to nebulize a small volume of sample fluid. Many researchers are still trying to find sample introduction devices that can handle small sample flow rates which maintain good transport and nebulization efficiency [4,5,18,26,27]. For example, it is not possible to use conventional pneumatic nebulizers for small sample flow rates because of two major drawbacks. First, these nebulizers consume 1 to 2 mL/min of a sample and, second, the transport efficiency is only 1 to 5%. For this reason, Fassel and co-workers introduced a new pneumatic nebulizer which they named the direct injection nebulizer (DIN). It was specifically designed for the introduction of small sample flow rates into the ICP. In the DIN, a very high velocity of gas (120 m/s) was used to nebulize liquid samples [25]. The DIN was used as an interface between HPLC and ICP [104]. The detection limit of elements by HPLC-DIN-ICP is compared with continuous sample introduction by using a conventional pneumatic nebulizer and it is comparable or inferior by a factor of 4. If the conventional pneumatic is used as an interface between HPLC and ICP, the detection limit of elements is one or more orders of magnitude inferior relative to the continuous sample introduction [104]. One of the shortcomings of the DIN is the high velocity of nebulizing gas which decreases the residence time of the sample in the plasma [25].

Electrospray provides a solution for some of the problems encountered in the nebulization of small sample flows. In fact, the capability of the electrospray for smaller sample flow rates improved from microelectrospray to nanoelectrospray to

picoelectrospray with picoliter per minute flow rates [105-108].

The aim of designing better nebulizers, pneumatic or ultrasonic, is to produce smaller "droplets" with a narrower size distribution, and to achieve a high transport efficiency. "Droplet" size is important since it is inversely proportional to the surface area per unit mass, and the finer droplets will be more completely vapourised than the larger ones during their residence time in the flame [109]. Therefore, the signal intensity increases with decreasing droplet size. The droplet size distribution is also important because it affects the flicker noise and consequently the detection limit [110-112]. Transport efficiency is another important criterion for nebulizers.

Generally, electrospray is a nebulization technique that works with small sample flow rates, from about 1 μL/min to 10 μL/min. Droplet size in electrospray depends primarily on the properties of the liquid and sample flow rates. Droplets which are emitted from the tip of a liquid cone have a diameter on the order of magnitude of one micron [113]. Following this, solvent evaporation causes droplet size to decrease by at least an order of magnitude. Transport efficiency is typically 100%. Therefore, in view of the above parameters (particle size, particle size distribution and transport efficiency), electrospray is an ideal nebulizer for small sample flow rates. In addition to these advantages, it does not have the residence time problem which was encountered with pneumatic nebulizers such as the DIN. This is because, in electrospray, an electric field, and not a high velocity gas, is used to nebulize the liquid. Ultrasonically assisted electrospray ("ultraspray") solved

the problem of ESI for different mobile phase compositions. Ultraspray has the capability of nebulizing virtually any type of LC solvent, regardless of its composition [114]. Other advantages of electrospray relate to its simplicity of operation and its low cost. It is worthwhile to note that, although the first generation of electrospray nebulizers was used for small sample flow rates, more recent applications are not limited to these small flow rates. Finnigan MAT introduced ESI sources applied in LC-MS. A heated metal capillary tube was used to enhance the desolvation process and the residual ions were transported into a mass spectrometer. In this technique a flow rate of up to 1 mL/min, typical of the output from a conventional 4.6 mm LC column, could be used. Fisons introduced an electrospray system known as "Megaflow Electrospray". They claimed that this method exhibits enhanced sensitivity (x100), a tolerance for highly aqueous solvent systems and the ability to handle liquid flow rates of up to 1 mL/min [80].

3.4 ELECTROSPRAY IN THE FLAME

It has been previously explained [87] that the solvent evaporation in a charged droplet is necessary for a coulomb explosion or the disintegration of a droplet into smaller droplets. To enhance the rate of desolvation, a capillary desolvation tube or a heated stream of dry nitrogen has been used [83]. Experiments with electrospray also indicated that slight heating allows aqueous solutions to be more readily electrosprayed, presumably due to the decreased surface tension [81]. The Perkin-Elmer Company passed a heated stream of dry

nitrogen into the evaporation chamber to accelerate the evaporation of solvent droplets. This process resulted in an improvement of up to 100 times in sensitivity over that obtainable with conventional ESI. Based on these results, electrospray in a flame should enhance the desolvation process and decrease the surface tension, ultimately leading to the stable production of smaller droplet sizes. The evaporation of the solvent is required to produce a very small droplets and consequently convert the liquid phase to the gas phase by either SIDT or IET mechanism. Therefore, the rate of liquid to gas phase conversion is controlled by solvent evaporation [93]. The rate of solvent evaporation under surface control is [115]:

$$dm/dt = -(\alpha v/4)\, 4\pi r^2\, p^{\circ} M/R_g T$$

where the dm/dt is the rate of change of droplet mass, α is the condensation coefficient (fraction of gas solvent molecules which condense on the droplet by collision with the droplet surface), v is the average velocity of gas solvent molecules, r is the droplet radius, p° is the solvent vapour pressure, M is the molecular weight of the solvent, R_g is the gas constant and T is the droplet temperature. The dm/dt is proportional to v and P° and inversely proportional to T. In flame with higher temperature, the rate of solvent evaporation increases and consequently the rate of conversion of liquid to the gas phase is enhanced.

3.5 ELECTROSPRAY EXPERIMENTS

Early experimental investigation for this thesis was based on the work of

V.G. Drozin [75]. A capillary tube was made by drawing out a capillary pipet so that the internal diameter of the capillary tip became approximately 0.1 mm. The capillary was inverted and the upper part filled with water. The water flow rate at the capillary tip was about 60 μL/min. A Spellman DC power supply (RHS5P30/CR/X769, Spellman, Bronx, N.Y, USA) (2 mA; 5 kV, and 5 MΩ resistors in series to limit the current for safety) was used and the high voltage cable was connected to the water. A grounded copper plate was placed about six centimeters from the needle tip of the capillary. The room was darkened so a flashlight could be used to observe the needle tip. The high voltage was increased gradually and at +3500 V a thread of droplets was observed. The experiment was repeated using a 4×10^{-4} M lithium chloride solution and, again, a thread of droplets was observed.

A glass tube (i.d. 0.3 mm, o.d. 2 mm) was used in a repetition of the experiment but no threads were observed. This experiment, therefore, indicated that the outer diameter of the capillary for making electrospray was an important parameter. Chait [116] also pointed out that the onset potential of electrospray was decreased by making the needle tip sharper. This experiment was repeated using a stainless steel needle (i.d. 0.15 mm) instead of a capillary glass tube, and again threads of droplets were observed. A further experiment was performed by putting the needle tip upright and placing the counter electrode about 2-cm away from the needle tip. A syringe pump (model 355 Sage Instruments Division of Orion Research Incorporated) was used to feed different sample flow rates, from 5 to

50 µL/min, into the needle. The voltage was increased to about 4000 V and dispersion of the liquid was observed. By increasing the sample flow rate, the thickness of the threads was increased.

3.6 ELECTROSPRAY EXPERIMENTS IN THE FLAME

In order to perform electrospray in a flame, a special burner was assembled according to Figure 3.1. A 5-cm quartz tube (i.d. 2 mm) was connected to a 0.63-cm o.d. brass union. A Teflon tube (i.d. 0.8 mm) was inserted into the union to prevent high voltage contacting the union. A needle capillary tube (i.d. 0.15 mm o.d. 0.30 mm) was inserted into the Teflon tube for sample introduction. The high voltage cable was connected to the needle and a Teflon valve was used between the luer connector of the needle and the metal luer lock of the syringe. In order to facilitate gas flow, a stainless steel mesh (with 1.1-mm holes, 2.3x3.7 cm^2) was used as a counter electrode. Entrained air was used as an oxidant to produce the flame. The experiment was conducted by passing hydrogen gas (without flame) around the needle, while a 4×10^{-4} M lithium chloride solution was fed into the capillary at a rate of 15 µL/min. A voltage of about 4000 V was applied. Hydrogen flow rates were changed from 60-200 mL/min. Increasing hydrogen flow rates increased the thickness of the threads of the droplets until ultimately larger droplets were observed at the needle tip. The electrical breakdown potential of gases is not the same [84]. For example O_2 has a higher electrical breakdown potential than N_2. From the observation, it can be said that by increasing the hydrogen flow, the

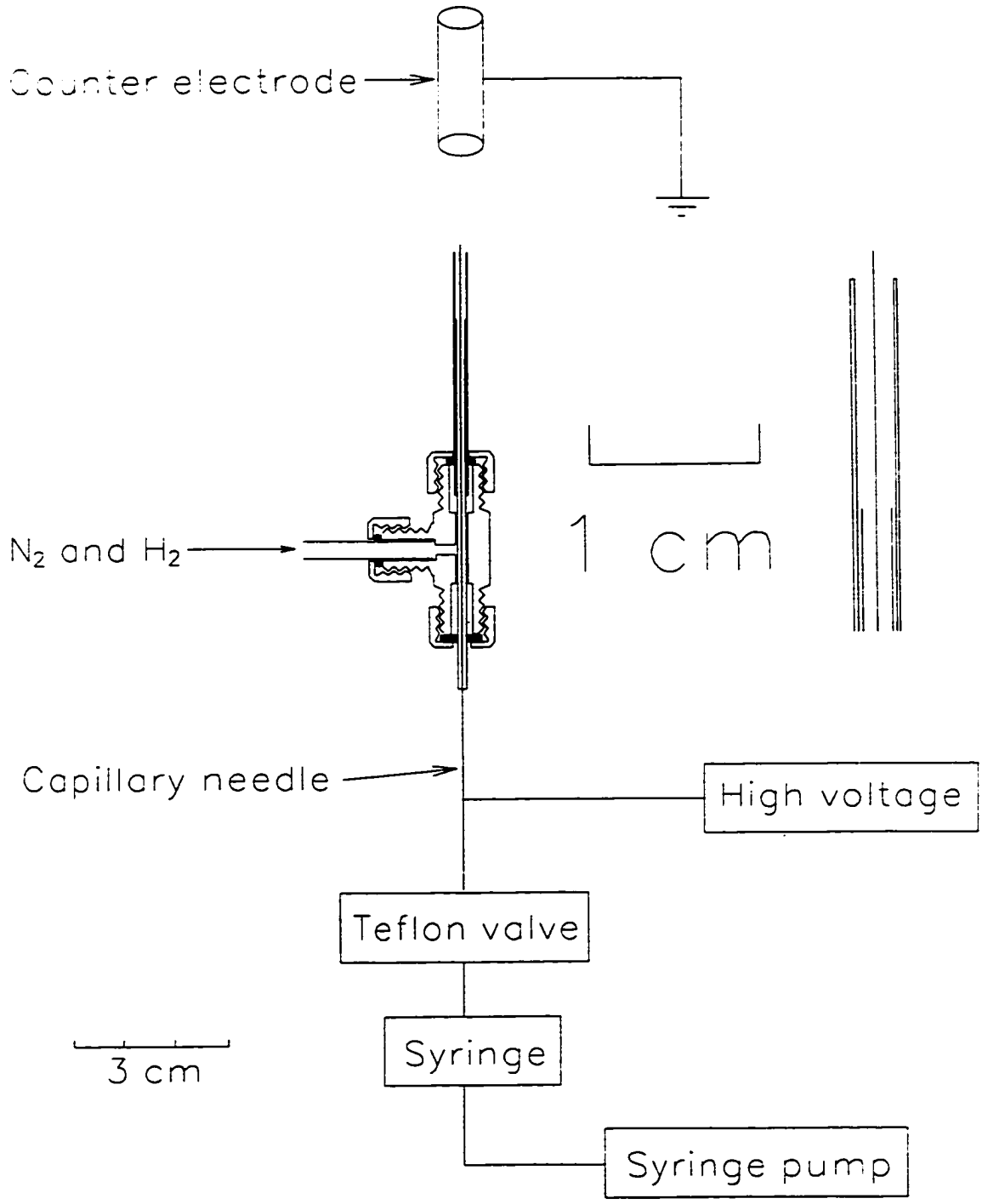

Figure 3.1 Schematic diagram of the electrospray in the flame.

corona discharge is increased and the performance of the electrospray becomes worse, which means that ultimately larger droplets are produced at the needle tip. These coarse droplets fell into the hydrogen tube and caused a connection between the high voltage source and the union, increasing the current in the circuit from μA to mA. This experiment was repeated with nitrogen instead of hydrogen, which resulted in a more stable electrospray. The above experiments showed, therefore, that different gases have diverse effects on the electrospray.

In order to make a stable electrospray with hydrogen flow around the needle, nitrogen at a flow rate of about 300 mL/min had to be mixed with the hydrogen flow to prevent the detrimental effect that pure hydrogen had on the electrospray. The other advantages of nitrogen will be discussed later. The flame was lit with 120 mL/min hydrogen and the voltage was increased to 4000 V. Water was fed at a rate of 30 μL/min and sparking took place. Droplets were observed that collided at the stainless steel mesh and a poor electrospray was produced.

A new counter electrode made of 0.63-cm copper tubing, 5-cm in length was assembled. The aim was to improve the electric field and to make a stable electrospray. A number of "threads" were observed when the hydrogen and nitrogen flow rates were 150 mL/min and 300 mL/min, respectively; the distance between two electrodes was about 1.8-cm; the applied voltage was approximately 5000 V; and water was fed into the capillary at 20 μL/min.

3.7 ELECTROSPRAY USING DIFFERENT SOLVENTS

The theory of electrospray suggests that the surface tension of the solution is important for producing a stable electrospray [117]: it should be low. To explore electrospray in different solvents, a 9.4 $x10^{-3}$ M lithium chloride solution was prepared in the following solvents: n-propyl alcohol, ethanol, water + hexadecyltrimethyl ammonium bromide (a surfactant), water + hydrochloric acid, acetic acid, formic acid, ethanol + water, and ethanol. A continuous and steady red emission (lithium) accompanied by a green emission (carbon) was observed when n-propyl alcohol, acetic acid and, formic acid were used.

Lithium emission from a formic acid solution was optimized by increasing the hydrogen flow rate to 200 mL/min and the voltage to 5000 V. The distance between the two electrodes was increased to 1.8-cm while the nitrogen flow rate was 300 mL/min and sample flow rate 12 µL/min. Using these conditions a very intense red color (not accompanied by green) was observed. The emission appeared even, smooth and stable. When the syringe pump was turned off, the emission disappeared and when it was turned on the signal was observed again. This experiment indicated that formic acid was a good solvent for making a stable electrospray. In this system a relatively high nitrogen flow was used. Therefore, it is worthwhile to explore whether the system is pneumatically assisted electrospray ("ionspray") or not. For this investigation, the linear nitrogen flow velocity in this system and in the ionspray system were compared with each other. Nitrogen flows through a quartz tube (i.d. 2 mm) at 300 mL/min. Therefore, the linear flow velocity

of nitrogen is calculated as:

$$V=r^2\pi v_g$$

where V = nitrogen flow rate; r = radius of the quartz tube ; v_g= linear flow velocity of the nitrogen gas. By substitution of their values, v_g is:

$$300/60=(2/2X10^{-1})^2X3.14Xv_g$$

$$v_g=159.2 \text{ cm/s}$$

Therefore, the linear flow velocity of nitrogen in this system is between 1.6 m/s to a maximum of 2 m/s, while in ionspray it is about 216 m/s [118]. Consequently, the electrospray in this system is not ionspray. However, nitrogen can have an affect on electrospray for the following reasons:

1. An normal flame is used and hydrogen is the flushing gas around the needle. Hydrogen has lower breakdown potential relative to nitrogen and as previously explained, use of nitrogen as a mixing gas improved the electrospray process by decreasing the corona discharge.
2. Nitrogen also removes the heat from the needle tip and prevents the needle tip from clogging.
3. Nitrogen dilutes the fuel and decreases the flame temperature, therefore improves the chemiluminescence reactions

Upon repetition of the above experiment the following general observations were made:

a. Formic acid was a good solvent for making a stable electrospray.

b. To make a stable electrospray in the flame, a clean and sharp needle tip was crucial, i.e. carbon deposits at and around the needle tip caused the electrospray to become unstable.
c. The position of the needle tip in the flame was important: when the distance between the needle tip and outlet of a hydrogen tube was increased, the probability of clogging was also enhanced.
d. Sample flow rates had to be increased or decreased gradually to prevent the sudden introduction of a large quantity of the sample into the capillary which could then create a "clogging" problem.

The capillary tip could be sharpened by using an electropolishing method [119]. The tip of the stainless steel capillary was electropolished from time to time by using the following conditions:

Anode: Sample capillary; Cathode: Lead; Voltage: 6 V; Electropolishing time: 5 min; Electrolyte solution: 60% phosphoric acid (85%), 20% sulphuric acid (98%) and 20% water.

Electropolishing removed a layer of the capillary and made the capillary tip sharper. The electrospray needle tip shape and its radius determine the onset voltage for electrospray and also the electric field at the needle tip [117,120]. The onset voltage is proportional to $(Tr)^{1/2}\ln(4h/r)$, where T is the liquid surface tension,

r is the radius of the needle tip, and h is the distance between the needle tip and a planar counter electrode. After examining the results of the above experiments, electrospray of different solvents containing lithium chloride was investigated. The solvent was considered a good solvent for electrospray if the emission was continuous, even and intense; otherwise, it was considered to be poor. The experiments were conducted using a sample flow rate of about 10 μL/min while the voltage was varied between 3 and 6 kV. The results are explained in Table 3.1.

Table 3.1 The evaluation of different solvents for the electrospray-FPD

Solvent	Electrospray
Pure water; glycerin; polyacrylic acid (100 ppm)	Poor
n-Propanol; 1:1 n-propanol and water; methanol; Ethanol; formic acid; 1:1 formic acid and water; Ethylene glycol; acetonitrile; 0.1% Triton CF-32	Good

Pure water was unsatisfactory. This experiment was repeated but the result was the same. It was possible to observe droplets emerging at the needle tip. Chait and associates [116] were able to make an electrospray of pure water by making the needle tip very sharp. The investigators produced finer droplets by sharpening the needle tip and discovered that the voltage needed for the onset of electrospray for pure water is decreased by making the needle tip sharper. Smith [117] was also able to electrospray pure water by using SF_6 as a highly efficient electron

scavenger [121,122] to prevent corona discharge.

During the introduction of lithium chloride in propanol into the flame, the counter electrode was moved and the lithium emission disappeared. When the electrode was moved back to its original position, the emission appeared again. This experiment shows that, without electrospray, the lithium emission is not observed. Ethylene glycol produced a distinct "smoke of droplets" around the flame. This experiment was also conducted without the flame and the amount of "mist" was less than in the previous case. Lithium emission, however, was not observed. It might be useful to insert a quartz probe tip into the flame to obtain a sample for MS analysis.

Additional trials with sodium chloride (NaCl) in formic acid showed an even sodium emission. Sodium dodecyl sulphate in pure water also produced an even and continuous sodium emission.

3.8 EXAMINATION OF DIFFERENT COUNTER ELECTRODES

The needle voltage is relative to another electrode which is named the counter electrode. The counter electrode is grounded and placed about 2-cm away from the needle tip. The shape of the counter electrode has an effect on the electric field distribution. The voltage power supply, the needle, the counter electrode, and ions between the needle and the counter electrode, originating from the flame and corona discharge, produce a closed circuit. Initially, a copper tube was used as the counter electrode, but its surface oxidized to copper oxide when

the flame touched it, and it became an insulator, a condition incompatible with successful electrospray. An aluminum tube (o.d. 6.3 mm) was examined which did not develop the same problem. Aluminum plates, with or without a hole in the center, were examined but were unsuccessful. It was concluded that a tube was better than a plate as a counter electrode. An aluminum tube was inserted into a hole in an aluminum plate. This also was unsatisfactory and sparking occurred at the union between the aluminum tube and the aluminum plate. A stainless steel tube (o.d. 6.3 mm) was examined and it performed well. Finally, a stainless steel tube (i.d. 3 mm), used as an air tube in the FID, was tested and proved to be superior to the previous arrangements. It was therefore, selected to serve as the counter electrode for the following studies.

3.9 CONSTRUCTION OF A NEW BURNER

To better control of the experimental conditions, a new burner was designed and constructed for use in the aluminum-block detector body (Figure 3.2). Two basic parameters had to be considered. First, the burner should easily connect and disconnect to/from the lower insert port of the block. Second, it should allow the simple insertion or withdrawal of the needle capillary tube (sample). The burner was constructed from five concentric tubes. The tubes from outer to inner were respectively, a 12-cm stainless steel tube (o.d. 6.3 mm), a 14-cm quartz tube (i.d. 2 mm), a Teflon tube (i.d. 0.8 mm, o.d. 1.3 mm), a 25-cm needle (i.d. 0.3 mm o.d. 1 mm), a 30.48-cm sample capillary needle tube (i.d. 0.150 mm, o.d. 0.30 mm).

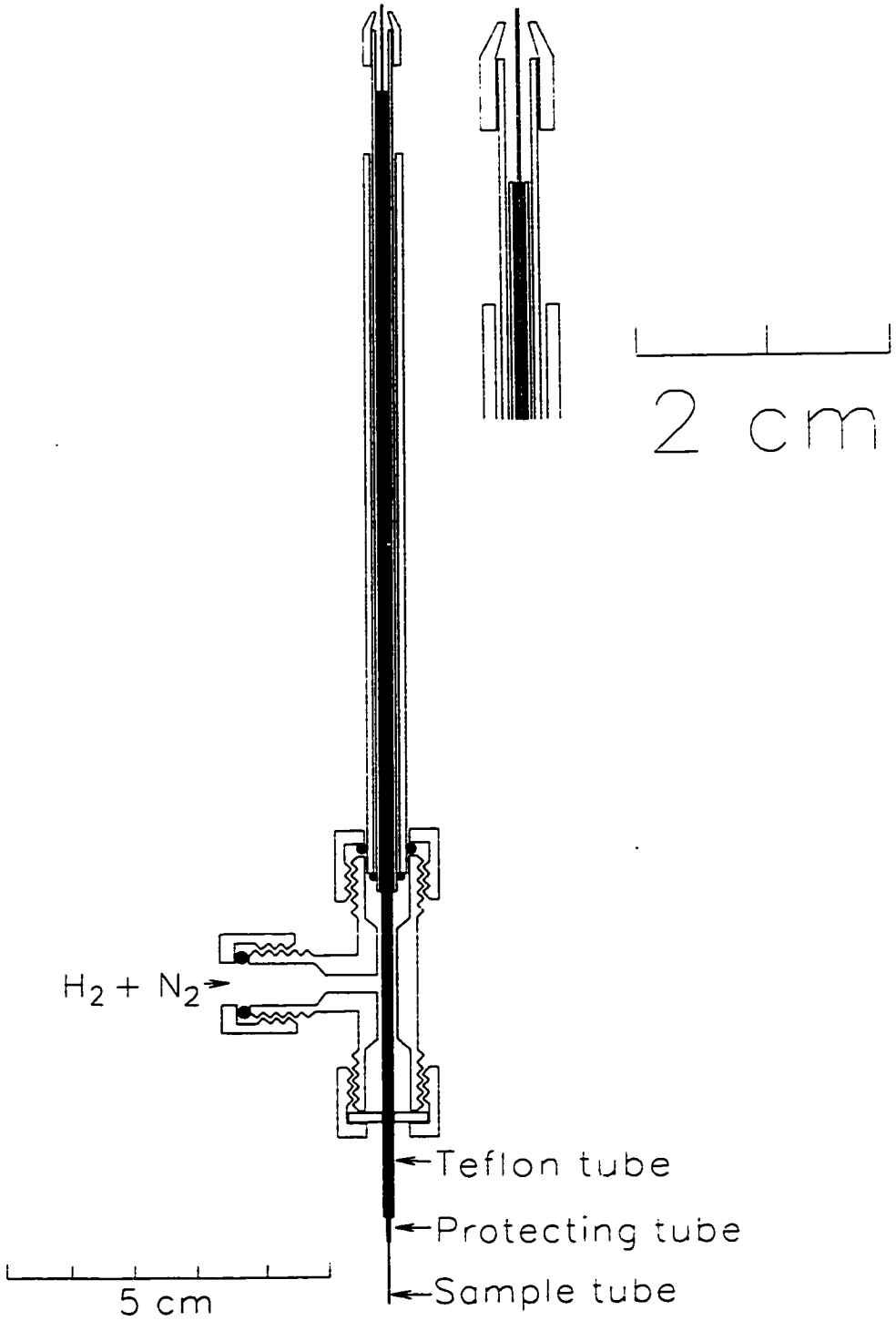

Figure 3.2 Schematic diagram of the burner.

A 14-cm quartz tube was inserted into a 12-cm stainless steel tube so that one end of the quartz tube protruded about 2 mm from the stainless steel tube. They were sealed together with epoxy glue. This stainless steel tube was used to protect the quartz tube and also to connect the burner to the lower insert port of the detector block. In other words, the 12-cm stainless steel tube is the body of the burner and it was connected to a stainless steel union. The Teflon tube was inserted into the stainless steel union and quartz tube to prevent a direct connection between the stainless steel needle capillary tube (which was connected to high voltage) and the union. A 25-cm stainless steel tube was inserted into the Teflon tube and it was used to protect the sample needle and also to connect the high voltage to this tube (because the sample capillary tube can be bent easily). A 30.48-cm sample capillary needle tube (Hamilton Co., 91080 N 730) was inserted into the 25-cm stainless steel tube. A stainless steel cap, 70 mm in length, with one end 2 mm (i.d.) and the other end 3.2 mm (i.d.), was placed on the quartz tube to suppress any background emission.

3.10 SPECTRA OF DIFFERENT ELEMENTS

3.10.1 INTRODUCTION

In atomic or molecular flame emission spectrometry, the first step in confirming analyte response is to obtain a spectrum of the analyte. The source of emission could be dominated by thermal or chemiluminescent reactions, depending on the flame temperature and other characteristics of both flame and analyte.

In FPD as typically used in gas chromatography [46,47], it is known that excitation occurs as a result of chemiluminescent reactions. The efficiency of these reactions is small, yielding a weak signal. Consequently, an interference filter instead of monochromator is usually used as a wavelength selector for measurements. To obtain spectra from various analytes in this type of flame, however, both monochromators and variable interference filters have been used. If the emission is a broad molecular band, the interference filter will yield a spectrum similar to the monochromator but does so at much lower analyte levels. Aue and coworkers [123,124] designed and constructed an FPD which included a rotating variable interference filter (wheel) to obtain spectra from chromatographic peaks. These spectra can be used as a diagnostic tool for compound identification, adding an additional (spectral) dimension to the chromatographic signal.

In this project, the filter wheel was used to obtain spectra of analytes with continuous sample introduction. A schematic diagram of the assembly for electrospray as a sample introduction system and the use of the wheel for obtaining the spectrum are shown in Figures 3.3 and 3.4. Each part will be described separately.

3.10.2 EXPERIMENTAL CONDITIONS

The following is a list of other equipment and experimental conditions used for our experiments. Certain experimental parts were extracted from two recently published papers from Aue and coworkers [123,124].

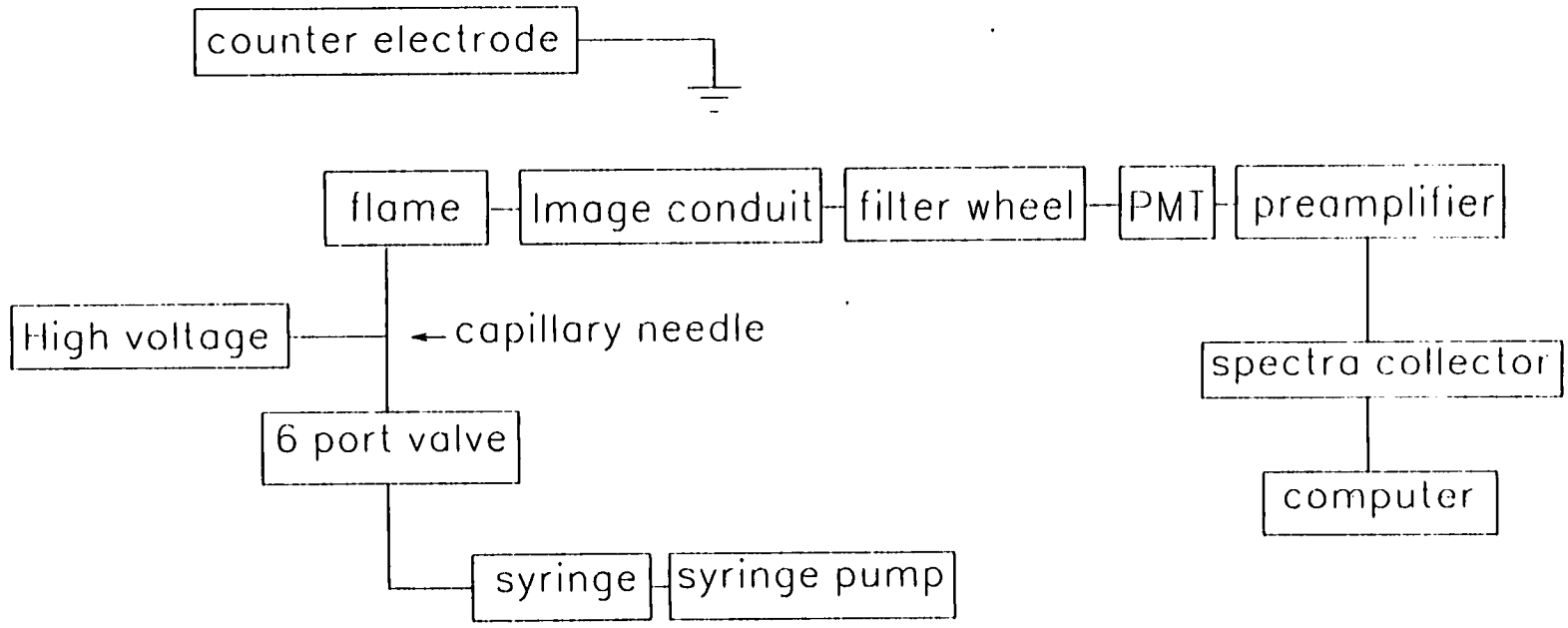

Figure 3.3 Schematic arrangement of modular components used for obtaining spectra by rotating a variable-wavelength interference filter (wheel).

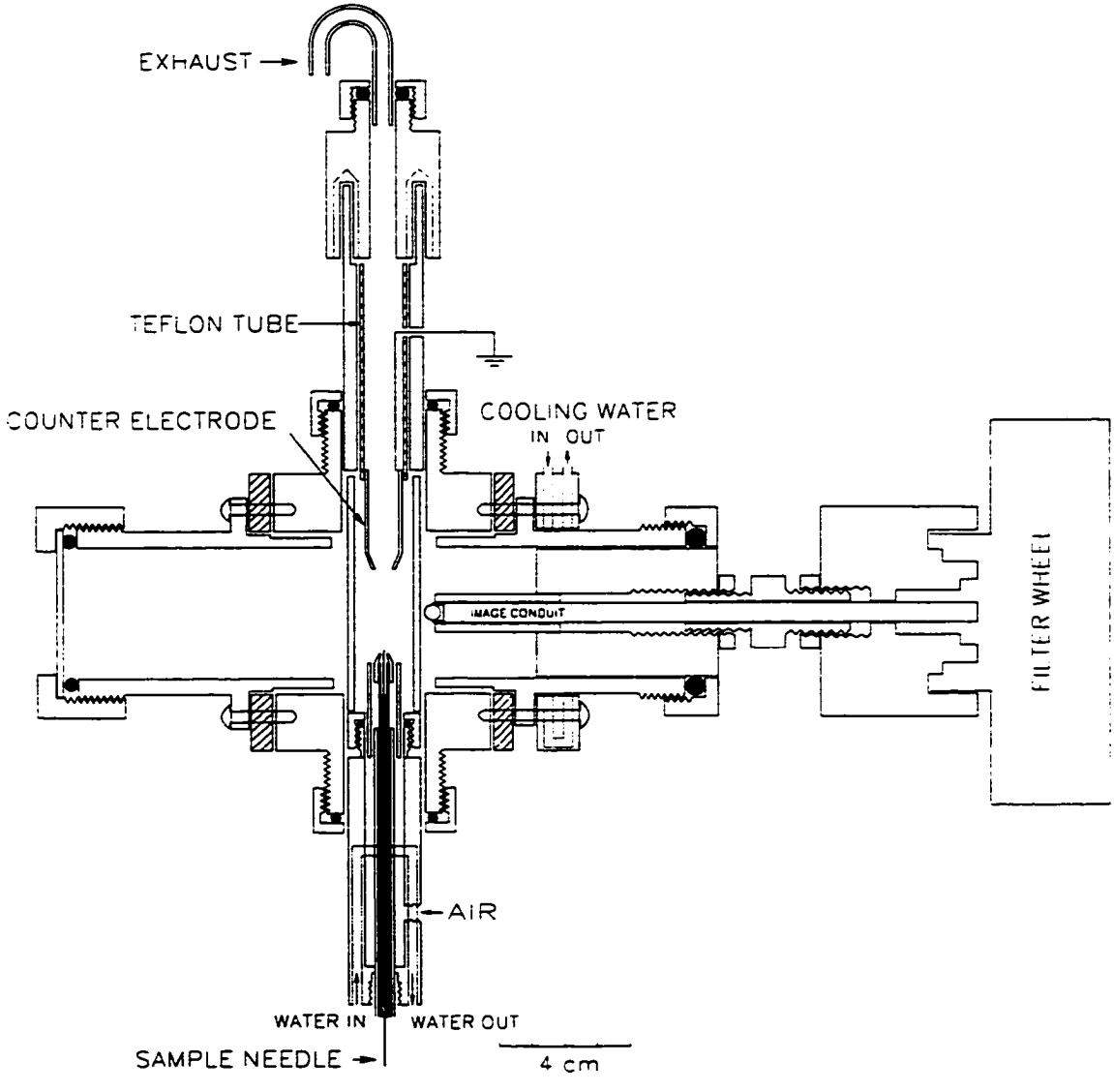

Figure 3.4 The detector and filter wheel.

SAMPLE INJECTION VALVE: A low-pressure sample injection valve (Model 5020, Rheodyne, Cotati, California, U.S.A.) was used to inject 10-12 µL/min samples into the flame.

REAGENT AND TEST SOLUTIONS: The test solution was prepared by dissolving reagent-grade metal ion compounds in deionized water. These solutions were modified by adding a surfactant such as Thorowet. Organic solvents were of analytical grade.

OPTICS: A ball lens of 10-mm diameters (item # 32748, Edmund Scientific Co., Barrington, NJ, USA) was installed in such a way that the lens was situated next to the chimney. The ball lens focused more light into the 15.24-cm glass image conduit (o.d. 0.63 cm) (item # 38307, Edmund Scientific Co., Barrington, N.J. USA). The object/image ratio was one. The light from the image conduit was focused on the rotating variable wavelength interference filter.

ROTATING INTERFERENCE FILTER: The circular variable interference filter rotated in a light-tight casing with 1" diameter entrance and exit ports. The filter wheel (item # 57496, Oriel Corporation, Stratford, CT, USA) was a four-inch diameter disk with a semicircular variable interference filter section. According to Oriel specifications, the filter covered the 400 to 700 nm wavelength range (over 172 degrees at a dispersion of 1.75 nm/degree) with a 17-nm maximum bandpass

and a 15% minimum transmission. The 180-degree opaque section served to balance the wheel for spinning. Data collection was synchronized with the filter rotation via an optical chopper mounted in the filter wheel assembly.

PHOTOMULTIPLIER TUBE: An R-1104 multialkali PMT (Hamamatsu Corporation, Middlesex, N.J, USA) was used for the spectra collector. The gain of the PMT at 1000 V was $2x10^7$ and typical dark current was 5 nA. The PMT channel was cooled by circulating water around the channel.

PREAMPLIFIER: A preamplifier circuit was built by the Chemistry Department's electronic shop. An OP-07 operational amplifier was used for current-to-voltage amplification. The gain was 10^9 V/A and in the circuit there was no analog filter to achieve the temporal resolution necessary for acquiring 100 data points per revolution of the filter wheel.

SPECTRA COLLECTOR: The signal from the PMT, after amplification, was inverted and fed to an analog-to-digital converter circuit which was built by Chemistry Department's electronic shop. The conversion time of the analog to digital converter is about 20 µs. The data collection was synchronized with the filter rotation via an optical chopper mounted in the filter wheel assembly. The spectra collector was designed by first considering the data collection rate (100 data points in 50 milliseconds). The microcontroller's role in the spectra collector was to collect

and sum, i.e., ensemble-average, one hundred digitized data points per scan, in 1.5-second packets of fifteen scans each, for transmission to the host computer (an Intel 486-class central processing unit running at 33 MHz).

SPECTRAL COLLECTION PROGRAMS: The spectra collection program [124] was started or stopped by start/stop buttons. During recordings (about 150 second), the screen showed the number of "samples" (each sample a 1.5-second packet) so far summed and the spectrum so far acquired. After the desired number of samples were obtained, the data were exported as an ASCII format file into a commercial program Sigma Plot (Jandel Scientific, San Rafael, CA, USA) for further data manipulation. Table 3.2 gives the experimental conditions for obtaining spectra of each element by the electrospray-FPD.

3.10.3 SPECTRA OF ELEMENTS

As described in the previous chapter, the detector block had four channels. Although it was possible to measure four elements simultaneously, each of these channels was used for a different purpose. Two channels were used for optical measurements (i.e., one channel for monitoring the analytical signal, and the other channel for such tasks as background correction, response ratio determination, etc). In a further channel, a movable mirror might be placed to focus more light into the wavelength selector, which could be an interference filter or a monochromator. The last channel was used for visually observing the flame. The

Table 3.2 Operating conditions for different elements by the electrospray-FPD

Element	Sample flow rate (μL/min)	Mass flow rate (ng/s)	C (ng/μL)	Air	H_2	N_2	Voltage (V)	PMT voltage (V)
				(mL/min)				
Na	10	15.9	95.4	220	150	330	3200	200
Li	10	21.5	129	230	200	330	4000	210
P (1)	12	61	305	220	220	330	2200	250
P (2)	10	61.7	370.2	250	330	330	2600	350
Cu	15	32.4	129.6	220	180	330	2700	400
Mn (1)	12	22.1	110.5	220	150	330	2500	300
Mn (2)	13	43.3	199.8	220	180	330	3600	380
Mn (3)	10	28.8	172.8	220	180	330	4000	400
Sr	16.2	51.9	192.2	220	180	330	3800	400
Ca	16.2	50.9	188.5	220	190	330	4400	400

C: Concentration; P (1): Triethyl phosphate; P (2): Phosphoric acid;
Mn (1): Methylcyclopentadienyl manganese;
Mn (2): Manganese (II) acetylacetonate in acetylacetone;
Mn (3): Manganese (II) acetylacetonate in propanol.

observation channel was a PMT housing with a glass filter; however, instead of the PMT as a detector, the human eye was used to monitor and also to evaluate flame conditions. This was a very useful channel because any changes in the flame could be readily observed. This channel was also used to obtain optimized conditions. Because the number of variables was relatively large, optimization of these parameters was done by changing each of these one by one and observing the effects they had on the flame and then analysing the emission. When satisfactory conditions were obtained, such as continuous, strong and even analyte emission, the channel was covered with aluminum foil and measurements were initiated. In the future, the simplex method might be used to optimize the variables for obtaining the minimum detection limit.

There were a number of reasons why conditions were favorable for electrospray in this type of flame:

1. The flame temperature was low.
2. The flame was hydrogen rich, and hydrogen was flowing around the needle tip. Because of the high thermal conductivity of hydrogen, heat was removed from the needle tip.
3. Nitrogen was mixed with hydrogen because nitrogen is an inert gas with good thermal capacity. It was a crucial factor in removing heat from the needle tip and producing a stable electrospray.
4. Samples were introduced into a hydrogen-rich atmosphere.
5. When surfactants were used as wetting agents in order to decrease the surface

tension of the solutions, they also helped to prevent the needle from clogging.

3.10.3.1 Spectrum of Sodium

The first spectrum was obtained by introducing sodium dodecyl sulphate (SDS) in aqueous solution into the flame. The atomic line of sodium is shown in Figure 3.5.

3.10.3.2 Spectrum of Lithium

The spectrum of lithium chloride in formic acid is shown in Figure 3.6. The atomic line of the lithium is observed. The atomic emission of lithium was very strong and in all of the electrospray experimental sections it was used to test the different variables that affected the electrospray process.

3.10.3.3 Phosphorus Spectrum

Phosphorus is the only element that other investigators have been testing for the microcolumn LC-FPD [3,16,66]. FPD is a very sensitive detector for phosphorus. In the electrospray-FPD, phosphorus spectra from triethyl phosphate (as a relatively volatile compound) and also phosphoric acid (as a nonvolatile compound) in aqueous solutions were obtained. These are recorded in Figure 3.7 and Figure 3.8, revealing the well known features of the HPO spectrum as conventionally seen in GC-FPD.

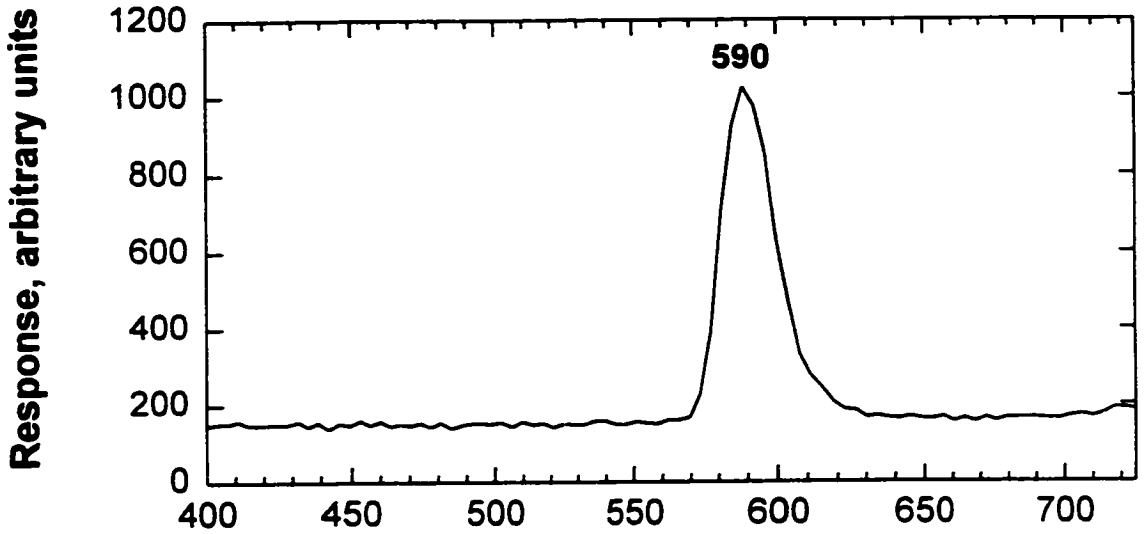

Figure 3.5 Sodium emission from sodium dodecyl sulfate in aqueous solution.

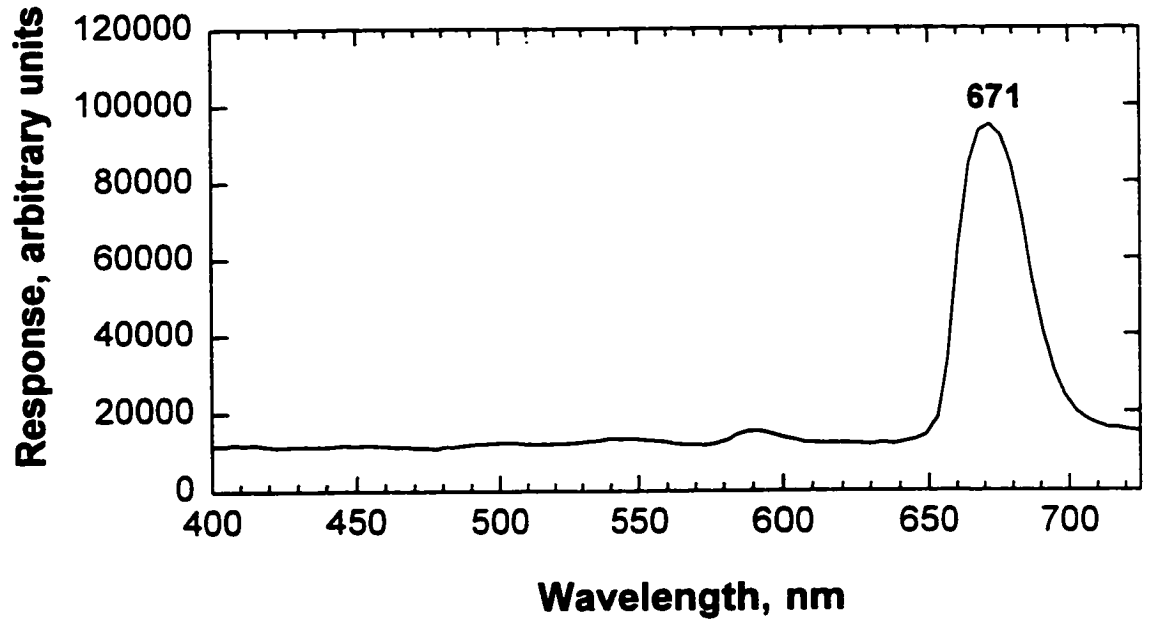

Figure 3.6 Lithium emission from lithium chloride in formic acid solution.

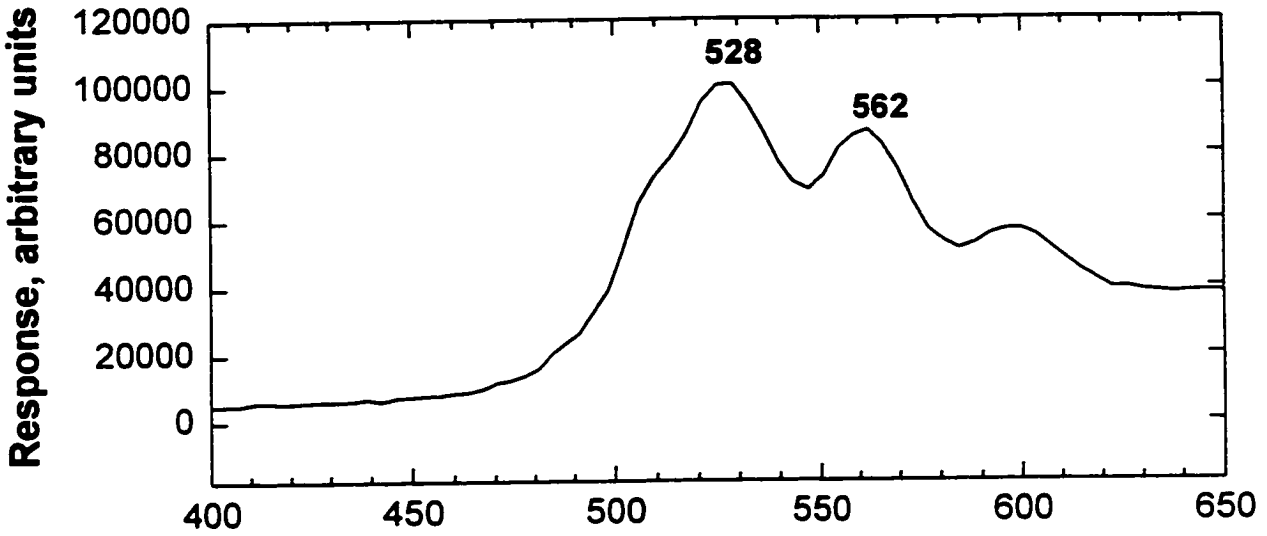

Figure 3.7 Phosphorus molecular band emission obtained from triethyl phosphate in aqueous solution (0.1% Thorowet).

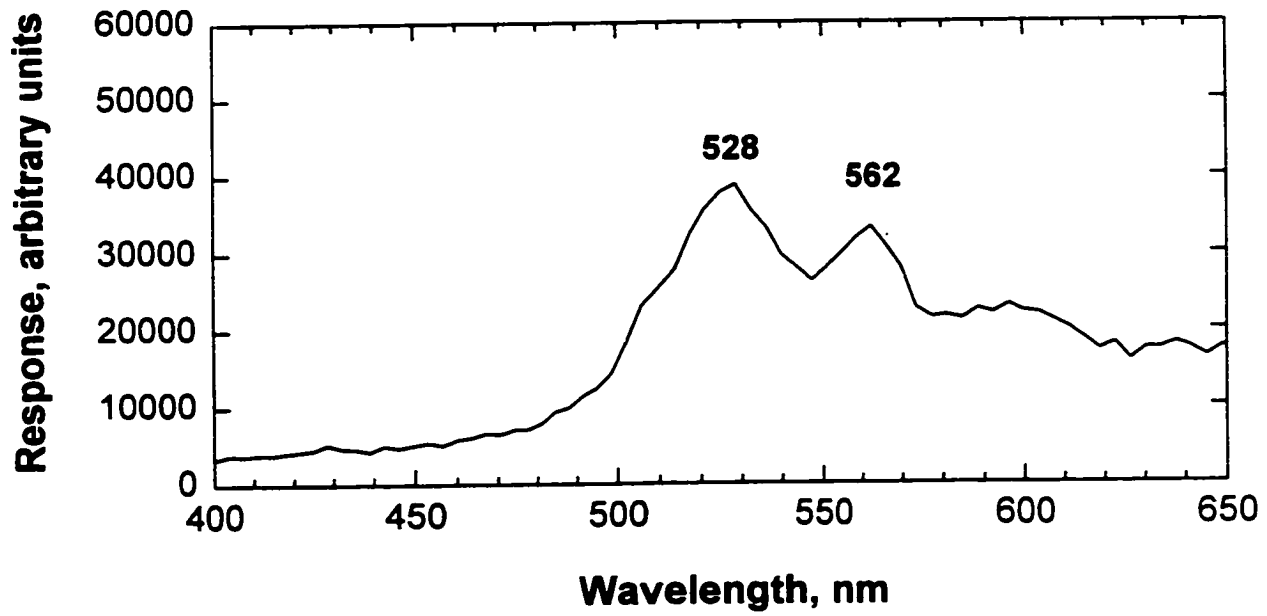

Figure 3.8 Phosphorus molecular band emission obtained from phosphoric acid in aqueous solution (0.1% Thorowet).

3.10.3.4 Spectrum of Copper Chloride

An aqueous copper chloride solution was prepared using 0.1% Thorowet, a nonionic surfactant with a special non-foaming property. Spectra of both test solution and the blank are illustrated in Figure 3.9. Based on data compiled by Pearse and Gaydon [125], CuOH has a strong diffuse band from 535-555 nm and a weaker band from 615-625 nm. The features in the copper chloride spectrum agree well with these values and consequently are assigned to CuOH. Alkemade and Hermann suggested that the chemiluminescent excitation of the CuH and CuOH bands is due to the following reaction [126]:

$$Cu + (O)\,H + X \longrightarrow Cu\,(OH)\,H^* + X$$

where X is a stable flame molecule (N_2, H_2O) that stabilises the recombination of the radicals through (partial) energy transfer.

In subsequent chapters, the mass detection limit of copper and other elements tested using electrospray-FPD will be compared with ICP as one of the best elemental analysis techniques. The potential of electrospray as a sample introduction technique will be clearly demonstrated.

3.10.3.5 Manganese Spectrum

The luminescence spectrum of methylcyclopentadienyl manganese tricarbonyl (MMT) is shown in Figure 3.10. The emission at 403 nm corresponds to the two strongest lines of atomic manganese, found at 403.076 and 403.307 nm (also to the strong line at 403.449) [127]. At 540 nm, another line of

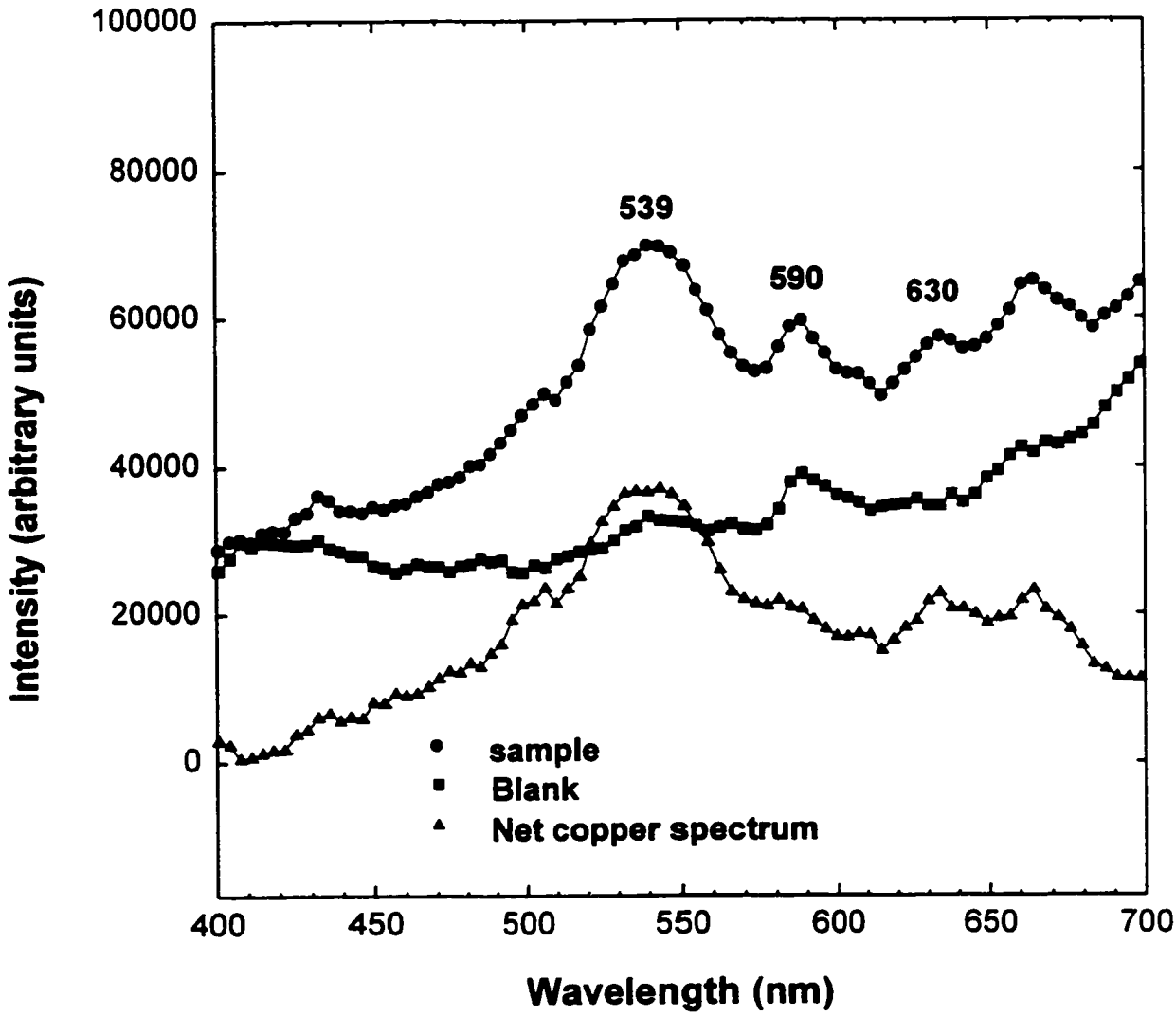

Figure 3.9 Copper molecular band emission obtained from copper chloride in aqueous solution (0.1% Thorowet).

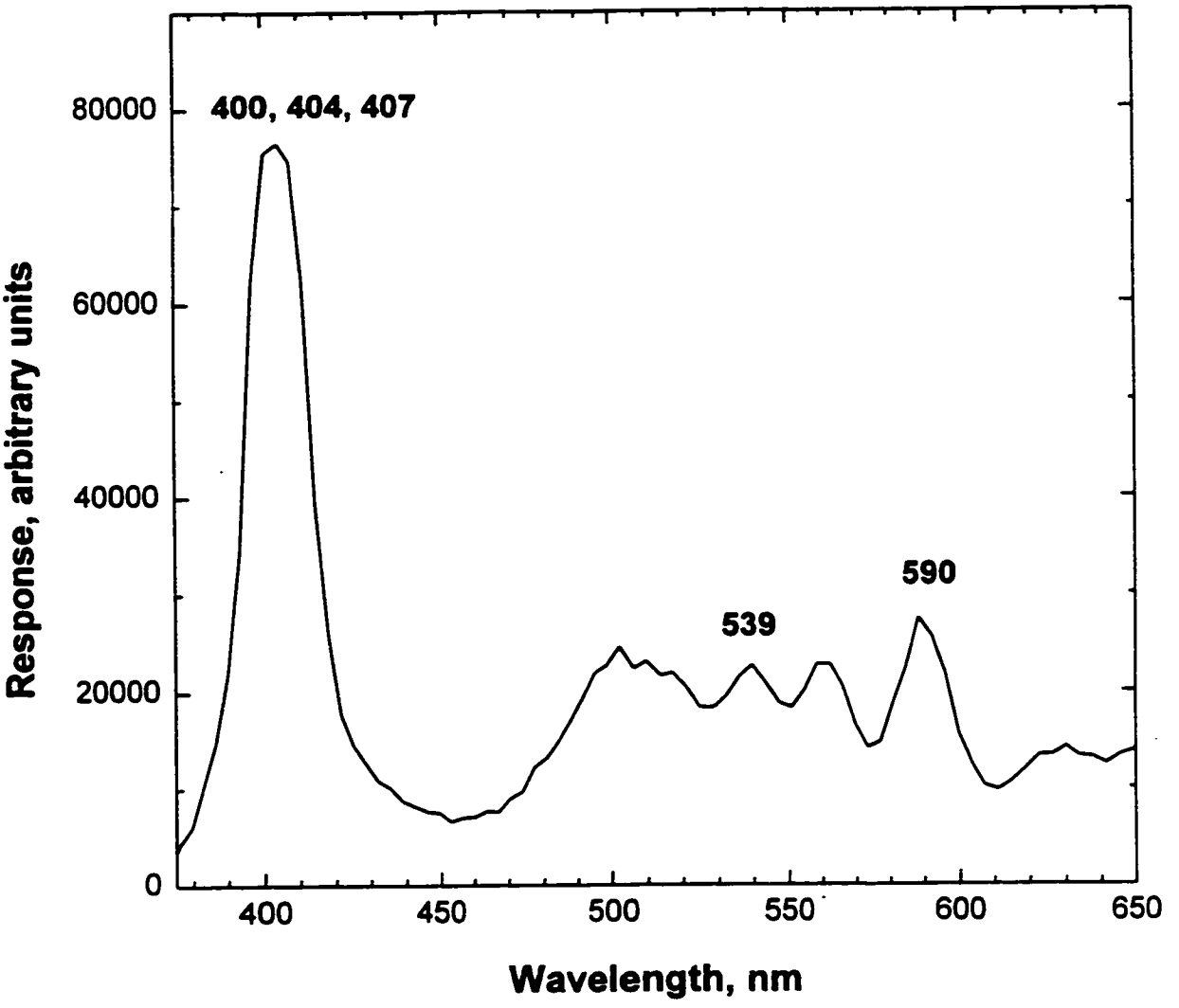

Figure 3.10 Emission obtained from methylcyclopentadienyl manganese tricarbonyl in aqueous solution (0.1% Thorowet).

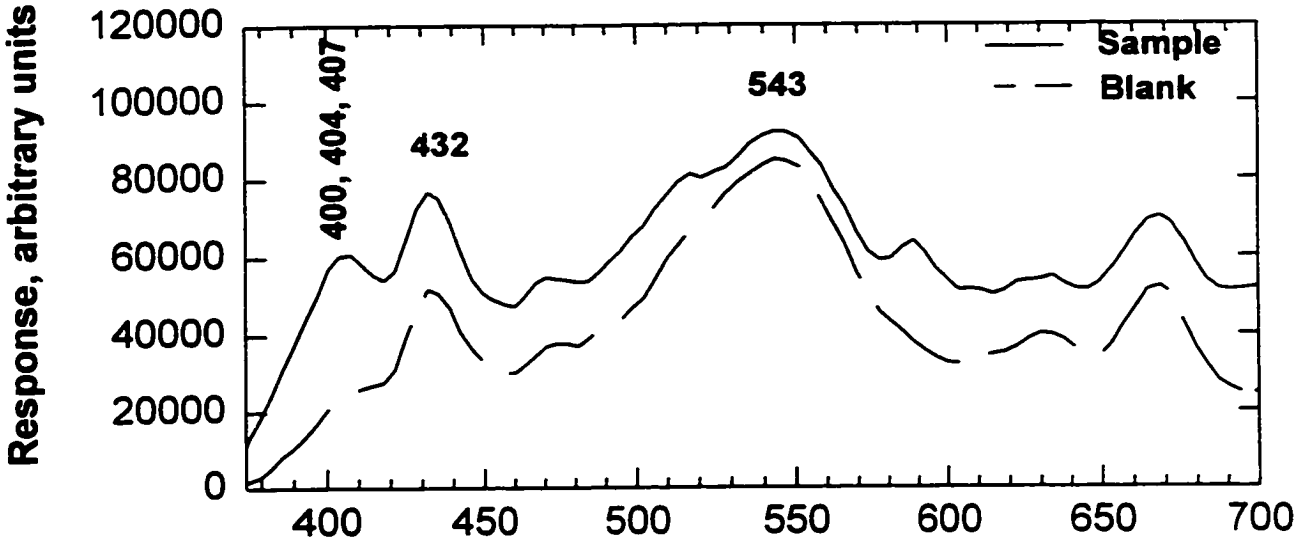

Figure 3.11 Emission obtained from manganese (II) acetylacetonate in acetylacetone.

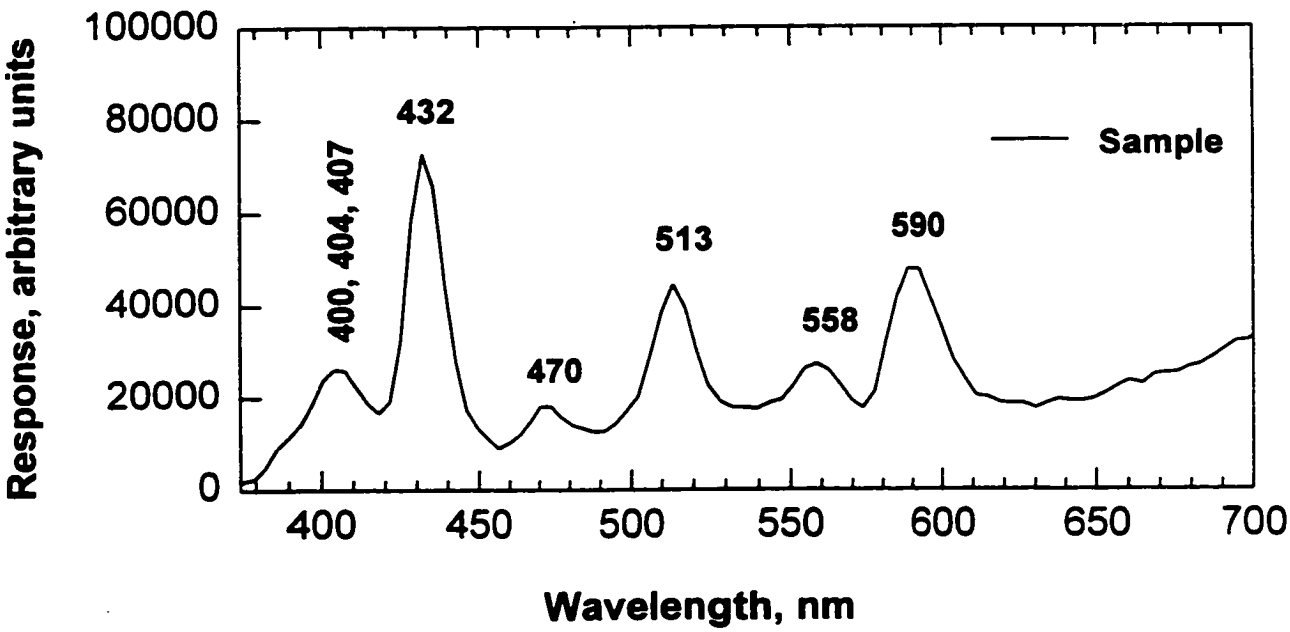

Figure 3.12 Emission obtained from manganese (II) acetylacetonate in n-propanol.

manganese appeared. The spectrum of MMT, a volatile compound, has been previously determined in GC-FPD (63). A manganese spectrum from manganese (II) acetylacetonate in acetylacetone and the blank solution (acetylacetone) were obtained and are shown in Figure 3.11. The spectrum of manganese acetylacetonate in n-propanol is shown in Figure 3.12. Manganese emission is observed at 403 nm along with strong carbon emission (C_2). The electrospray-FPD technique has a very good sensitivity for manganese. This good sensitivity will be shown in the following chapters, where the mass detection limit of manganese from manganese chloride solution (i.e., from a non-volatile analyte) will be reported.

3.10.3.6 Strontium spectrum

The spectrum of strontium is shown in Figure 3.13. The sodium emission in the spectrum originates from distilled water or contamination. James and Sugden [128] studied the source of the emission of strontium in different gas compositions of hydrogen, oxygen and nitrogen flames and confirmed that strontium emission at 600-610 nm and 685-690 nm belonged to SrOH. Alkemade and Hermann [126] reported SrOH band wavelengths and Pungor and Hegedus [129] showed that Sr produced a molecular band emission with the maximum at 670 nm, a wavelength that is in good agreement with the illustrated spectrum.

3.10.3.7 Calcium spectrum

The calcium spectrum is shown in Figure 3.14. Based on Pearse and

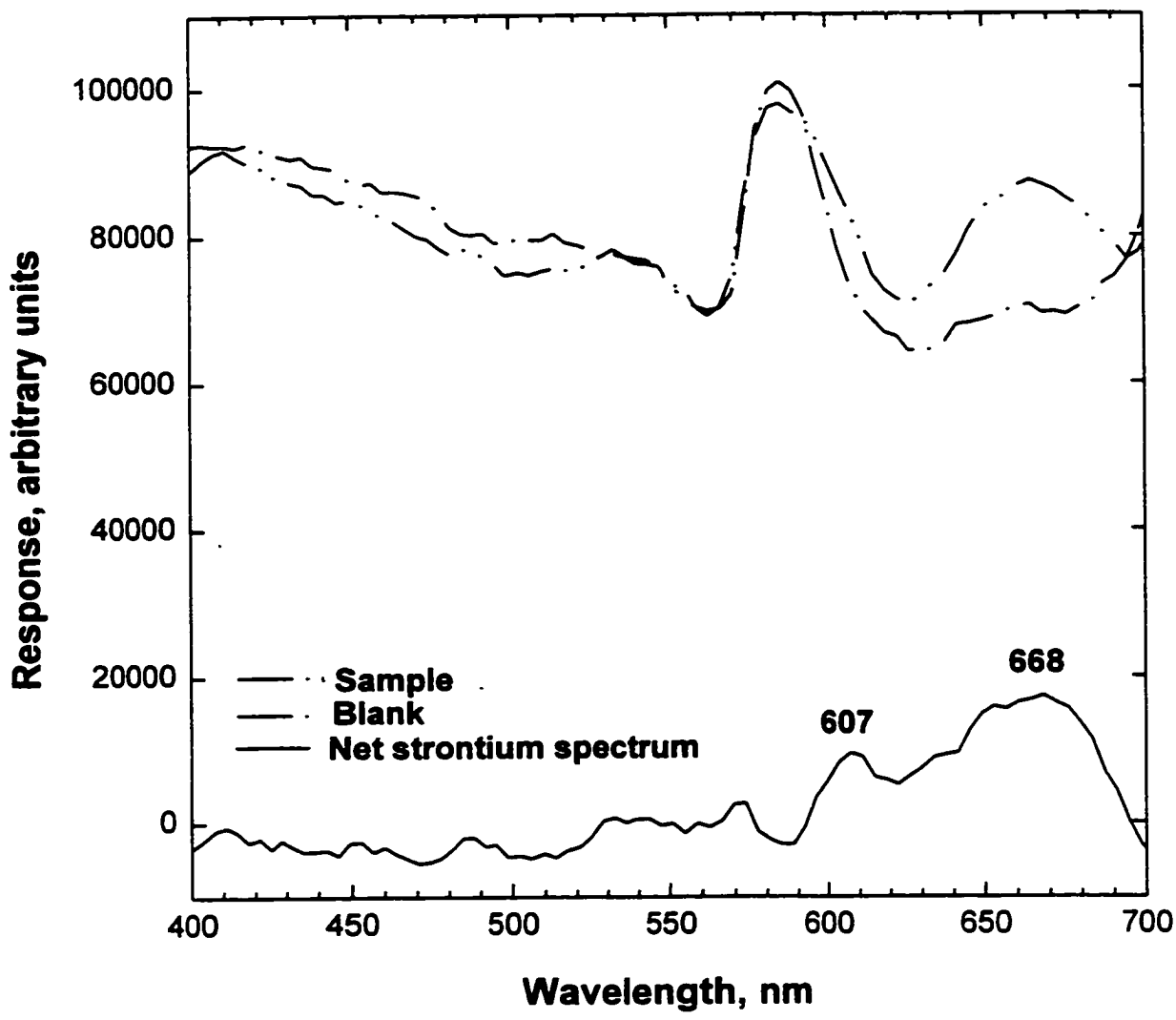

Figure 3.13 Strontium molecular band emission obtained from strontium chloride in formic acid solution.

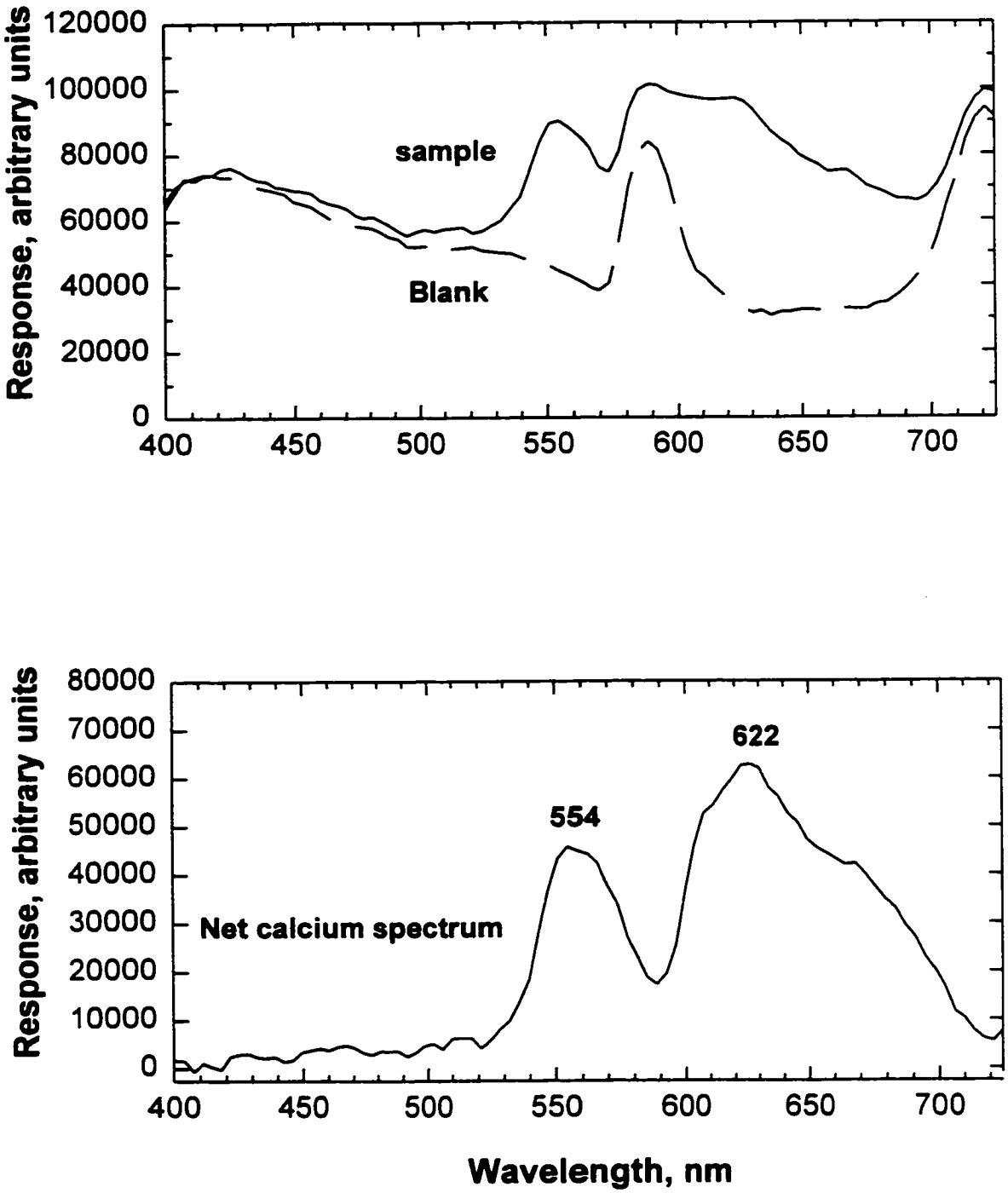

Figure 3.14 Calcium molecular band emission obtained from calcium chloride in formic acid solution.

Gaydon [125], CaOH has a green band in the region 553-557 nm, and an orange-red band which is very diffuse and has a maximum at 623 nm; these are accompanied by a much weaker diffuse band at 603.8- 641.5 nm. These bands correspond to the features of the present spectrum; consequently, the molecular band emission probably originates from CaOH molecules. Pungor and Hegedus [129] also showed that calcium had molecular band emissions at 554 and 624 nm. These wavelengths again correspond to the given calcium chloride spectrum.

3.11 CONCLUSIONS

The experimental results of this chapter are:

1. The detector and the burner were constructed and the experimental conditions for the optimum performance of the electrospray-FPD were established.
2. The application of different solvents for electrospray-FPD was investigated. Aqueous solution with SDS as a modifier was able to produce an even and stable electrospray. This result was used later for the electrospray of aqueous solutions.
3. The spectra of the elements Na, Li, Mn, Ca, Sr, Cu and P were determined. This suggested that electrospray-FPD has potential as a sample introduction device for the FPD. The exploration of spectra for other elements and determination of detection limit, calibration curve and dynamic range for some elements are the next step for further investigation of the potential of electrospray-FPD.

4. Electrospray as a sample introduction technique has a special advantage for FPD because the flame temperature is low and eletrospray provides a gas phase of the analyte without the necessity of resorting to a high flame temperature or other techniques for sample evaporation.
5. Electrospray-FPD does not have clogging problems.

Chapter 4

NOISE IN THE ELECTROSPRAY FLAME PHOTOMETRIC DETECTOR

4.1 INTRODUCTION

In this chapter the noise power spectrum (NPS) is used as a diagnostic tool to determine the frequencies of the noise on the signal and the limiting form of noise in the system. Noise is any component of a signal which impedes observation, detection or utilization of the information that the signal is carrying [130,131]. The magnitude of noise affects precision, and detection limit in a chemical analysis [132]. Noise can be divided into two categories [133]: cyclic and random noise. Cyclic noise is any kind of interference noise which repeats itself through each experimental cycle. Examples of random noise are white noise and flicker noise. Sources of noise include shot noise and Johnson noise. In spectroscopy, shot noise originates from the random arrival of photons at the PMT. Shot noise follows a Poisson distribution and is therefore proportional to the square root of the signal strength [134]. In some systems shot noise is the dominant noise. Examples include noise found in measurements of light intensity in the FPD, or noise originated from changing the number of the β particles in the ECD [135,136]. Flicker noise, which originates from the relatively slow drift in the instrumental components [132] and the introduction of droplets by the nebulizer [110,111,112], has a magnitude that is inversely related to noise frequency, and is proportional

to the signal strength. It causes the signal to noise ratio (noise on the signal) to be independent of the signal strength (e.g., the noise of the signal using direct current plasma techniques [137]). Random noise is measured by the standard deviation or peak-to-peak fluctuation; two measurements that can be converted into each other by using a factor that depends on the time constant of the analog filter [135]. Normally noise is measured on the signal and on the blank. In spectroscopy, noise on the signal is related to precision and detection limit [132]. It is the noise on the signal (or on the blank near the detection limit) that should be considered when evaluating experimental variables in a system and the signal intensity to background intensity ratio (sometimes used in spectroscopy) may be a misleading value. However, if the limiting noise in a system is related to the spectral background, then the noise of the blank can be used [138]. The noise of the blank in spectroscopy or chromatography is used to calculate the detection limit. For example, the noise of a blank solution in LC-FPD or the noise of the flame alone in GC- FPD is used in determining the detection limit. All efforts to deal with noise are designed to decrease noise and/or increase signal intensity. In other words, the aim is to enhance the S/N. To do this, information about noise, the identification of some sources of noise (if that is possible), the definition of the "limiting" noise in a system, and the application of some remedies based on controlling and reducing this limiting noise is essential.

The noise power spectrum (NPS) is a powerful diagnostic tool for obtaining information about noise and noise frequencies in a system [137,139]. The noise

power spectrum can be used to determine the limiting noise in a system, to investigate the effects of different experimental variables, to choose conditions under which the system has less noise, and finally to select suitable hardware devices or data processing software for enhancing the S/N to obtain a better detection limit. There are a variety of hardware and software methods to enhance a signal to noise ratio [140,141]. These techniques should be selected based on limiting noise in the system. In other words, modifications made to the system, or application of the different types of data manipulation, are dependent upon defining the limiting noise of the system. For example, GC-FPD is a shot-noise limited system [136], therefore in this system enhanced light gathering or increased integration time improve the S/N and hence the detection limit. However, when a system is flicker-noise limited, this remedy is not useful. Shot noise is proportional to the square root of the light intensity or the integration time, and flicker noise is proportional to the integration time or light intensity. Signal in any case is proportional to the light intensity or integration time. Therefore, S/N enhancement is proportional to the root square of the light intensity or integration time when the system is shot noise limited, and there is no enhancement when the system is flicker noise limited. This result can be explained in another form based on the frequency bandwidth changes of the system with integration time. Root mean square (rms) of the noise current when the system is shot noise limited (i_N) and flicker noise limited (i_F) are [142]:

$$i_N = [2ei\Delta f]^{1/2}$$

$$i_F = [Ki^{\alpha}\Delta f/f^{\beta}]^{1/2}$$

where i_N is the rms shot noise current; e is the electron charge, i is the average current; Δf is the frequency bandwidth of the system; i_F is the rms flicker current; α and β are approximately 2 and 1; f is the average noise frequency. Δf is inversely proportional to the integration time; consequently, when the system is shot noise limited, Δf decreases by integration. However, when system is flicker noise limited, the noise is proportional to the root mean square of $\Delta f/f$ where Δf and f are dependent variables. When Δf decreases, f is also reduced because f must fall within the Δf. Therefore, increasing the integration time or reducing the frequency bandwidth of the system does not improve S/N ratio when system is flicker noise limited.

Coping with flicker-noise is not simple, especially when the signal is in the low frequency ranges. This is because the amount of the flicker noise is inversely proportional to the frequency of the noise. There are several methods to deal with flicker noise. One of them is to change the frequency of the signal, provided that the noise frequency does not change. In other words, signal modulation should occur before the noise adds to the system [134]. For example, modulation of light from/through the flame (by using a chopper) will change the signal and the noise frequencies simultaneously; therefore, it cannot be used as a method to reduce noise sources in the flame. However, it can be used to diminish the dark current. A second method is to change some experimental conditions or some equipment function and investigate the effect of these changes on the noise. Hopefully it can

then be determined which experimental condition favours minimal noise and hence provides the best detection limit [132]. This method has been applied to investigate the effects of different variables on the noise of the plasma [132].

Sample modulation is another technique to enhance S/N ratio when the system is flicker noise limited [143]. This technique was implemented for flame photometry to decrease background flame emission. Another method, introduced by Winefordner and co-workers [144], suggests that, in the case of multiplicative noise, two channels can be used. The signal and the reference channel were monitored simultaneously and the ratio of these two channels was used to calculate the detection limit. This method was applied by Karnicky [16] in LC-FPD to reduce flicker noise arising from fluctuations in the nebulizing efficiency of the ultrasonic nebulizer. The authors claim this approach improved the detection limit by a factor of five.

Cyclic noise is another kind of the noise which is a systematic noise [133]. Based on this definition it can be inferred that any spectral, physical, chemical and instrumental interferences which repeat themselves in a cyclic manner are cyclic noise. In addition to chemical, physical, and instrumental methods exist to cope with cyclic noise, there are also mathematical tools to cope with cyclic noise such as partial least squares [145]. In our system, the cyclic noise was observed and the application of ratioing two signals (analytical/reference) to decrease this interference noise is demonstrated. In the following, the procedures to obtain the noise power spectrum (NPS) for different sampling frequencies of a single channel

and a ratio channel will be described, and an application of a dual channel method to enhance the S/N ratio and also reduce interference noise is discussed.

4.2 GENERAL NOISE POWER SPECTRUM FEATURES FOR FLAME EMISSION FROM AN ELECTROSPRAYED SODIUM DODECYL SULPHATE SOLUTION

The first experiment was conducted to obtain the noise power spectrum of 5.19-mM sodium dodecyl sulphate (using noise on the signal). In this experiment, the same module components, as shown previously in Figure 3.3, were used. The sodium emission was monitored with a 600-nm interference filter and the filter wheel-PMT setup was used in the data acquisition system. There was no analog filter in the circuit and the time constant of the fast amplifier was 1 ms. The main difference between this experiment and the earlier experiment is that in this experiment the data were collected at 600 nm. In the earlier experiment, the filter wheel was scanned to collect a spectrum. The procedure can be summarised as follows:

a. The spectra collector was triggered to obtain 100 data points from the same wavelength (600 nm). This procedure was repeated automatically 15 times to obtain ensemble averaging of the cycles. The collected data were saved and considered to represent one sample. The data were acquired over 1.5 seconds for each sample.
b. Forty samples were collected. In this experiment, 100 data points were acquired during 50 ms. Therefore, the sampling frequency was 2000 Hz with a resolution

of 1000/50 or 20 Hz.

4.2.1 Calculation of the noise power spectrum

After the data were obtained, NPS calculations were performed by using a 00method described by Hieftje and co-workers [137]. An algorithm was written using MATLAB 4.0 (The Math Works Inc., Natick, MA) for fast Fourier transformation (fft) calculations. First, the mean value was calculated for every sample, and this value was subtracted from every point in the same sample. With this method, the DC part of the signal was eliminated. Then the Fourier transform of each sample was calculated. These calculations were repeated for all 40 samples. Finally, the average NPS was calculated for 40 samples in the frequency domain and the NPS shown in the Figure 4.1 was plotted from zero to 1000 Hz with 50 points. This NPS demonstrates that the system is flicker noise limited because the noise power at the low frequencies dominates the spectrum.

4.3 NOISE POWER SPECTRUM OF SODIUM CHLORIDE IN FORMIC ACID

With the filter wheel and its data acquisition equipment, it was not possible to decrease the sampling frequency or increase the number of data points in order to increase resolution. To obtain the NPS at lower sampling frequencies, a digital oscilloscope (Tektronix Model 2232, Beaverton, OR) in the sampling mode was used as a data acquisition system, and a sampling frequency of 200 Hz was

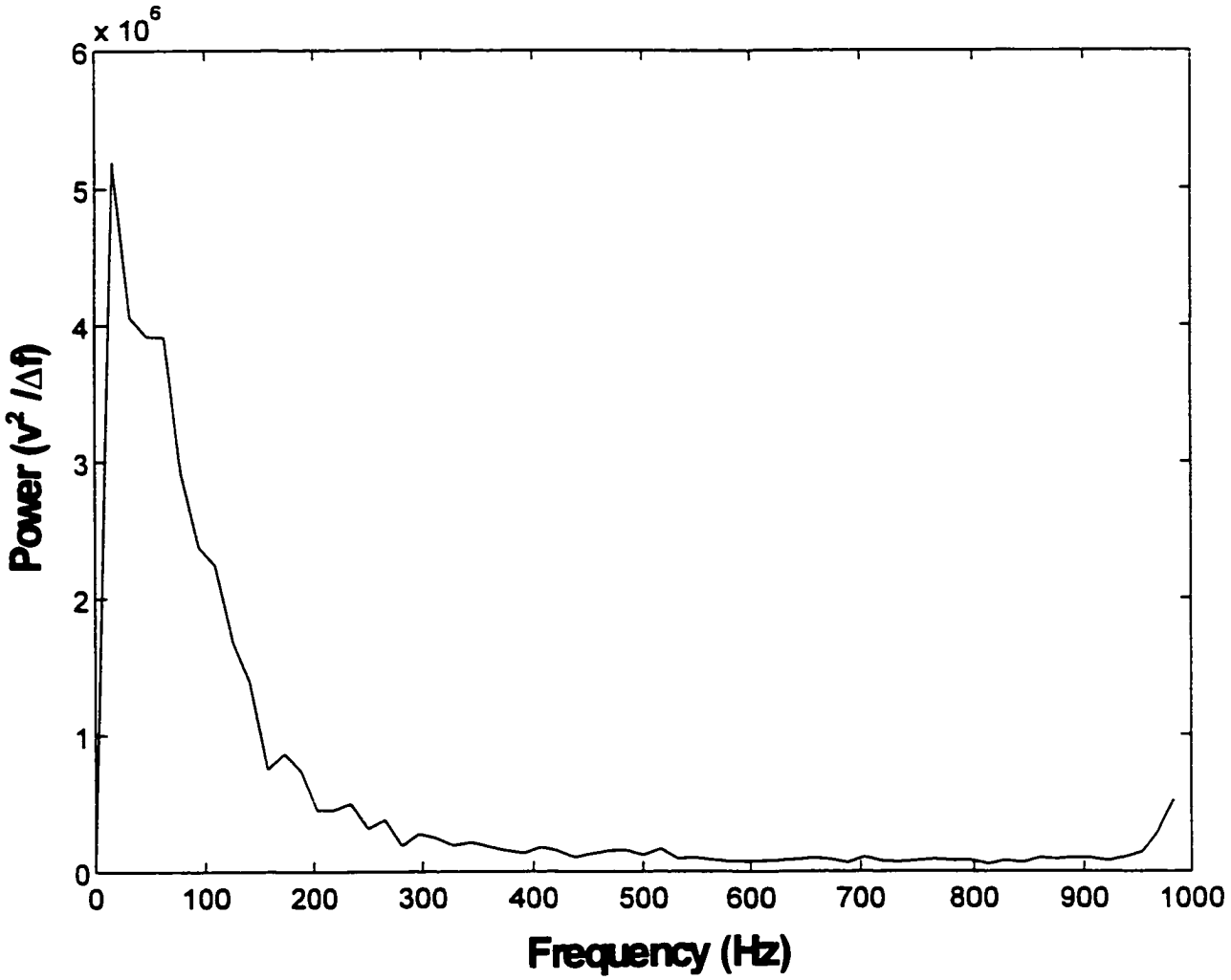

Figure 4.1 Noise power spectrum from sodium emission (SDS) in aqueous solution. Hydrogen: 200 mL/min; Air: 230 mL/min; Nitrogen: 330 mL/min; Voltage: 3500 V; Interference filter: 600 nm WB; PMT: R-1104; Sample flow rate: 35.8 ng Na/s. For other conditions see the text.

selected. In this experiment, 1000 data points were acquired for each data set, resulting in a noise spectrum containing 500 points. Therefore, the resolution was 100/500 = 0.2 Hz. In order to prevent aliasing (the effects of higher frequency masquerading on those of lower frequency), an analog filter with a 0.0125 second time constant was used before the analog signal was converted to digital format. After data were collected (by the oscilloscope), the stored data were exported to an ASCII file using a written program by Dr. Wentzell [146]. Time domain noise and frequency domain noise during the introduction of sodium chloride in formic acid are shown in Figures 4.2 and 4.3. The NPS of sodium emission shows a large contribution at low frequencies (< 0.4 Hz), indicative of drift.

4.4 NOISE POWER SPECTRUM OF THE ANALYTICAL SIGNAL AND OF THE RATIO ANALYTICAL SIGNAL / REFERENCE SIGNAL

The objective of this experiment was to compare the analog signal and the NPS of lithium emission (the analytical signal) in a single channel and also in the ratio of two channels (the analytical signal over the reference signal). The signal channel monitored emission of lithium, the reference channel that of potassium.

4.4.1 Experimental conditions

A 0.125-m monochromator (model 77250 Oriel, Stratford, C. T., U.S.A.) with a 1200 groves/mm ruled grating and 0.02 to 3.2 mm variable slits was used to monitor the lithium resonance line at 670.8 nm. A-765 nm interference was

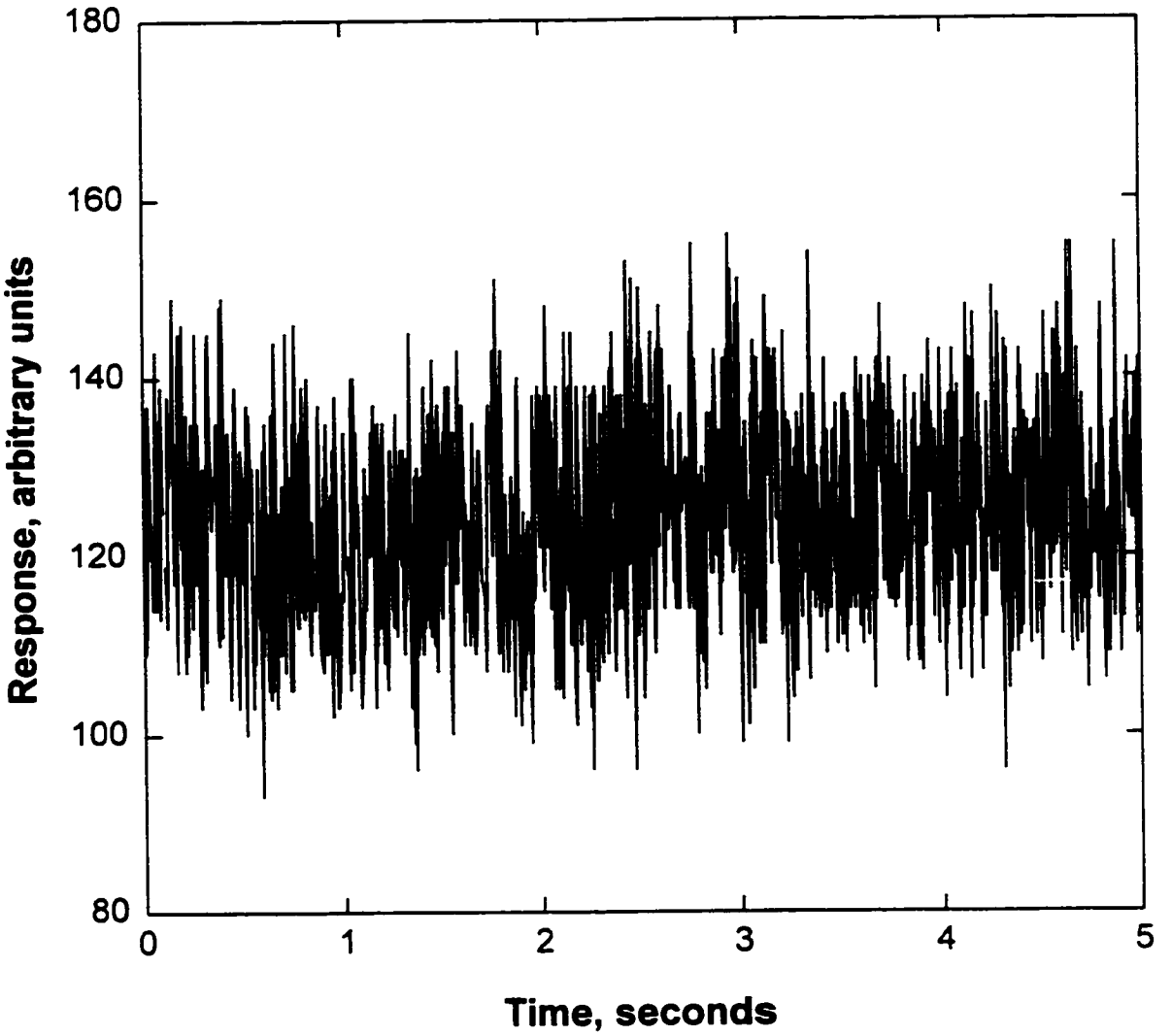

Figure 4.2 Noise of the signal (sodium emission) from sodium chloride in formic acid solution; Hydrogen: 200 mL/min; Air: 230 mL/min; Nitrogen: 330 mL/min; Voltage: 4000 V; Interference filter: 600 nm; PMT: R-268; Sample flow rate: 17.6 ng Na/s.

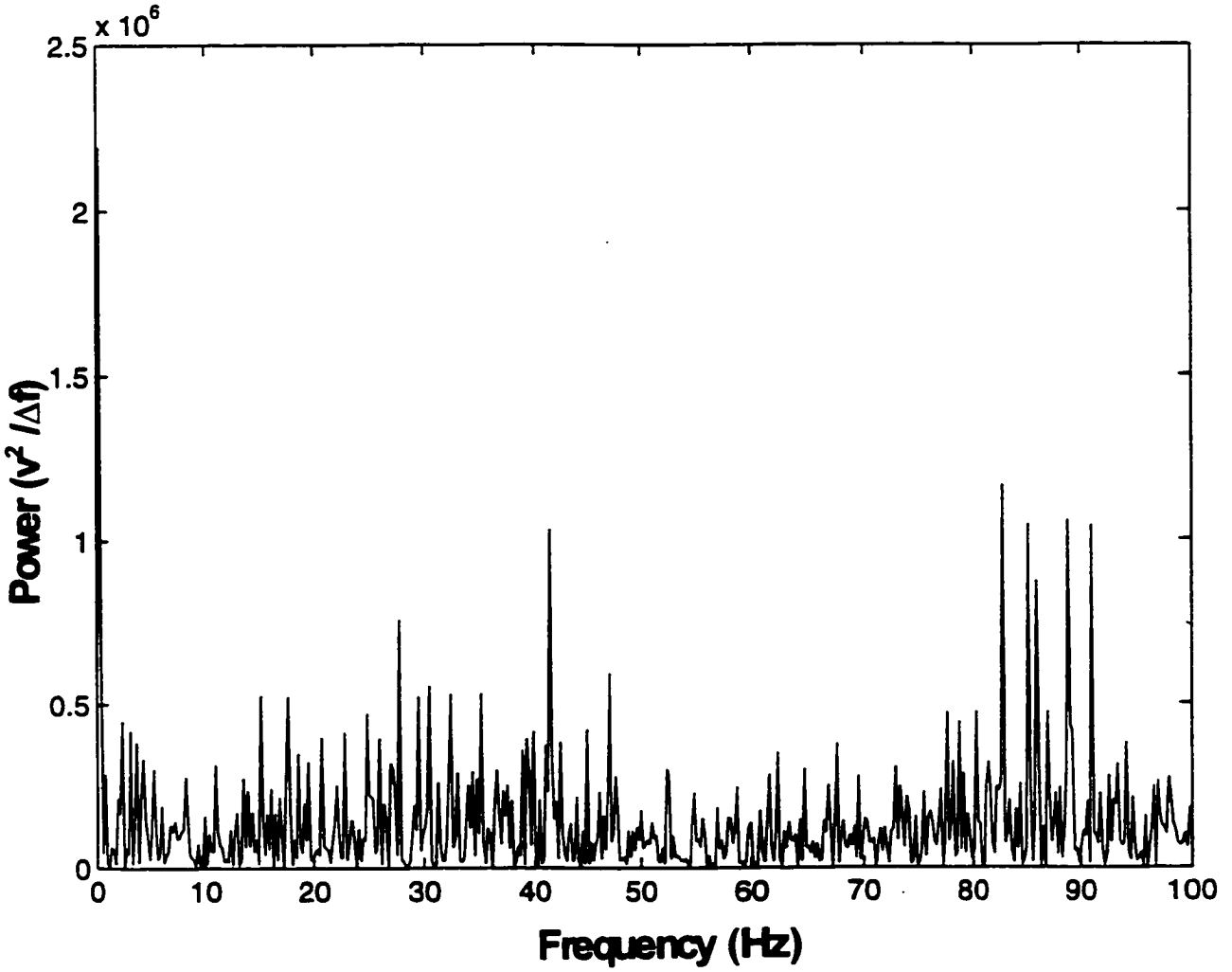

Figure 4.3 Noise power spectrum of the sodium emission signal shown in Figure 4.2.

used as a wavelength selector for recording the potassium emission. The data acquisition system differed from that of previous experiments. For each channel, the output of the PMT was connected to the electrometer which was connected to a simple RC filter to filter, prior to sampling, frequencies above 5 Hz. The analog detector output signal was then converted to a digital value. A voltage to frequency converter was used to transform the signal to a digital pulse train, and a counter accumulated these pulses over 0.1 second intervals. A full scale input signal could produce a digital count value of 16000 [47]. In this experiment, 6649 data points were acquired for one scan. Therefore, the resolution for the NPS was 5/6649 = $7.51X10^{-4}$ Hz. Other modular components were described previously. The operating conditions for the experiment were:

Hydrogen: 200 mL/min; Air: 230 mL/min; Nitrogen: 330 mL/min; Voltage: 5100 V; 1/8 meter grating monochromator with R-374 PMT for monitoring Li; 765 nm interference filter with R-374 PMT for monitoring K; Li sample flow rate: 23.7 ng Li/s; K sample flow rate: 27.6 ng K/s; Solution flow rate: 11 µL/min.

4.4.2 Results and discussion

Lithium and potassium signals and the ratio of the two, are shown in Figure 4.4. The NPS for lithium and potassium emissions and for the ratio of lithium over potassium emission were calculated and the results are shown in Figures 4.5, 4.6 and 4.7. In this case, the NPS of lithium shows an interference frequency (cyclic) noise with its frequency harmonics. The same frequency noise is also observed

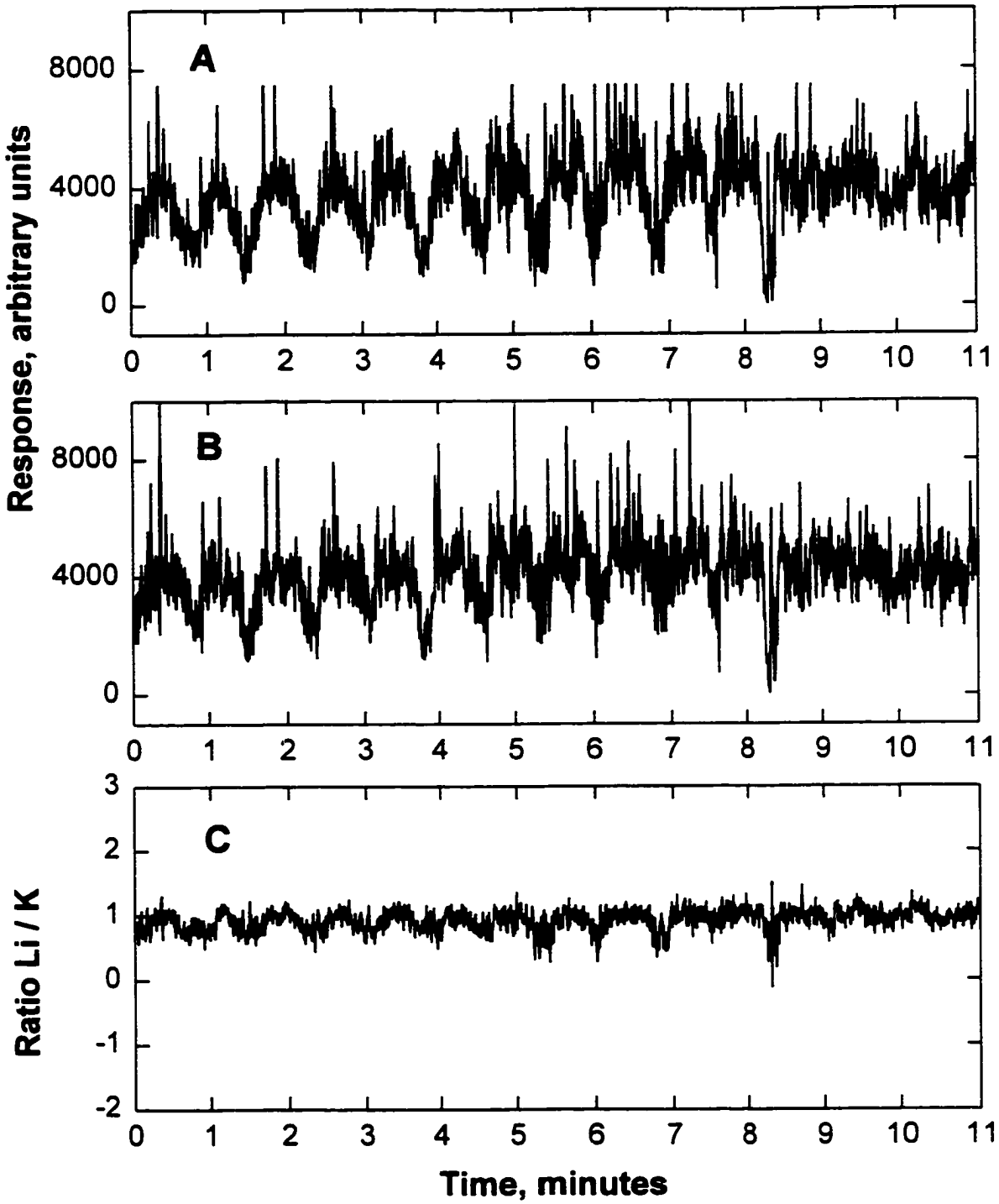

Figure 4.4 a: Lithium emission at 670 nm; b: Potassium emission at 767 nm; c: Ratio Li/k. Experimental conditions are in the text.

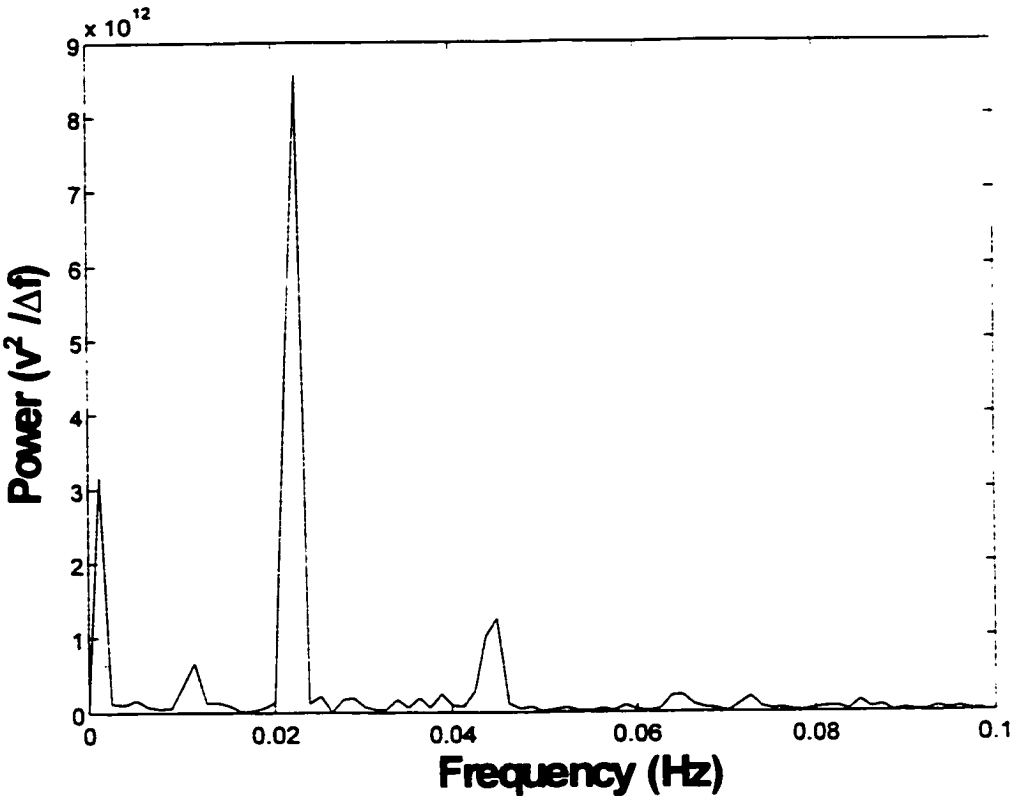

Figure 4.5 Noise power spectrum of the lithium emission signal shown in Figure 4.4 (a).

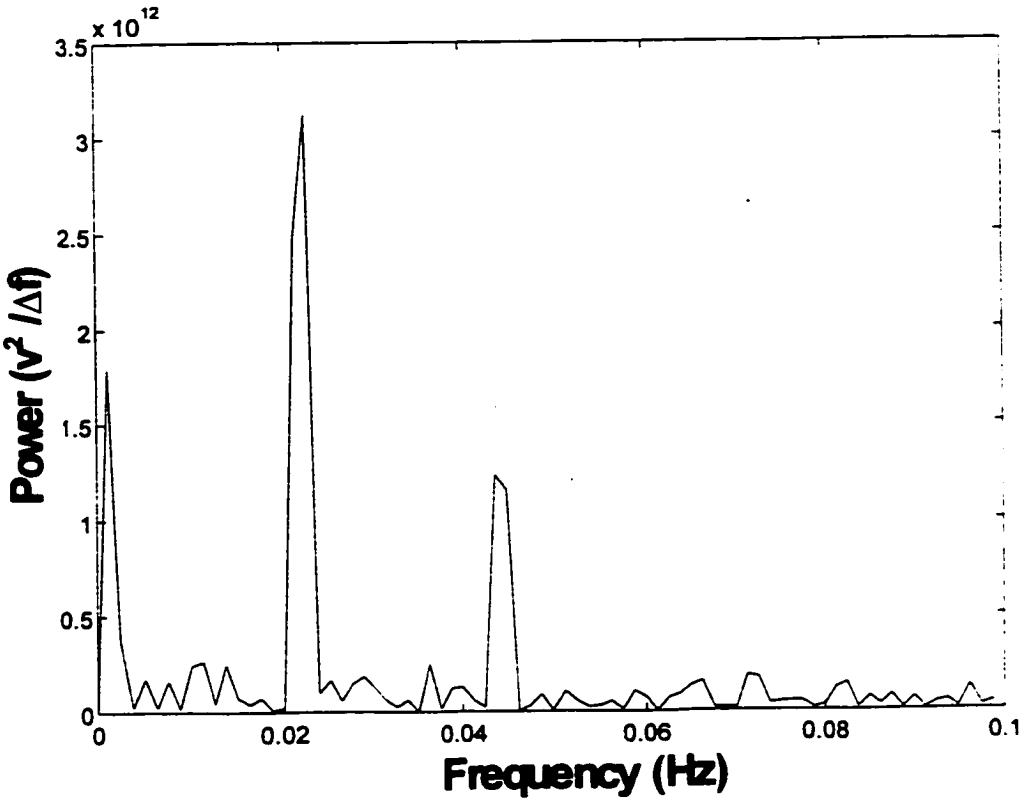

Figure 4.6 Noise power spectrum of the potassium emission signal shown in Figure 4.4 (b).

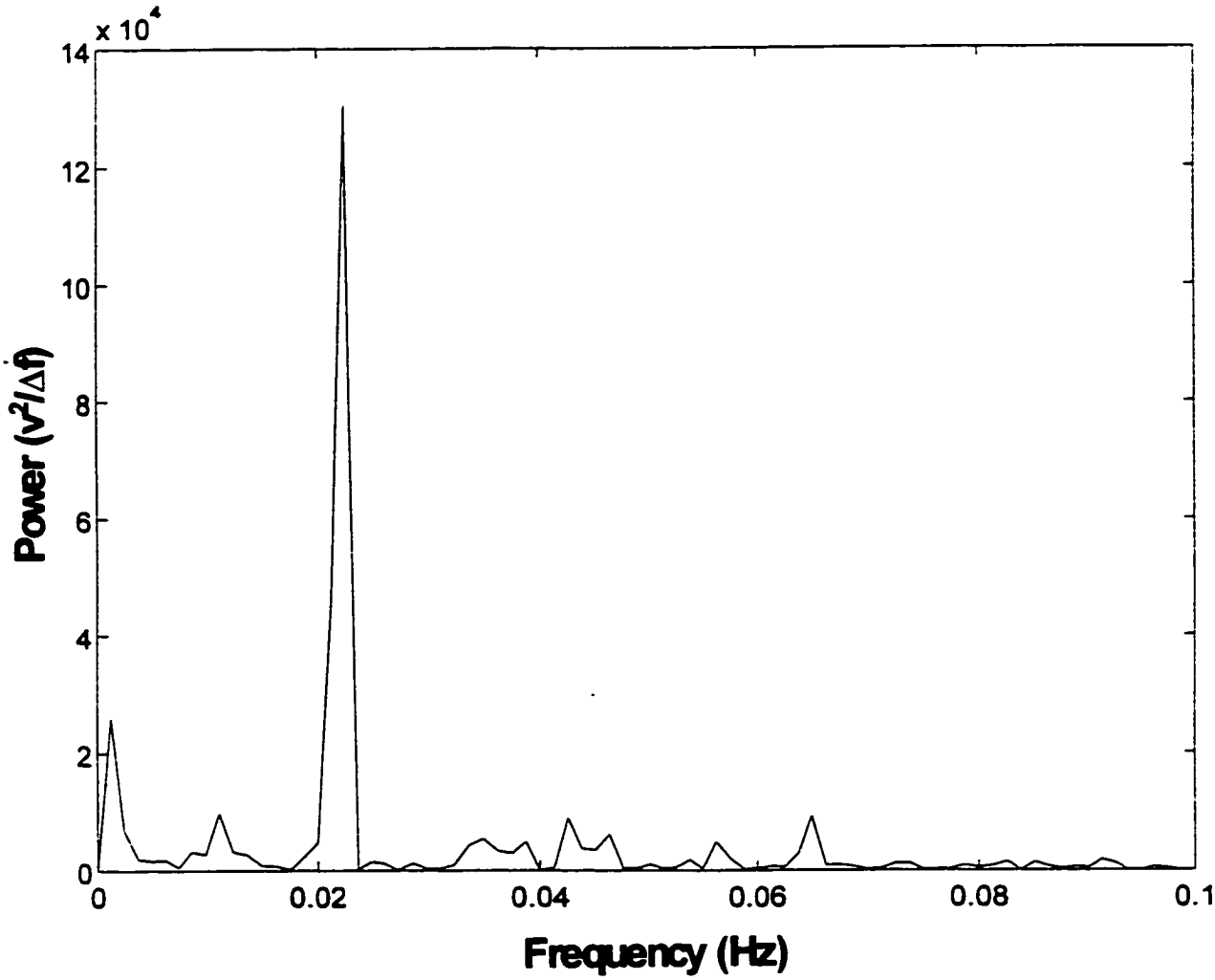

Figure 4.7 Noise power spectrum of ratio Li/K shown Figure 4.4 (c).

in the NPS of potassium. Therefore, it is apparent that interference noise originates from the syringe pump, air flow or other experimental source. This is in contrast to the earlier experiments which suggested flicker noise as the dominant source. The difference is probably due to the relative time scale of the two experiments. Since the earlier experiments had a wider frequency resolution, this likely hid the presence of interference noise. In either case (flicker or interference noise), an internal standard can be used to reduce the overall noise. The amplitude of the interference noise is reduced when the ratio is used as shown in Figure 4.7. The interference noise in the ratio of the two signals is less than the analytical signal due to the correlation between noise sources in the analytical signal and reference signal. Therefore, the ratioing is a useful method to suppress the interference noise and any correlated noise such as drift or flicker noise originating in the analyte emission. An application of the ratio channel to improve the detection limit will be described in the next section. It is worthwhile, theoretically to investigate the parameters determining the factor of improvement in order to choose a suitable internal standard and experimental conditions [147]. Based on propagation of the error, the division operation can be expressed [148] as:

$$[\sigma_{A/R} / (I_A/I_R)]^2 = (\sigma_A/I_A)^2 + (\sigma_R/I_R)^2 - 2\, r\, \sigma_A\sigma_R/(I_A I_R)$$

where:

I_A = average of the analytical signal over the measurement time

I_R = average of the reference signal over the measurement time

σ_A = standard deviation of the analytical signal

σ_R = standard deviation of the reference signal

r = correlation coefficient of the noise in the two channels

The factor of noise reduction achieved by ratioing can be calculated by the following equation:

$$R = (\sigma_A / I_A) / [\sigma_{A/R} / (I_A / I_R)]$$

If two conditions simultaneously meet: (1) the analytical signal and the reference signal are completely correlated (r=1) and (2) the relative amplitudes of the fluctuations of two signals are the same or In other words $\sigma_A/I_A = \sigma_R/I_R$, then the $\sigma_{A/R}$ becomes zero. That means that on the ratio signal, there is not any correlated noise and it is eliminated completely. In other situations, depending on how far the conditions are from the ideal conditions, the reduction of correlated noise in the ratio is varied. The factor of improvement (R) for ratioing of the lithium emission over the potassium emission was calculated and the results are:

$$\sigma_A/I_A = \sigma_{Li}/I_{Li} = 0.3295$$

$$\sigma_R/I_R = \sigma_K/I_K = 0.2708$$

$$r = 0.8707$$

$$[\sigma_{Li/K} / (I_{Li}/I_K)]^2 = (0.3295)^2 + (0.2708)^2 - 2 \times 0.8707 \times 0.3295 \times 0.2708$$

$$[\sigma_{Li/K} / (I_{Li}/I_K)]^2 = 0.02652 \quad \text{which gives} \quad [\sigma_{Li/K} / (I_{Li}/I_K)] = 0.1628$$

By substituting the calculated values in improvement equation (R) :

$$R = 0.3295/0.1628 = 2.023$$

Therefore, in this experiment, ratioing can theoretically reduce correlated noise on the signal by a factor of about 2. It is shown in the next section that this is in good

agreement with the experimentally observed value. However, the degree of improvement and the improvement factor (R) depend on the experimental conditions, the analyte and the reference elements.

4.5 APPLICATION OF THE INTERNAL STANDARD TECHNIQUE BY USING THE RATIO OF AN ANALYTICAL CHANNEL AND A REFERENCE CHANNEL

One of the methods to cope with flicker and interference noise is to use an internal standard, to measure the signal and the reference signal simultaneously, and to take their ratio. This method decreases the noise amplitude and improves the detection limit, provided the reference element was selected properly. In other words, the internal standard line should be selected with the same noise behaviour as the analyte [147,149].

4.5.1 Experimental conditions

The experimental setup of this method was the same as that of the previous experiment. The emission from lithium in formic acid solution was monitored as the analytical signal, and potassium emission was measured as the reference signal. The experimental conditions were:

Hydrogen: 200 mL/min; Air: 230 mL/min; Nitrogen: 330 mL/min; Voltage: 5000 V; 1/8 meter grating monochromator with R-374 PMT for monitoring Li; 765 nm interference filter with R-268 PMT for monitoring K; Li sample flow rate: 20.7 Li/s; K sample flow rate: 21.1 ng K/s; Solution flow rate: 10 µL/min.

4.5.2 Results

In Figure 4.8, the lithium emission, the potassium emission, and the ratio of these two emissions are shown. The S/N ratio improved by a factor of 2.3 which corresponds to the theoretically predicted value.

4.6 CURRENT THROUGH THE FLAME AS AN INTERNAL STANDARD

4.6.1 Experimental setup

An experimental setup (Fig 4.9) was used to record emission and electrical signals simultaneously. The emission signal from lithium was recorded by the monochromator while flame conductivity was measured by an electrometer. The neon lamp (NE-2) was used as a variable resistor, where its resistance is changed by the current, to prevent damage to the electrometer.

4.6.2 Results

When a voltage of about 3000 V was applied between the capillary needle and the counter electrode and the flame was lit, a current passed through the flame. The current was dependent on the flame conditions; it decreased with increasing nitrogen flow or decreasing hydrogen flow. The crucial factor influencing the current was the air flow, and decreasing it reduced the current sharply. When a sample was introduced into the flame, the current signal decreased and the resulting signal was evaluated as an internal standard. The data in Figure 4.10 illustrate that there is a correlation between noise sources on the optical signal and

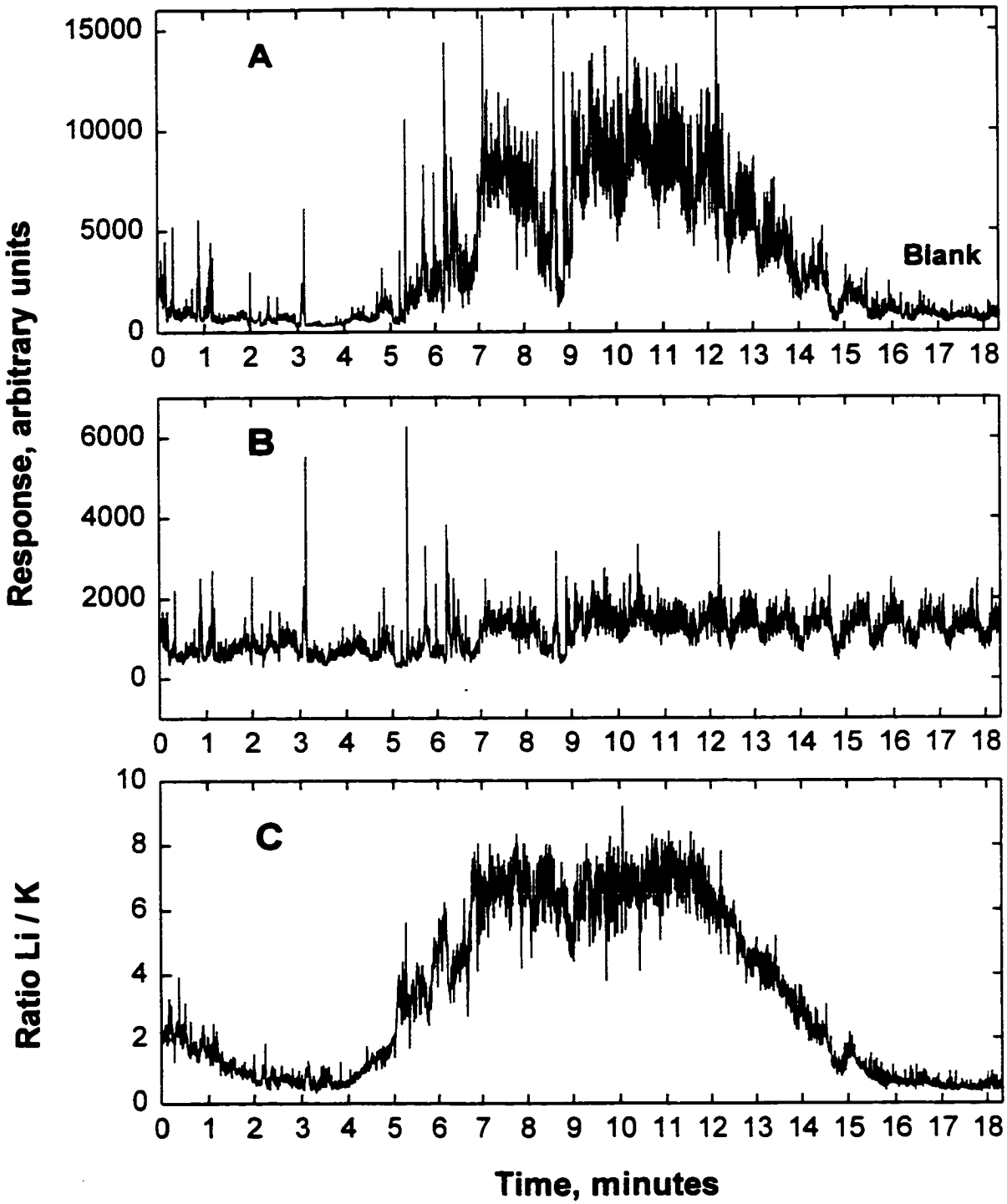

Figure 4.8 a: Lithium emission at 670 nm; b: Potassium emission at 767 nm; c: Ratio Li/K. Experimental conditions are in the text.

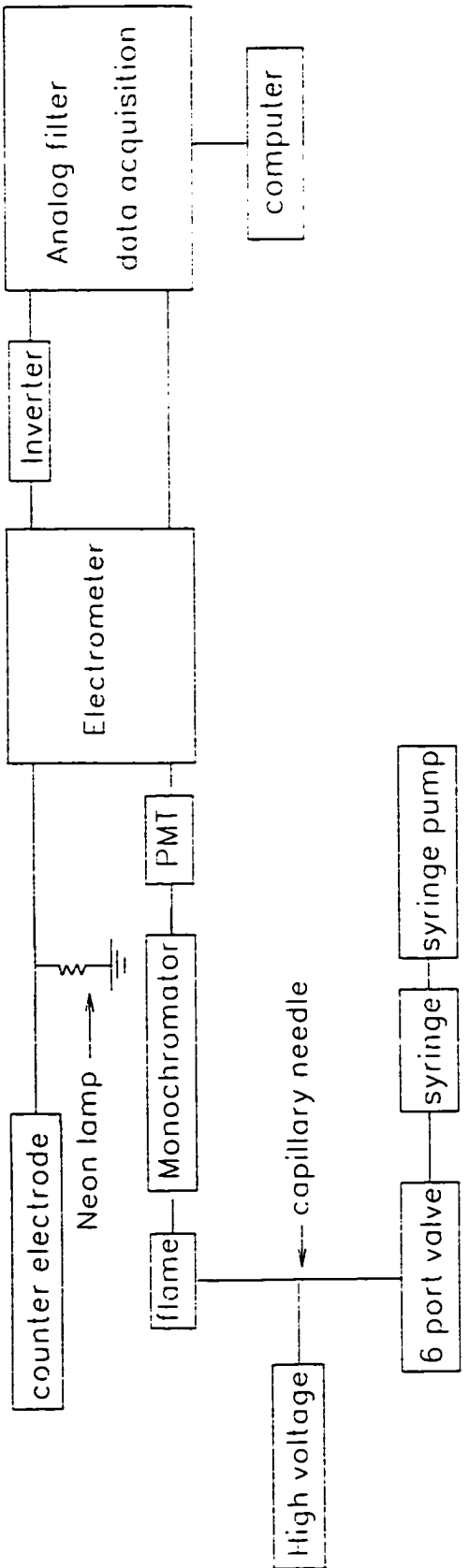

Figure 4.9 Block diagram of modular components for measurements of electrical and optical signals.

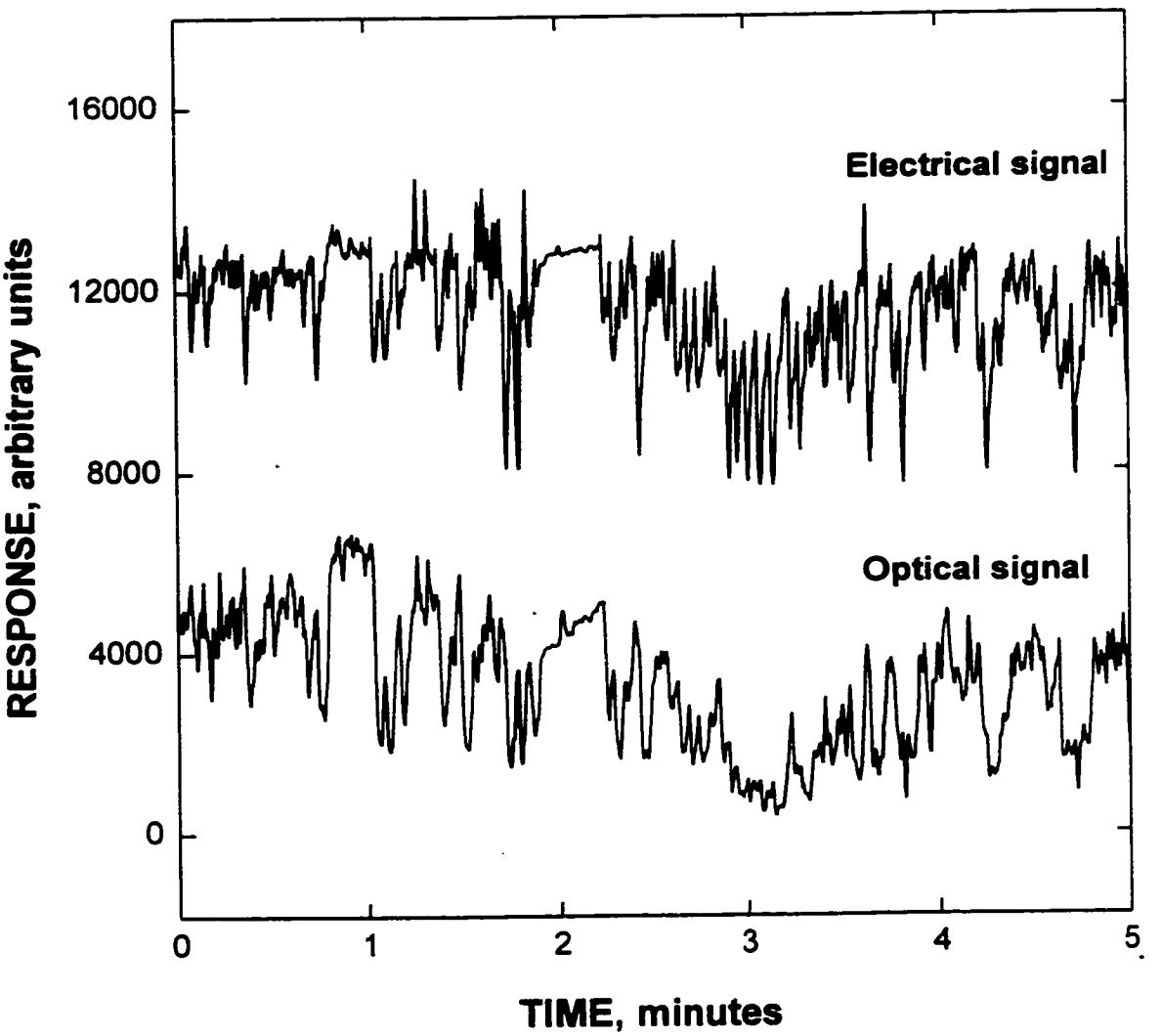

Figure 4.10 Noise of the optical signal (lithium emission) from lithium chloride in formic acid and noise of the electrical signal (current through the flame. Hydrogen: 150 mL/min; Air: 220 mL/min; Nitrogen: 300 mL/min; Voltage: 3800 V; 1/8 meter grating monochromator with R-1104 PMT; Sample flow rate: 15.1 ng Li/s.

the electrical signal with a correlation coefficient of 0.8062. Therefore, it may be possible to use the ratio of optical signal/electrical signals to reduce the correlated noise on the signal. The source of the current in electrospray-FPD and its interaction with the sample are discussed in the next chapter.

Chapter 5

SPECTRA OF SELECTED ELEMENTS

5.1 INTRODUCTION

After obtaining the spectra of some elements with the filter wheel as a wavelength selector, it was decided to use the monochromator to obtain spectra with better resolution. Two modifications also were implemented for the FPD. First, the air tube was brought to within a few millimeters below the cap (the hydrogen tube) to decrease the flicker noise originating from the instability of the flame when a sample was fed into it. Second, a movable spherical mirror (r = 35.8 mm) was positioned in the channel opposite the PMT channel. The radius of the mirror was selected to focus the emission and enhance light throughput from the flame onto the entrance slit of the monochromator. Aqueous solutions were used to record a series of spectra. Surfactants such as SDS or polyoxyethylene sorbitan were added to the solution to improve electrospray nebulization. Spectra from selected elements in the periodic table were then recorded.

5.2 EXPERIMENTAL CONDITIONS

Diagrams of the experimental setup used for obtaining spectra are shown in Figures 5.1 and 5.2. Table 5.1 gives the experimental conditions for obtaining spectra of selected elements by the electrospray–FPD. The modular parts were described in previous experiments. The reciprocal linear dispersion of the

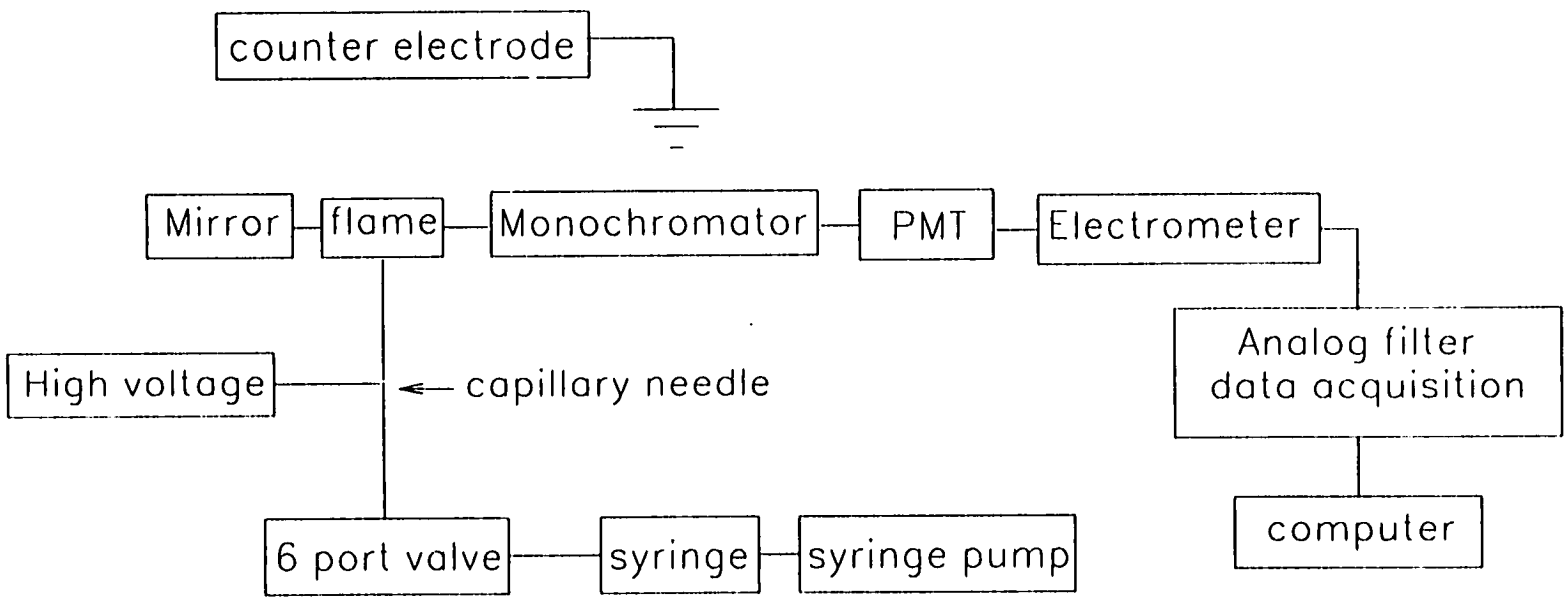

Figure 5.1 Block diagram of modular components for obtaining spectra by monochromator.

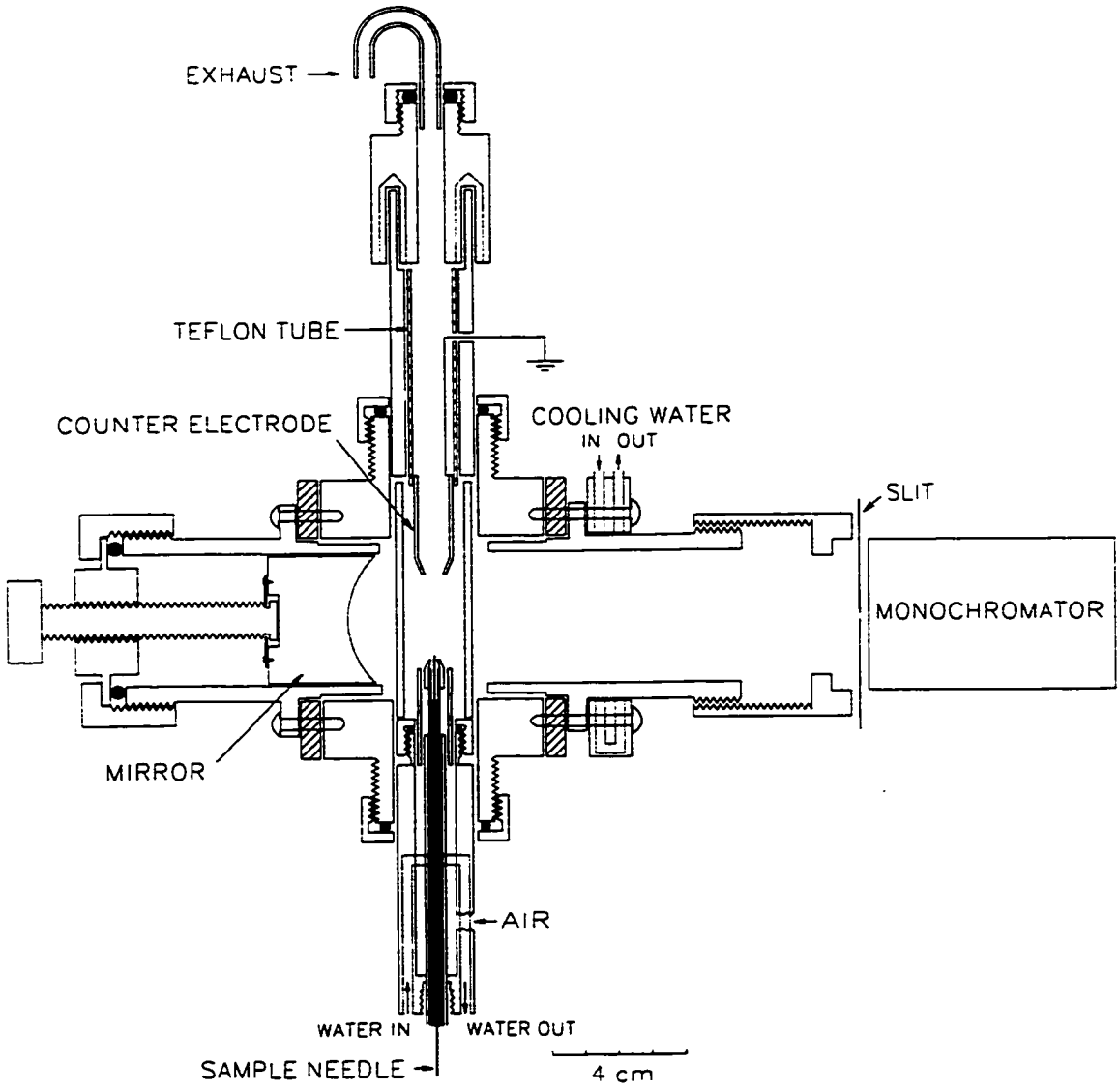

Figure 5.2 The detector and monochromator.

Table 5.1 Operating conditions for selected elements by the electrospray-FPD

Element	Sample flow rate (mL/min)	Mass flow rate (ng/s)	C (ng/mL)	Air	H_2	N_2	Voltage (V)	PMT voltage (V)
				(mL/min)				
NSP	-	-	-	181	187	330	5000	600
SDS (1)	10	20	120	170	140	330	4850	690
SDS (2)	12	33.5	167.5	176	250	330	3600	650
SDS (3)	10	20	120	206	150	330	variable	387
SDS (4)	10	24	144	176	120	330	4000	500
P (1)	10	41	246	176	140	330	3500	550
Cu	11	21.6	117.8	206	175	330	4500	575
Mn	11.2	31.3	167.6	170	140	330	4200	520
Ag	12	54.5	272.5	176	150	350	4700	700
P (2)	10	51.2	307.2	210	300	330	4200	700
Cd	10	44.1	264.6	176	150	320	4800	700
In	10	71	426	206	150	330	4800	650
Sc	10	17	102	180	150	330	4200	700
Mg	10	28.4	170.4	170	150	330	4200	700
Ba	12	57	285	180	200	330	3700	700
Se	12	55	275	176	170	330	3800	700
B	10	143	858	176	160	300	4800	700
As	10	199	1194	176	150	330	3800	700
Ni	10	32.2	193.2	170	140	130	4850	690

C: Concentration; P(1): Adenosine 5-monophosphate; P(2): Disodium hydrogen phosphate; SDS (1), SDS (2), SDS (3), and SDS (4) are experimental conditions of sodium dodecyl sulphate for Figures 5.4, 5.9, 5.5, and 5.6 respectively.

monochromator was 6.4 nm/mm and it used a simple drive built by the Chemistry Department's electronic shop. The starting wavelength and scan speed were selected manually. Data acquisition was conducted at 10 Hz and stored data were exported in ASCII format to the commercial program SigmaPlot (Jandel Scientific, San Rafael, CA, USA) for further manipulation.

REAGENT AND TEST SOLUTIONS: Test solutions were prepared by dissolving reagent-grade ionic compounds in water. These solutions then were modified by the addition of a sodium dodecyl sulphate (SDS) solution so that the final concentration of SDS in the sample was 5.2 mM. In cases where precipitates were formed from ionic metals and dodecyl sulphate, the concentration of SDS was increased to 17 mM. The critical micelle concentration of SDS is 8.1 mM [150]; therefore, by enhancing the SDS concentration from 5.2 to 17 mM, SDS micelles are formed. Once a sufficient concentration of micelles is present, the metal cations are solubilized by binding to the micelle surface, and precipitation of $M^{n+}(DS)_n$ (M = metal cation, n^+ = charge of the metal cation, DS = dodecyl sulphate) is prevented. when sorbitan was used as the surfactant, the concentration of sorbitan in the final solution was 0.1% w/v.

HIGH VOLTAGE POWER SUPPLY: A DC power supply (model # R10B, Hipotronics, Brewster, N.Y. USA) (5 mA; 12 kV and 5 MΩ resistors in series to limit the current for safety) was used for the electrospray.

5.3 RESULTS AND DISCUSSION

5.3.1 Nitrogen second positive system

In the course of obtaining the chromium spectrum, it was found that, at certain high voltages, some additional peaks appeared in the spectrum. In order to investigate the source of these peaks, a number of experiments were conducted. At high voltages (5 kV) a corona discharge produced the nitrogen molecular emission. The results of experiments at selected high voltages are shown in Figure 5.3. These molecular band emissions originate from the radiative decay of a triplet state of nitrogen molecules [151,152]: $N_2(C^3\Pi_u) \longrightarrow N_2(B^3\Pi_g)$, with an electronic energy level above 9.76 ev. These molecular band emissions are referred to as the nitrogen second positive system. Clearly the corona discharge can exist without a flame. However, the nitrogen second positive appeared strongly with the flame. Therefore, the flame seems to play a role in the appearance of a strong nitrogen second positive band system.

5.3.1.1 Interpretation of the nitrogen second positive system

The nitrogen second positive emission (NSP) originates from a relaxation of the nitrogen molecule from a triplet state [$N_2(C^3\Pi_u)$] to a lower state [$N_2(B^3\Pi_g)$]. The energy of $N_2(C^3\Pi_u)_{\upsilon=0}$ is 11.1 eV above ground state and, in order to observe the second positive emission, the $N_2(C)$ state must be populated [152]. One mechanism for the production of $N_2(C)$ is the collision of two A-state metastables (6.2 eV) to populate the C state (11.1 eV) via an efficient energy pooling

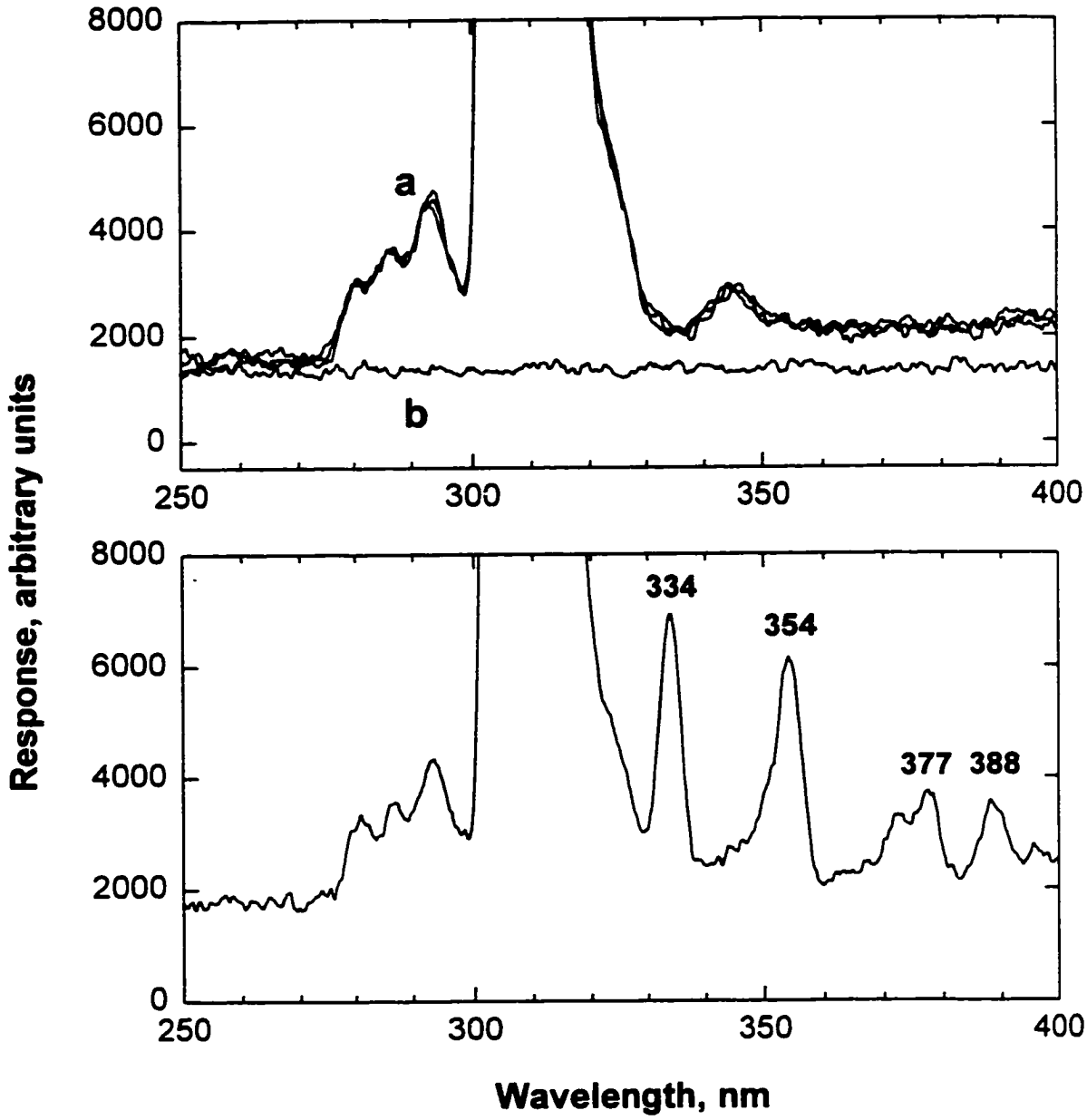

Figure 5.3 Spectra at different voltages with and without flame.
Top: a. Flame spectra at 2000, 3000 and 4000 V.
b. Wavelength scan without flame at 5400 V.
Bottom: Spectrum of the flame and nitrogen second positive system at 5000 V.

reaction [153,154]:

$$N_2 (A^3\Sigma_u^+) + N_2 (A^3\Sigma_u^+) \longrightarrow N_2 (C^3\Pi_u) + N_2 (X^1\Sigma_g^+)$$

Another mechanism for producing N_2 (C) has been suggested by Ung [155]:

$$N_2 (A^3\Sigma_u^+) + N_2 (X^1\Sigma_g^+)_\upsilon \longrightarrow N_2 (C^3\Pi_u) + N_2 (X^1\Sigma^+)$$

$N_2 (X^1\Sigma_g^+)_\upsilon$ represents vibrationally excited ground state nitrogen (υ>20) with an excitation energy greater than 5 eV. For these two mechanisms to proceed, metastable nitrogen molecules $N_2 (A^3\Sigma_u^+)$ are first necessary. The mechanism for producing these molecules, as proposed by Berkowitz [156], starts by the collision of two nitrogen atoms and a third body for energy conservation in the collisional reactions. Borst and Chang [157] also suggested that the excitation of the A state occurred directly from the N_2 ground state by electron impact:

$$N_2 (X^1\Sigma_g^+) \longrightarrow N_2 (A^3\Sigma_u^+) \qquad \text{(direct excitation)}$$

The authors concluded that the upper vibrational levels υ>8 are populated mainly by direct excitation.

Another mechanism suggested for producing N_2 (C) from a recombination of an electron with an ionized nitrogen molecule in the ground state [158] is:

$$N_2^+ (X^2\Sigma_g^+) + e \longrightarrow N_2 (C^3\Pi_u) + h\upsilon$$

Based on this information it can be postulated that the reason for a strong nitrogen second positive system in the flame is direct excitation of the nitrogen molecule and the production of N_2 (A) followed by collision of two A-state metastables to populate N_2 (C) via an efficient energy pooling reaction.

Metastable nitrogen molecules as an energy transfer medium have been

used as an analytical technique for determination of some metals and as a detector in GC [152,159,160]. Aue and co-workers [160] used NSP as an energy source for excitation of a number of aroyl compounds. Fassel and associates [159] used the active nitrogen as an energy source for the excitation of atomic lines of some elements such as As, Bi, Ge and Pb by introducing the volatile hydride of these elements into the active nitrogen atmosphere. The strong appearance of a nitrogen second positive in the flame suggests potential for further investigation.

5.3.2 SODIUM DODECYL SULPHATE

Sodium dodecyl sulphate is a surfactant. It was added to aqueous solutions to decrease the surface tension of the aqueous solution in order to produce a stable electrospray. It also serves as a wetting agent to prevent needle tip clogging. A number of experiments were conducted to investigate the effects of different variables on the electrospray process itself, or on flame emission. The results of these experiments and the spectra of SDS under different experimental conditions are described below.

5.3.2.1 Spectrum from sodium dodecyl sulphate (sodium emission)

Two kinds of emission spectra were obtained for SDS depending on gas flow rates. The spectrum shown in Figure 5.4 shows no sulphur emission; only OH (first and second orders) and Na emissions appeared. In Figure 3.5, the first and the second order of the OH emission is not observed because the filter wheel does

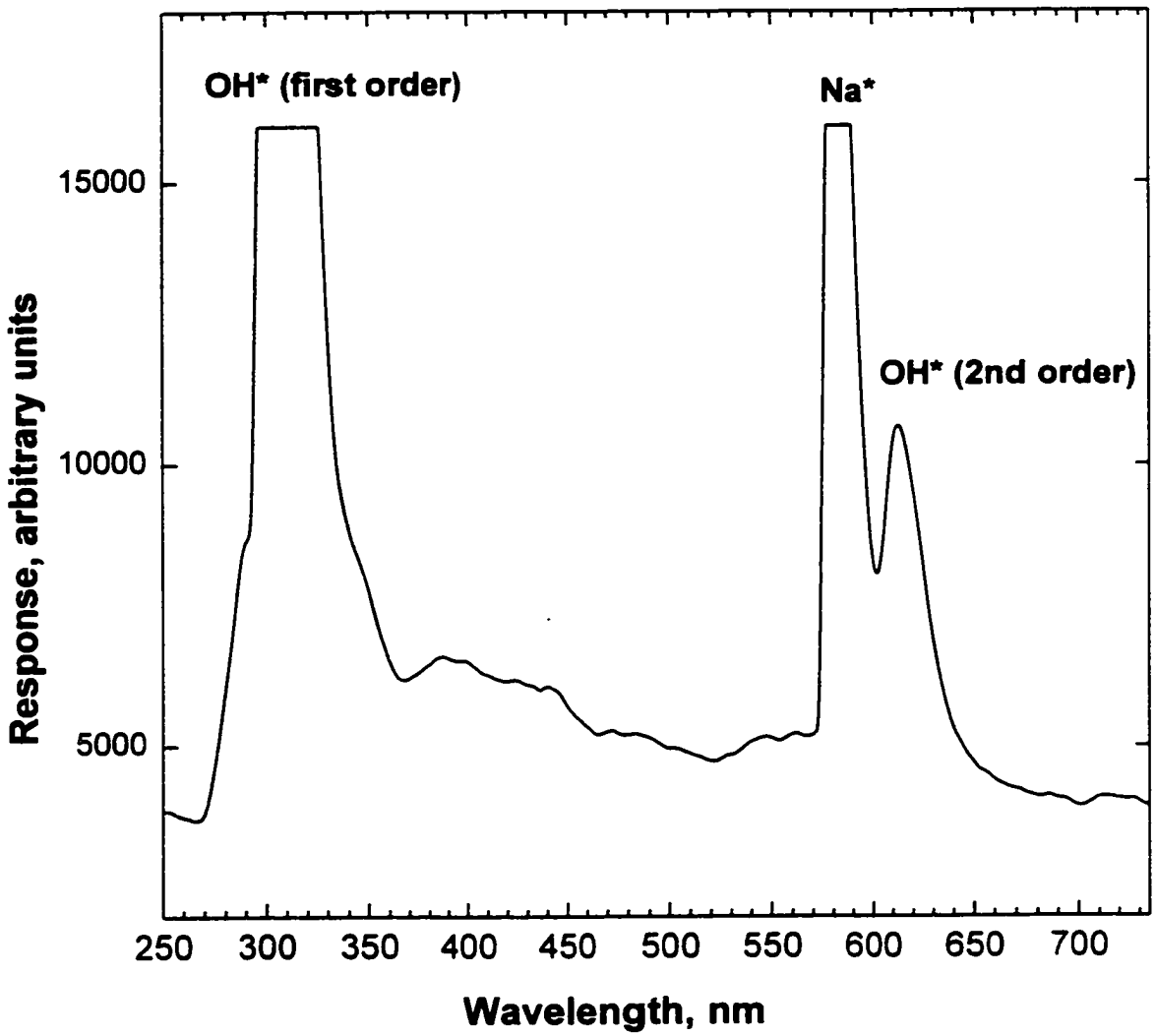

Figure 5.4 Spectrum from sodium dodecyl sulphate in aqueous solution.

not transmit the wavelengths below 400 nm. Sulphur emission was observed under different experimental conditions and as discussed under Section 5.3.2.5. The experimental conditions under which sulphur spectrum (from SDS) did not appear was preferable, as this eliminated any spectral interferences from sulphur.

5.3.2.2 Sodium emission versus electrospray voltage

The effect of electrospray voltage on the intensity of sodium emission is shown in Figure 5.5. When the voltage was increased beyond 4600 V, sparking occurred. Below 2000 V, the flame was extinguished and electrospray was not effective. In this case, the sample accumulated at the needle tip and was suddenly pulsed as a large droplet into the flame. These pulsations occurred a few times until the flame was extinguished. It is clear from the Figure 5.5 that higher voltages are necessary for obtaining a larger signal.

5.3.2.3 Investigation of the negative mode of electrospray

Electrospray was examined in the negative mode by applying a negative voltage to the capillary needle. It was not possible to operate below -2000 volts when the sample was introduced into the flame. Furthermore, the sodium emission was very noisy, making it difficult to distinguish the signal from the noise. Therefore, electrospray in the negative mode in these conditions did not work for FPD. A corona discharge is easily formed in the negative mode electrospray [118]. Fenn [87] also pointed out that corona discharge in the negative mode starts at a

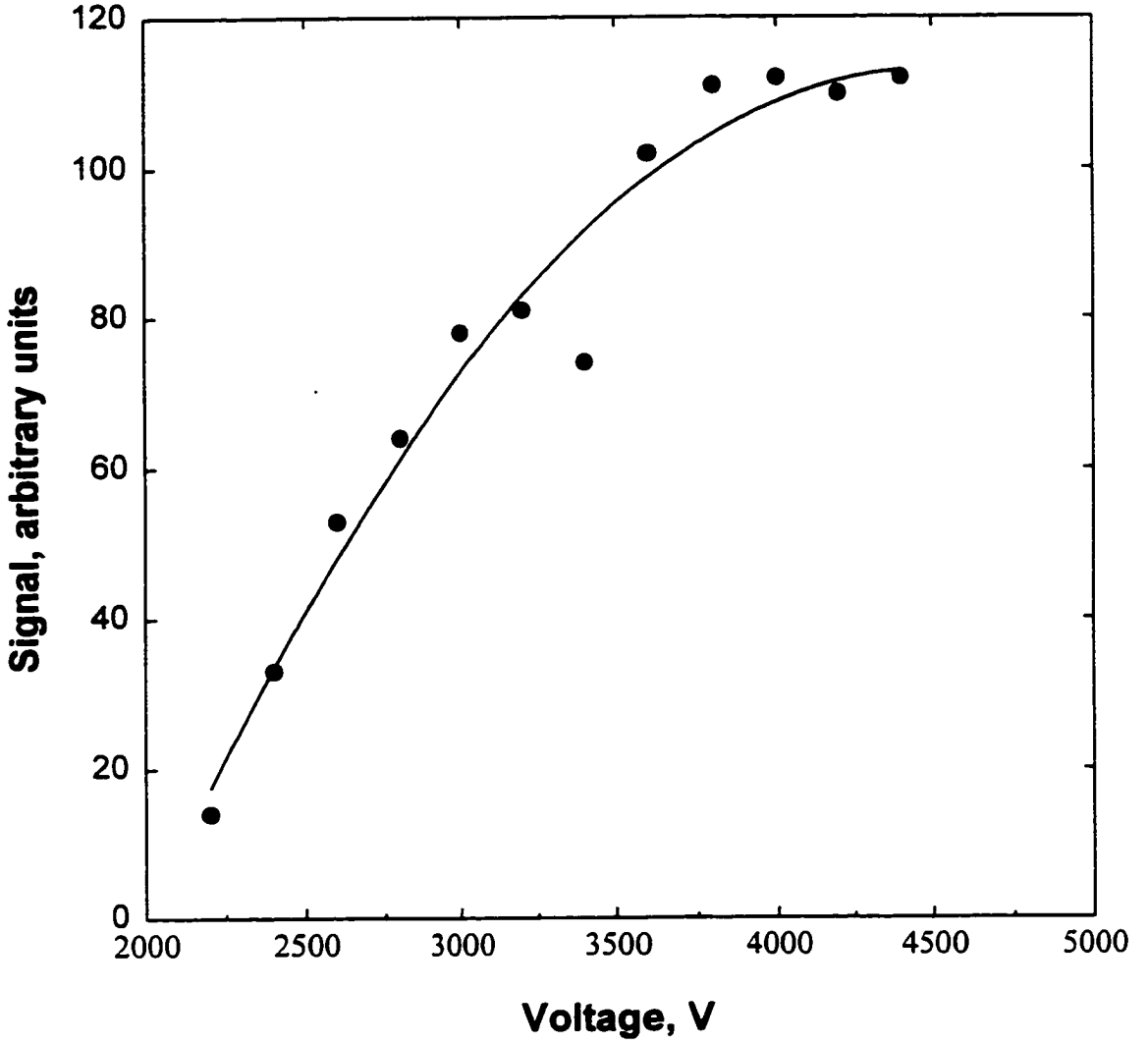

Figure 5.5 The effect of electrospray voltage on sodium emission (SDS) in aqueous solution.

lower voltage than in the positive mode. There are several methods to reduce corona discharge. SF_6 as a highly efficient electron scavenger [121,122] can be used in this capacity. Pure oxygen suppresses corona discharge because oxygen is able to capture electrons [79]. Henion [118] found that air or nitrogen doped with Freon can also prevent corona discharge. Therefore electrospray in the negative mode may be possible if an electron scavenger is used to reduce corona discharge.

.

5.3.2.4 Optical and electrical signals

The sodium emission and current signal through the flame were measured simultaneously for the introduction of SDS into the flame. The experimental setup was the same as that in Figure 4.9 except that, instead of the monochromator, a 600-nm interference filter with a 40-nm bandpass was used. The result of this experiment is shown in Figure 5.6. Although electrospray-FPD is a very sensitive method for sodium measurement, the more interesting part of this experiment was the flow of current through the flame as an electrical signal. In order to explain Figure 5.6, it is necessary to clarify that, before SDS is introduced into the flame, there is a background current which originates from ion species in the flame and the corona discharge arising from the application of the high voltage across the flame. When SDS is introduced into the flame, this background current decreases. This is, presumably, due to the reduction of charged species. Introduction of SDS into the needle starts the electrospray and this may reduce the corona discharge

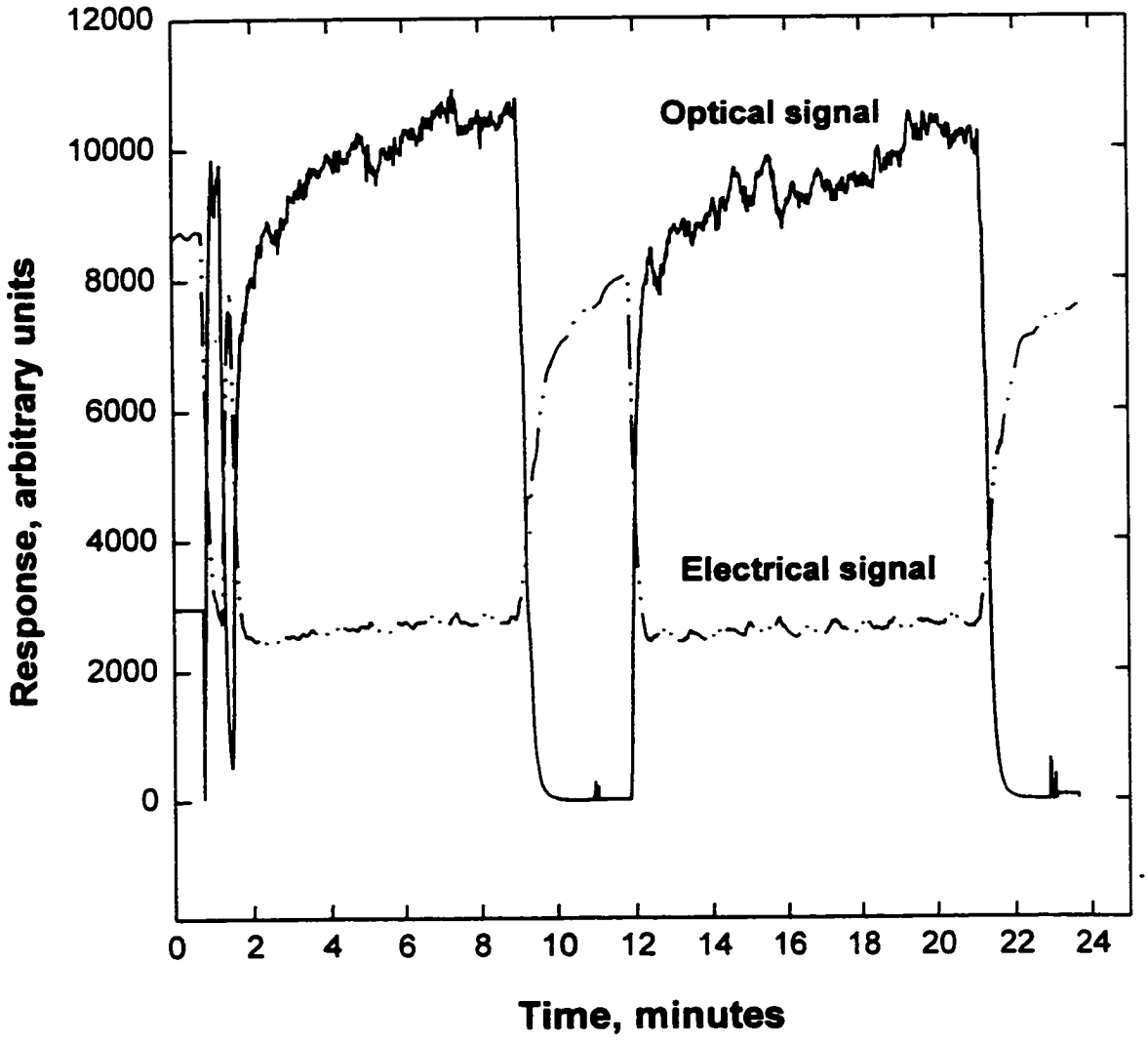

Figure 5.6 Optical and electrical signal obtained from sodium dodecyl sulphate in aqueous solution.

and consequently ion species that are produced by the discharge. Therefore introduction of SDS decreases the current. The flow of current through the flame, its interaction with the sample, and the application of the current as an analytical signal are very interesting subjects which require more investigation.

Several experiments were conducted to establish the relationship between current and flame parameters.

a. The effects of gas flow rates on the current signal

The effect of nitrogen flow rates on the current is shown in Figure 5.7. As noted previously (section 4.6), the current is decreased by reducing hydrogen and air flow rates. However, the air flow rate had a greater effect on changing the current than the hydrogen flow. Nitrogen dilutes the fuel and decreases the flame temperature. Also, the flame becomes more hydrogen rich by reducing the air flow and the temperature decreases. Therefore, it might be concluded that the flame temperature (at a certain voltage across the flame) affects the production of ions and consequently the current.

b. The effects of voltage on the current signal

The effect of voltage on the signal current from the flame is shown in Figure 5.8. The current increased at higher voltages due to an enhanced electric field at the needle tip and improved conditions for ionization of species.

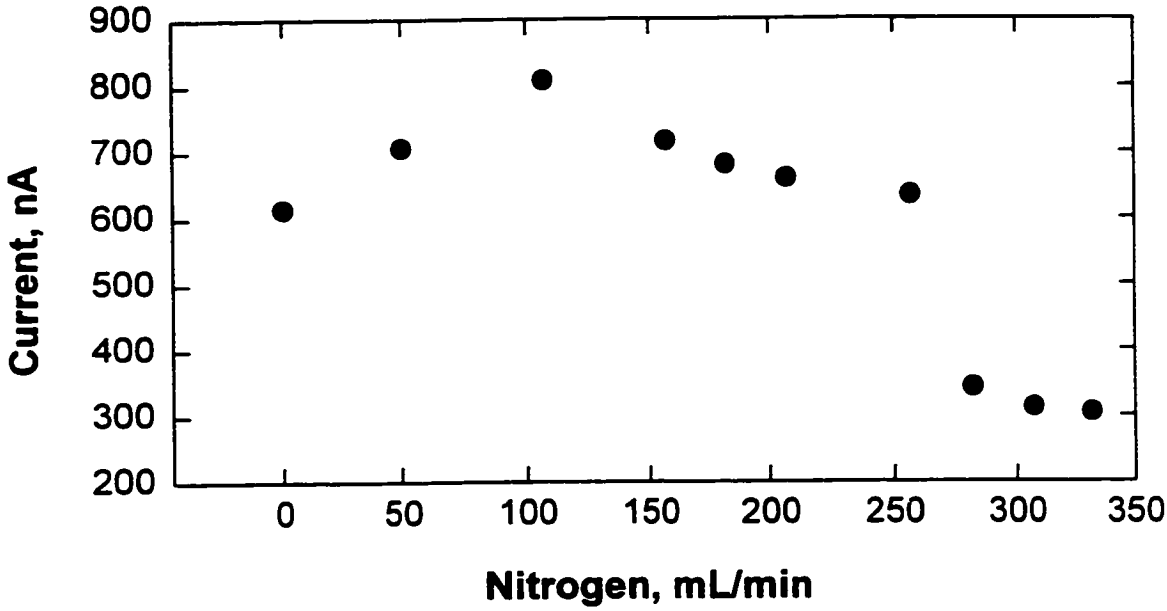

Figure 5.7 The effect of nitrogen flow rate on the current through the flame. Hydrogen: 170 mL/min; Air: 176 mL/min; Voltage: 2800 V

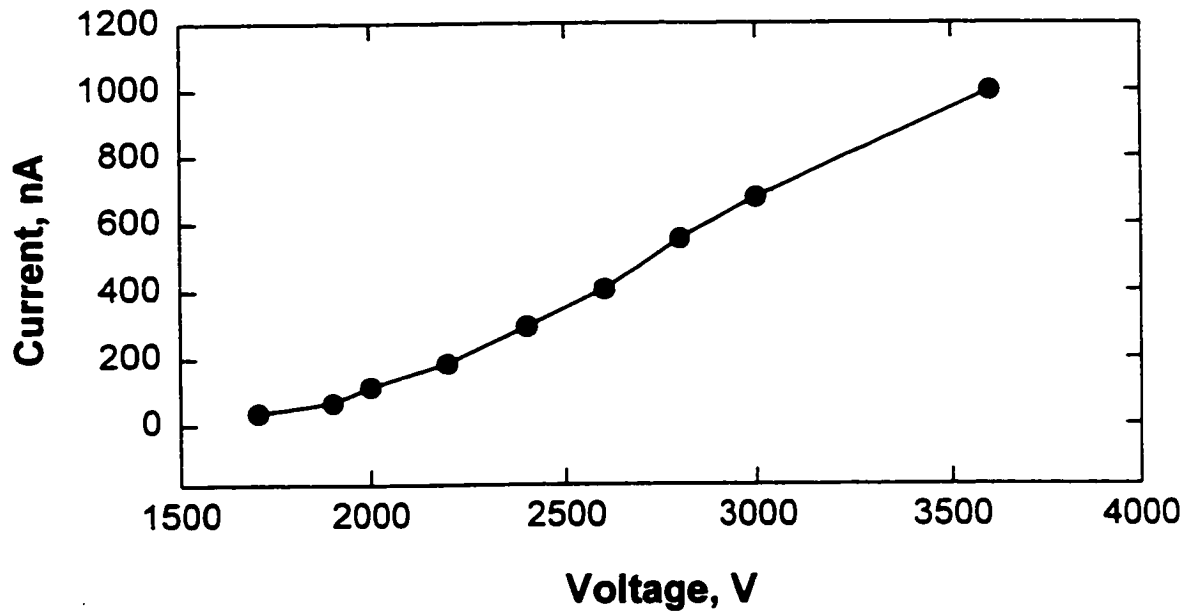

Figure 5.8 The effect of voltage on current through the flame. Hydrogen: 180 ml/min; Air: 250 mL/min; Nitrogen: 300 mL/min.

5.3.2.5 Sulphur spectrum from sodium dodecyl sulphate

The spectrum of sulphur from SDS is shown in Figure 5.9. The sulphur emission needs a cool flame [51]. The flame temperature is decreased by enhancing hydrogen flow rate and consequently the sulphur spectrum appears. The S_2 spectrum is well known in GC-FPD and it will not be described here. The main point is that it was possible to obtain the sulphur spectrum from an ionic compound by electrospray-FPD. The application of electrospray-FPD for sulphur analysis in biological samples is described later.

5.3.3 SPECTRA OF SELECTED ELEMENTS BY THE ELECTROSPRAY FLAME PHOTOMETRIC DETECTOR

5.3.3.1 PHOSPHORUS

Adenosine 5'-monophosphate (AMP) is a nucleotide or monomeric unit of deoxyribonucleic acid (DNA) and ribonucleic acid (RNA) [161]. The spectrum of AMP is shown in Figure 5.10 and is similar to the spectrum of volatile phosphorus compounds using GC-FPD. This suggests that electrospray-FPD is useful for the analysis of phosphorus in biological samples. The analytical utility of this technique, the detection limit, calibration curve and dynamic range for AMP were determined. In addition, several experiments were also conducted to investigate the effect of the sample flow rate on the signal to noise ratio, the quenching effects, and finally the nature of the baseline noise. These experiments are described below.

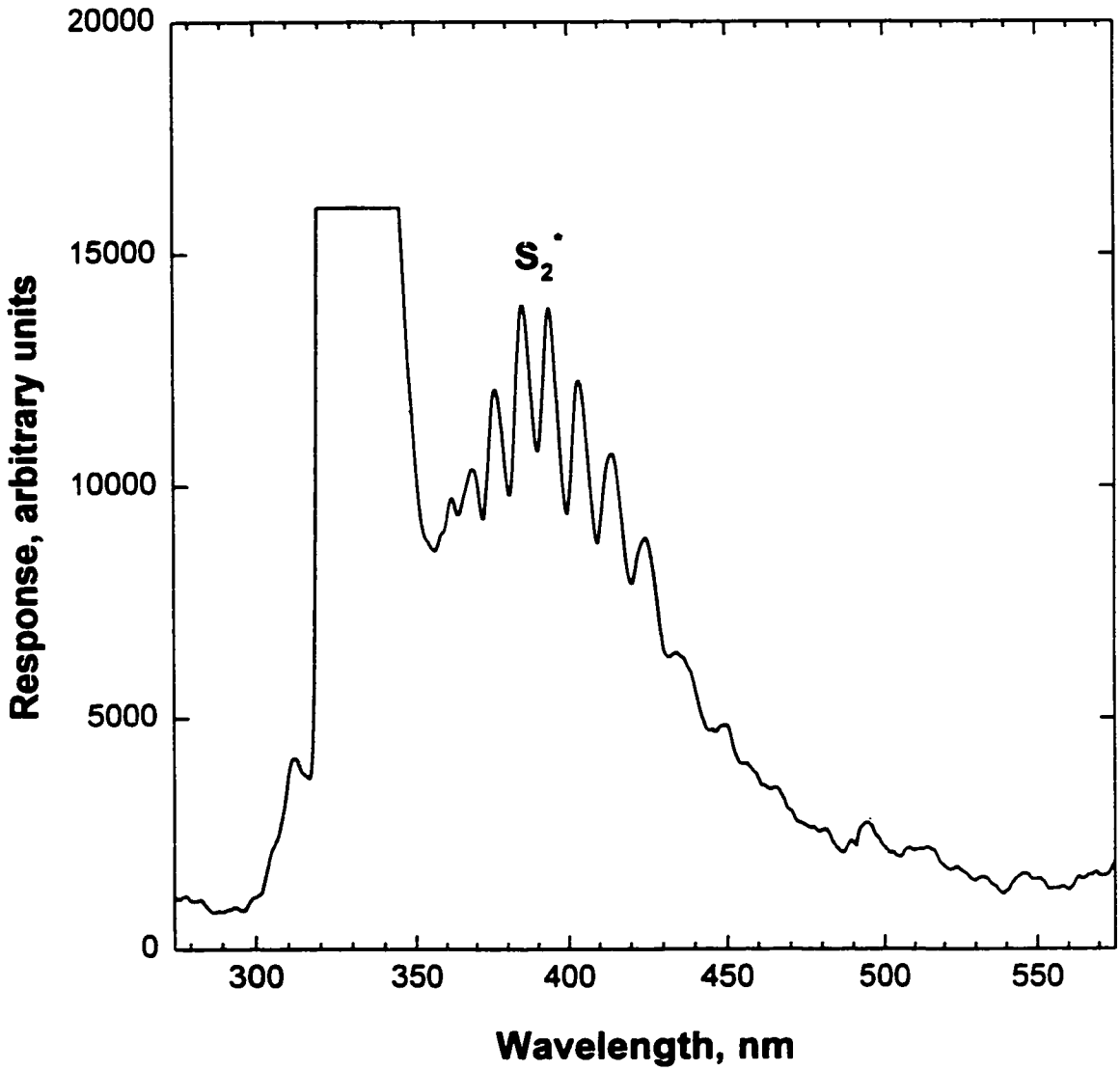

Figure 5.9 Sulphur spectrum obtained from sodium dodecyl sulphate in aqueous solution.

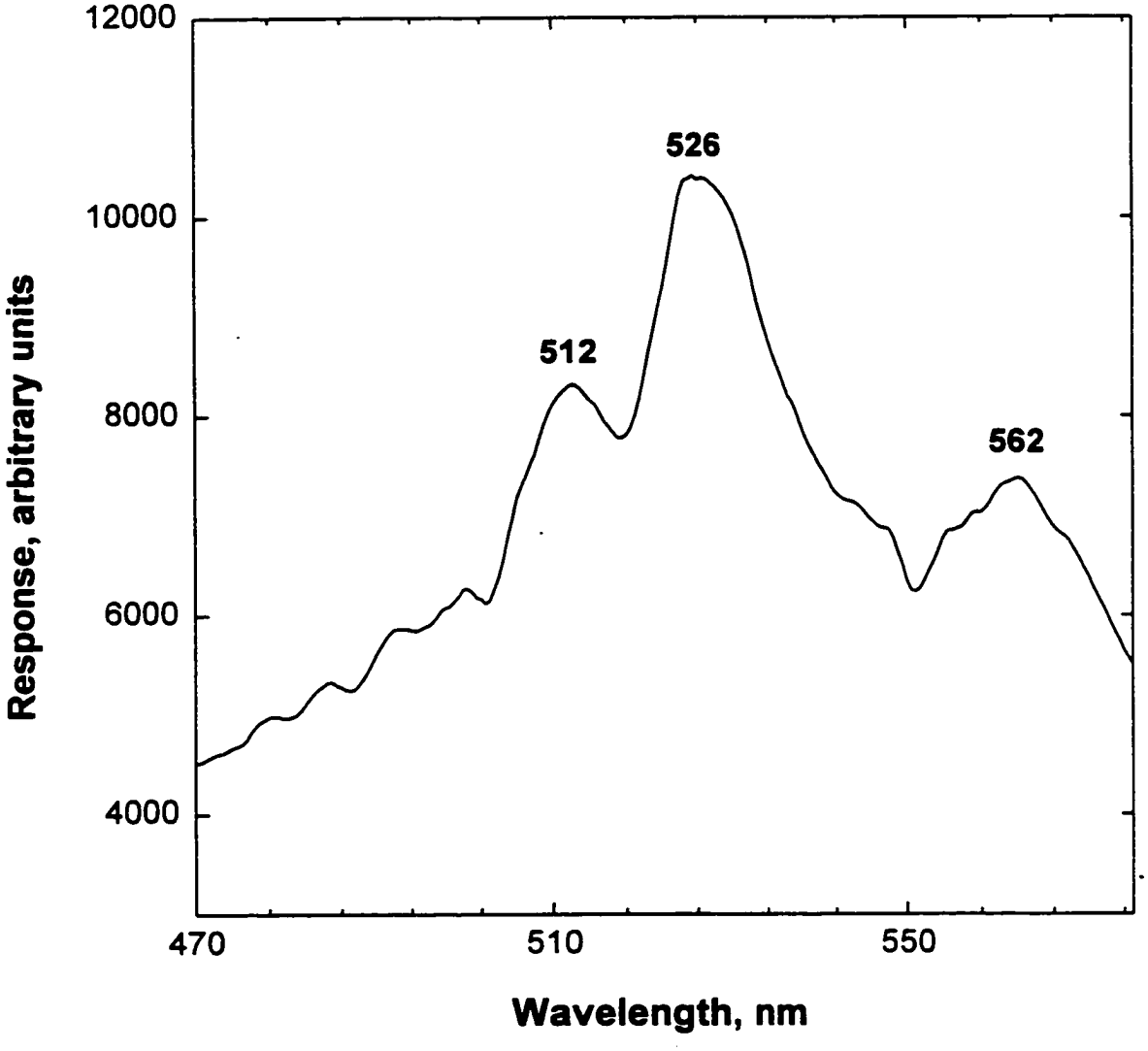

Figure 5.10 Emission bands obtained from adenosine 5'-monophosphate in aqueous solution.

5.3.3.1.1 Experimental conditions

The experiment was conducted by reducing the i.d. of the air tube (i.d. 4 mm) and placing the cap over the air tube instead of the hydrogen tube. The experimental conditions for obtaining the calibration curve were:

Hydrogen : 270 mL/min; Air: 160 mL/min; Nitrogen: 360 mL/min; Voltage: 4000 V; Interference filter: 524 nm (40 nm bandpass); PMT type and voltage: R-268 and 600 V; Sample flow rate: 10.5 µL/min; Time constant of the analog filter: 1.8 seconds. The SDS concentration in all solution is 5.2 mM.

The phosphorus emission is monitored by a 524 nm wide band interference filter and at the same time sodium emission is measured in another channel with a 589 nm interference filter.

5.3.3.1.2 Calibration curve

The recorded signal from the phosphorus emission using a 524 nm interference filter and the calibration curve are shown in Figures 5.11 and 5.12. The detection limit is about 1 ng P/s or 5.9 ng P/µL. In order to evaluate the performance of the electrospray-FPD, the detection limit is compared, for the same compound (AMP), with ICP and ICP MS as selective and sensitive elemental detectors. Heine and coworkers [161] determined phosphorus in AMP by HPLC-ICP by monitoring phosphorus emission at 213.6 nm and obtained a detection limit

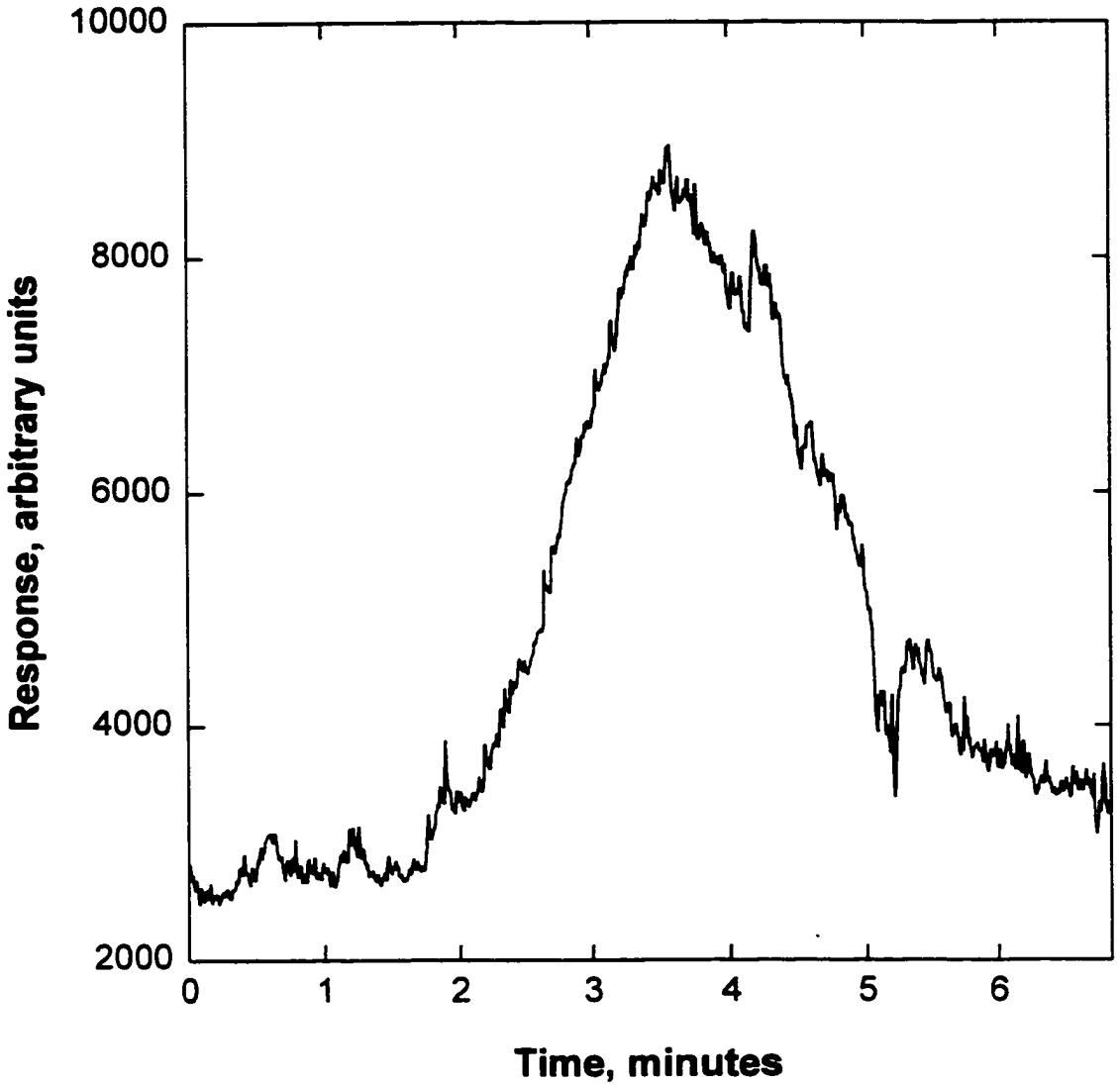

Figure 5.11 Emission at 524 nm (interference filter) from injection of 45 μL of an aqueous solution of adenosine 5'-monophosphate. Experimental conditions are in the text. Sample flow rate: 14.4 ng P/s.

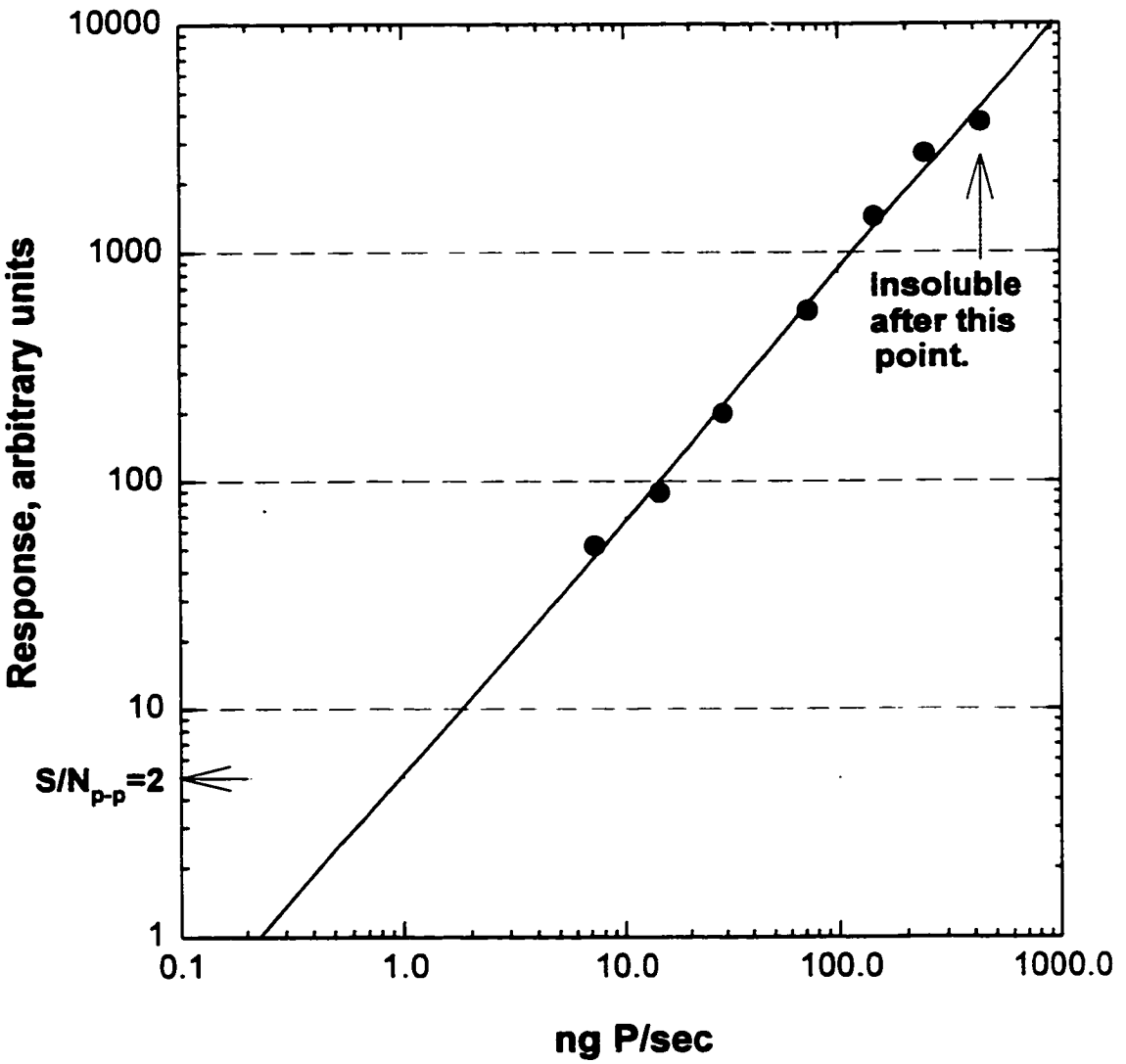

Figure 5.12 Calibration curve for adenosine 5'-monophosphate. Experimental conditions are in the text.

of 7.5 ng P/μL or 187 ng P/s. Yoshida and coworkers [162] also determined phosphorus in twelve common 5'-ribonucleotides by HPLC-ICP using a concentration gradient method. The detection limit for AMP is 0.37 μg P/mL or 8.6 ng P/s. ICP-MS offers detection limits for the elements generally in the range of 5 - 50 pg/mL [163]. One of the advantages of the ICP-MS over the ICP is the lower spectral interference [164]. Hiefje [165] suggested that the ICP-MS shows a better detection limit for elements because of the lower background and noise, which is shot noise limited. However, there is a serious mass isobaric interference at $^{14}N^{16}OH^+$ for phosphorus determination by ICP-MS [166]. Houk and Jiang [163] determined phosphorus in AMP by HPLC-ICP-MS using an ultrasonic nebulizer with aerosol desolvation. The authors used an ultrasonic nebulizer to improve the detection limit, and desolvation to reduce the amount of the solvent (hence oxygen) reaching the plasma and consequently reduced spectral interference from $^{14}N^{16}OH^+$. The detection limit for phosphorus in AMP by using this relatively sophisticated technique is 16 ng P/mL or 426 pg P/s, which is more than an order of magnitude better than the detection limit of phosphorus by ICP. The detection limit was calculated based on the signal over standard deviation of the background equal to three ($S/\sigma = 3$). The detection limit of the phosphorus in AMP using electrospray-FPD is 1 ng P/s based on $S/N_{p-p} = 2$. The comparison of the two mass detection limits demonstrates the ability and potential of the electrospray-FPD as an inexpensive and simple technique.

5.3.3.1.3 The effect of sample flow rates on the signal to noise ratio

The effect of sample flow rates on the signal to noise ratio was explored by introducing the same amount of 1.1 mM AMP at varying flow rates and monitoring the phosphorus emission. Signal to noise ratio in different flows is calculated and then it is divided by the corresponding flows to evaluate the signal to noise ratio for the unit phosphorus mass flow. The result shown in Figure 5.13 suggests that signal to noise ratio improves with lower flows. At lower flow rates, electrospray produces smaller droplets and consequently higher sensitivity and signal to noise ratio. This experiment also demonstrates that in optimum experimental conditions, electrospray-FPD is able to perform at a very small sample flows typical of capillary column HPLC and capillary zone electrophoresis.

5.3.3.1.4 Noise of the baseline (blank)

In spectroscopy, the noise of the signal is related to the precision and detection limit of the method [132], because lower noise means better reproducibility. The lower the noise of the signal, the smaller the signal that can be determined, so the lower the detection limit [132]. In applying chromatography as a separation technique, the analyte appears as a peak, so near the detection limit it is the noise of the baseline that is important [167]. Therefore, the noise of the blank solution for the phosphorus measurement was investigated. The blank noise was smoothed by using a moving average filter with a varying number of data points in the window. The result is shown in Figure 5.14 and it suggests that the

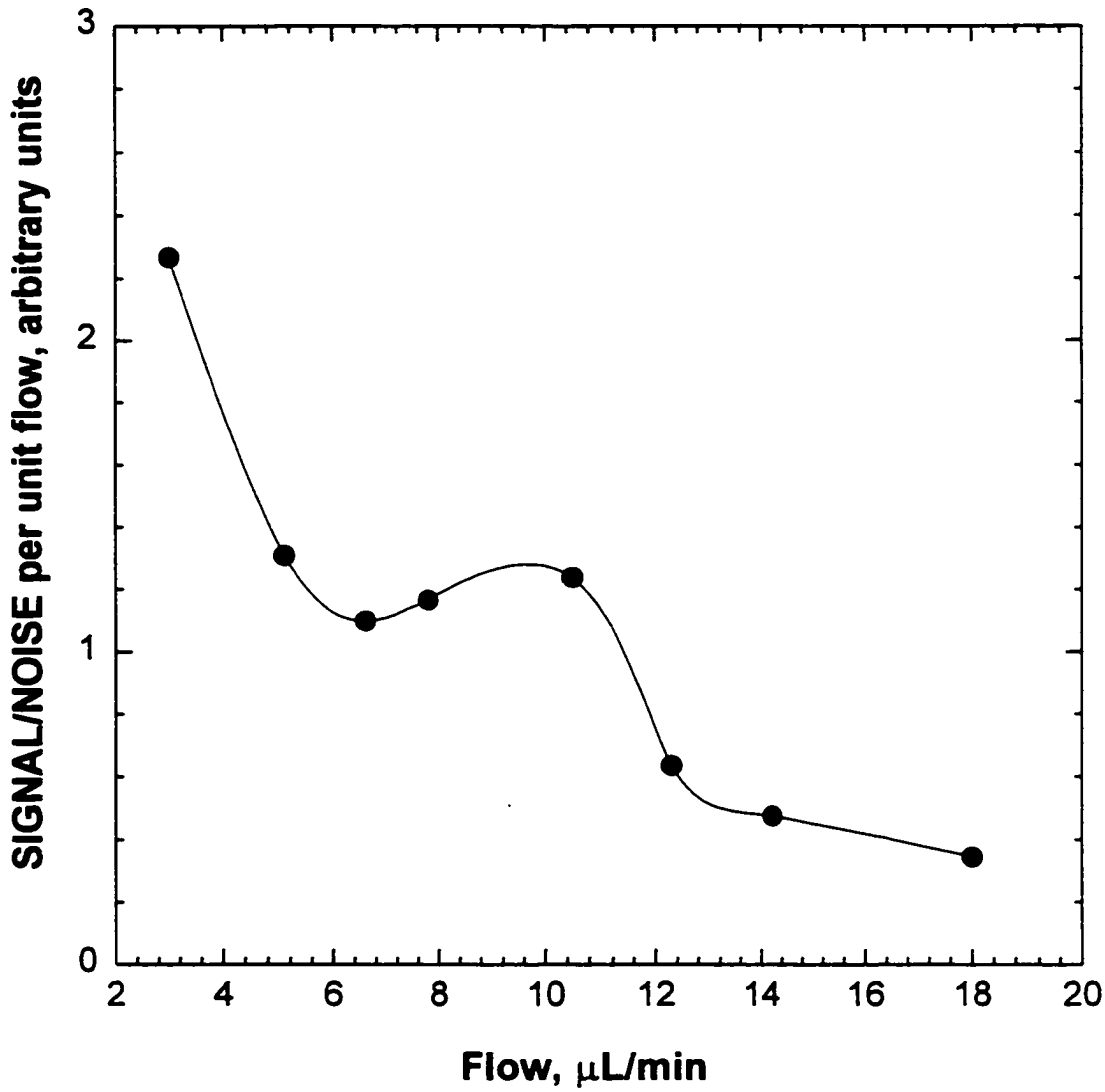

Figure 5.13 The effect of sample flow rates on signal to noise ratio of phosphorus emission.

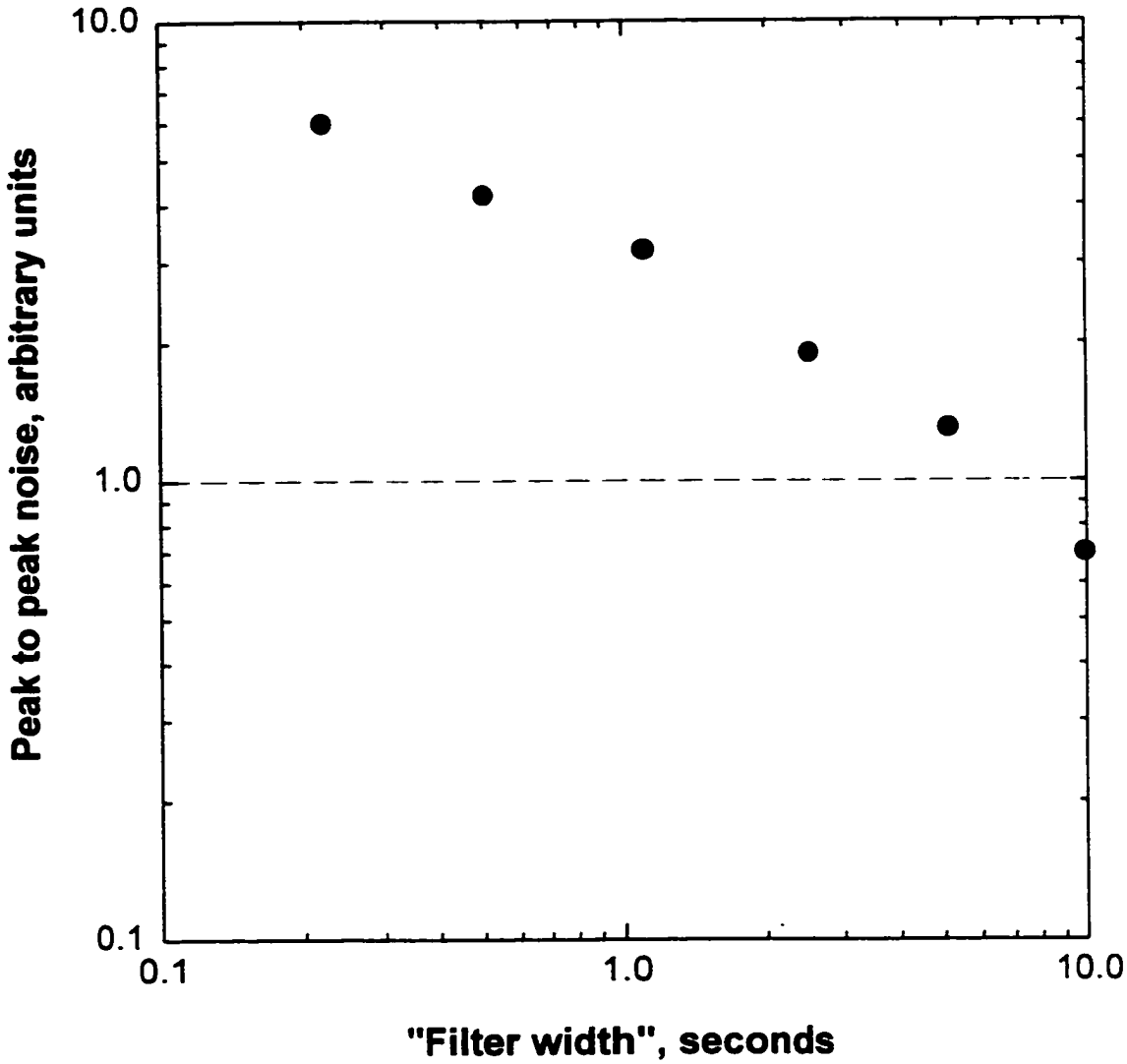

Figure 5.14 The effect of moving average filter width on baseline noise.

noise of the blank is white, since it is inversely proportional to the square root of the number of the data points in the window or, in other words, the time constant of the filter [135].

5.3.3.1.5 Quenching effects

Quenching of the HPO emission by carbon is a well known phenomenon in GC-FPD [71] and LC-FPD [67]. This quenching was investigated at constant AMP concentration (11.44 mM) and different carbon concentrations by adding normal propanol to the aqueous AMP solution. Phosphorus emission is monitored with a 524 nm interference filter and also with a 510 nm (9-nm band pass) interference filter. The response ratio (response with adding propanol/response without adding propanol) is shown in Figure 5.15. The result shows that the quenching in the electrospray-FPD is approximately the same as that in GC-FPD. Quenching in the FPD is a poorly understood phenomenon and there is controversy over mechanism. It is not clear whether the quencher quenches the exited analyte or the flame species which participate in chemiluminescence reaction.

5.3.3.2 COPPER

Figure 5.16 shows the luminescence spectrum of a copper chloride solution containing lithium dodecyl sulphate as a surfactant. As previously noted, the features of the spectrum can be interpreted from the work of Pearse and Gaydon [125]. A strong diffuse band (535-555 nm), and a weaker band (615-525 nm)

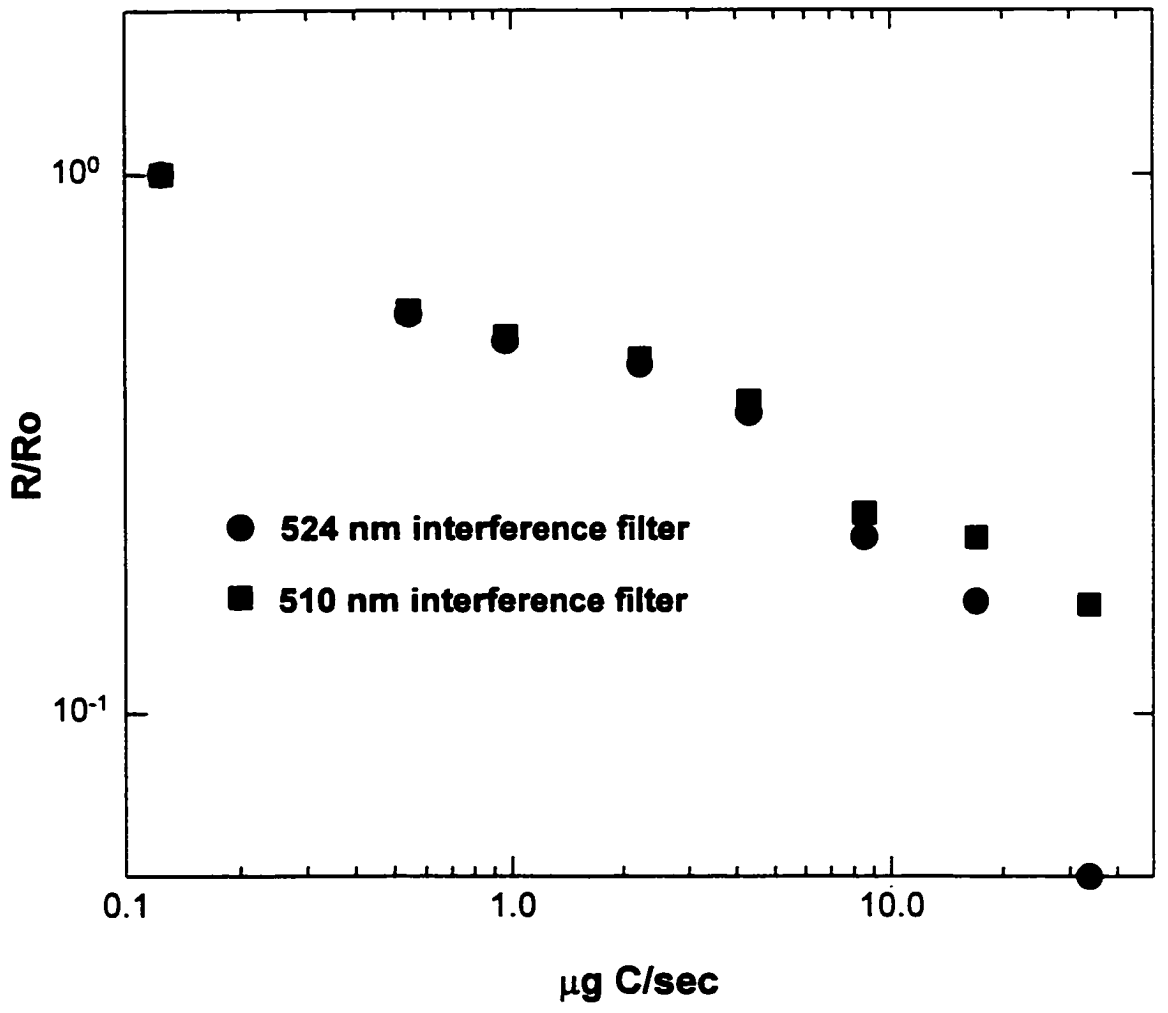

Figure 5.15 Quenching of phosphorus emission by carbon (n-propanol)

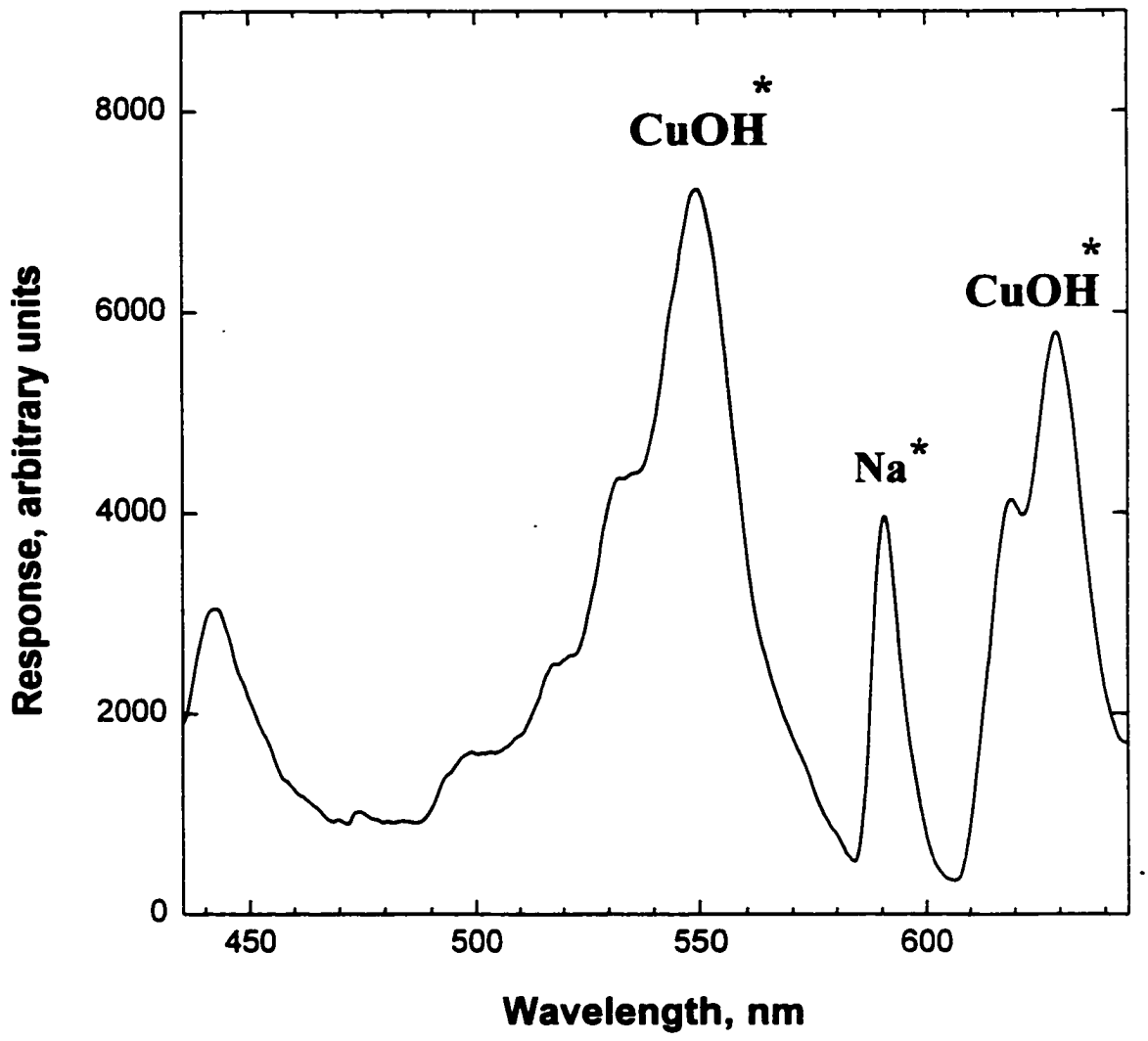

Figure 5.16 Emission bands obtained from copper chloride in aqueous solution.

appears for CuOH. The sodium emission in the spectrum originates from distilled water or contamination. Improved analytical sensitivity is obtained if an interference filter is used that has a bandpass in the range of 535-555 nm. The recorded signal from the copper emission using a 540 nm interference filter with a 9 nm bandpass is shown in Figure 5.17. The injection volume was about 110 µL. Copper shows a very good response using electrospray-FPD. In the following sections, the experimental conditions and calibration curve are described.

5.3.3.2.1 Experimental conditions

The experimental conditions used to obtain the calibration curve were:

Hydrogen: 260 mL/min; Air: 175 mL/min; Nitrogen: 270 mL/min; Voltage: 4200 V; Interference filter: 540 nm (9 nm bandpass); Sample flow rate: 10.5 µL/min; PMT type and voltage: R-268 and 500 V. Time constant of the analog filter: 1.8 seconds. A 540-nm interference filter with a 9-nm bandpass was used to monitor the CuOH emission.

5.3.3.2.2 Calibration curve

The calibration curve is shown in Figure 5.18. The detection limit, based on a signal level which is twice the peak to peak fluctuation of the blank solution, is 0.6 ng Cu/s. If the standard deviation of the noise is considered, the spectroscopic detection limit can be calculated based on $S/\sigma=3$ (IUPAC definition). However it

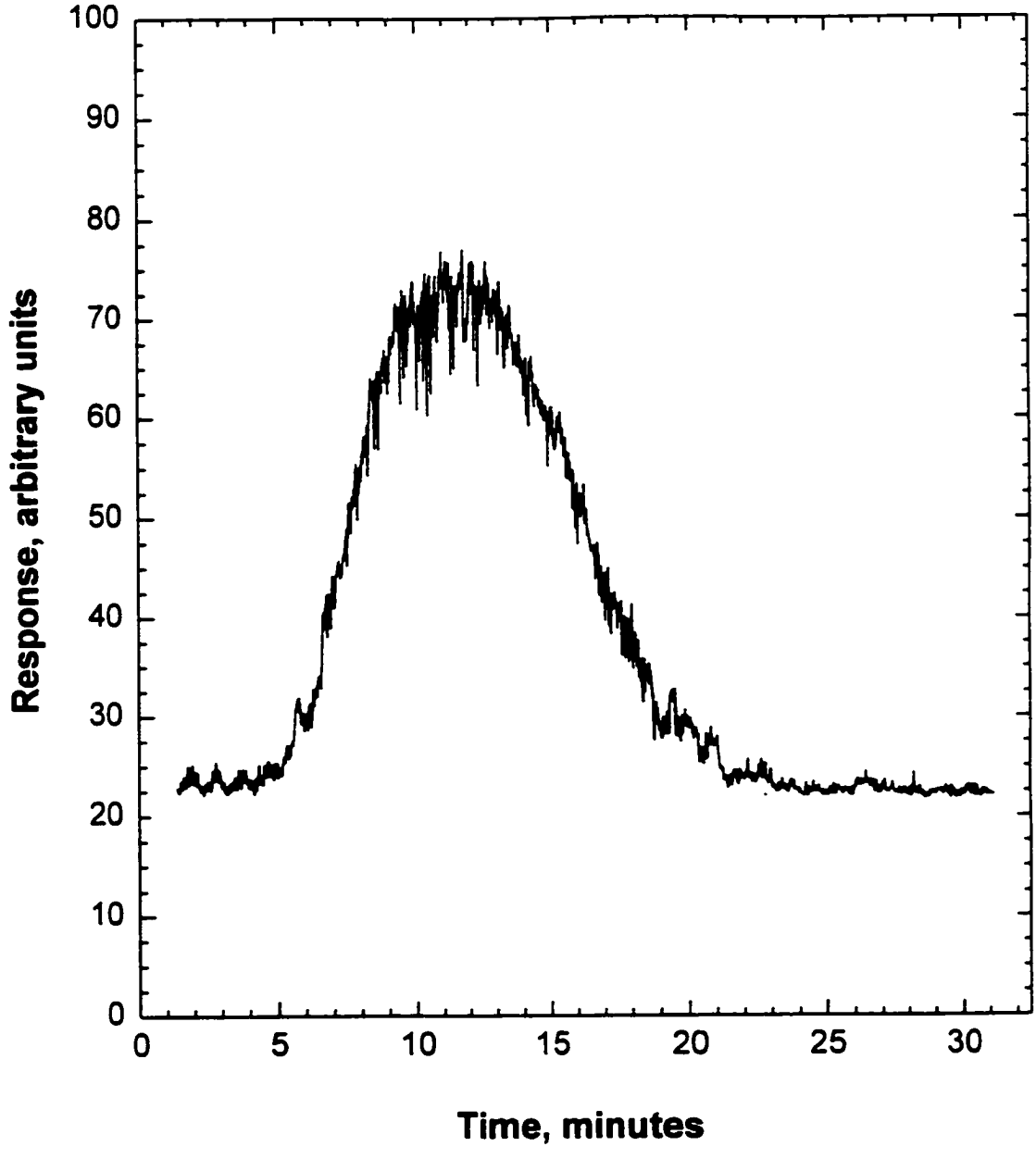

Figure 5.17 Emission at 540 nm (interference filter) from an aqueous solution of copper chloride.

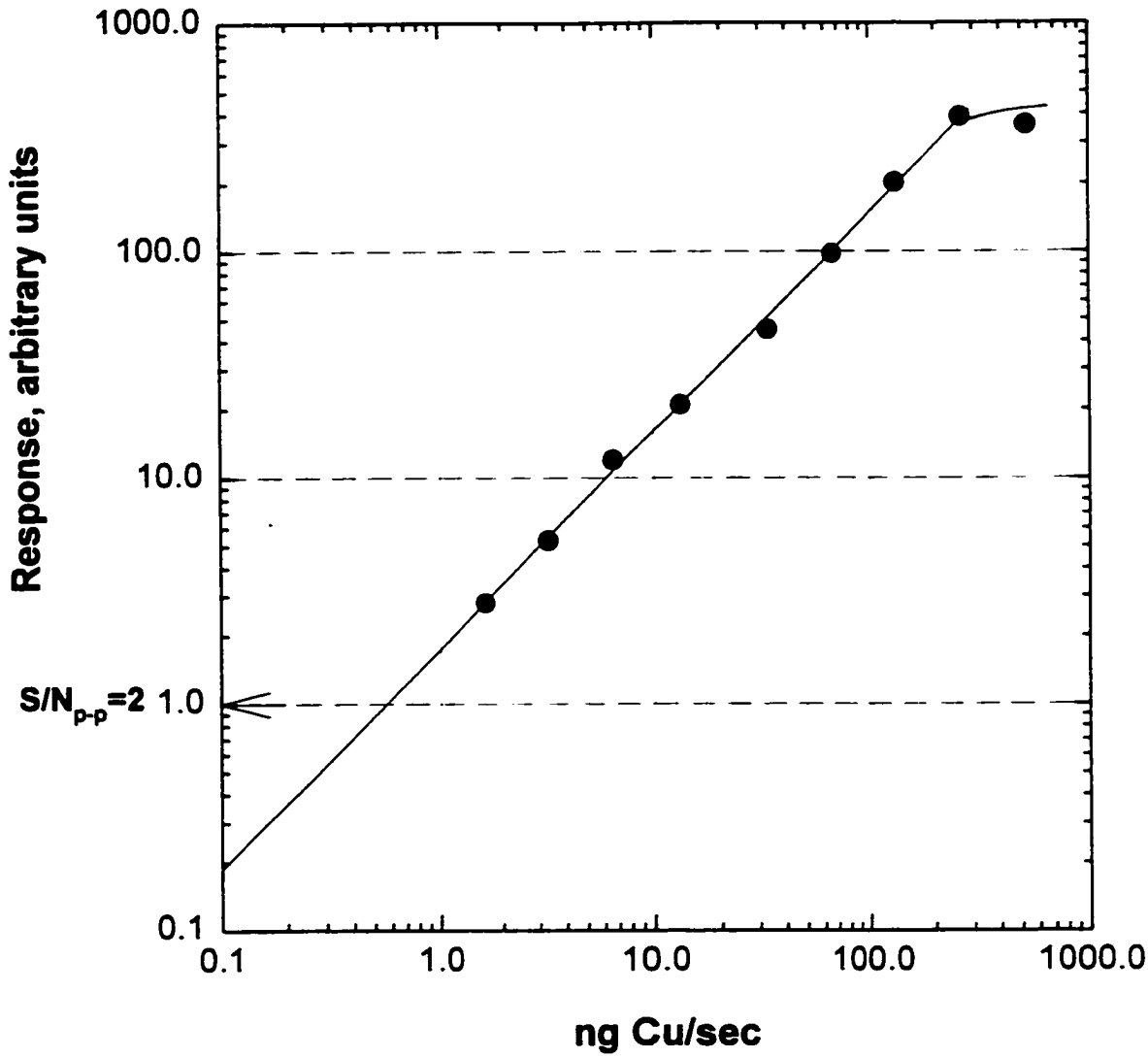

Figure 5.18 Calibration curve for copper chloride. Experimental conditions are in the text.

should be noted that the peak to peak noise is larger than the standard deviation of the noise by a factor of 5 to 6.8, depending on the time constant of the filter [135]. The mass detection limit of copper by using HEN in ICP is 1.2 µg Cu/L or 1 pg Cu/s [27]. It is clear that the detection limit for copper by ICP is superior to that by electrospray-FPD. However, this is the first report on the analytical utility of the FPD for ionic compounds. This experiment also shows that electrospray-FPD is useful not only for nonmetals such as phosphorus, but also for metals such as copper.

5.3.3.2.3 The effect of sample flow rates on signal to noise ratio

A constant concentration of copper chloride solution (2.4 mM) was used to investigate the effect of sample flow rates between 3 µL/min and 18 µL/min on the S/N. The calculated S/N at any flow rate then is divided by the same flow rate to compare the S/N at a unit sample flow rate. The result is shown in Figure 5.19 and it shows that at lower flows, the S/N is higher. The reason, as previously noted, is the production of smaller droplets by the electrospray at lower flow rates and consequently a higher sensitivity and signal.

5.3.3.3 MANGANESE

The luminescence spectra from manganese chloride and also SDS as the blank is shown in Figure 5.20. The manganese spectrum does not have spectral interference from the blank. The emission at 403 nm corresponds to the two

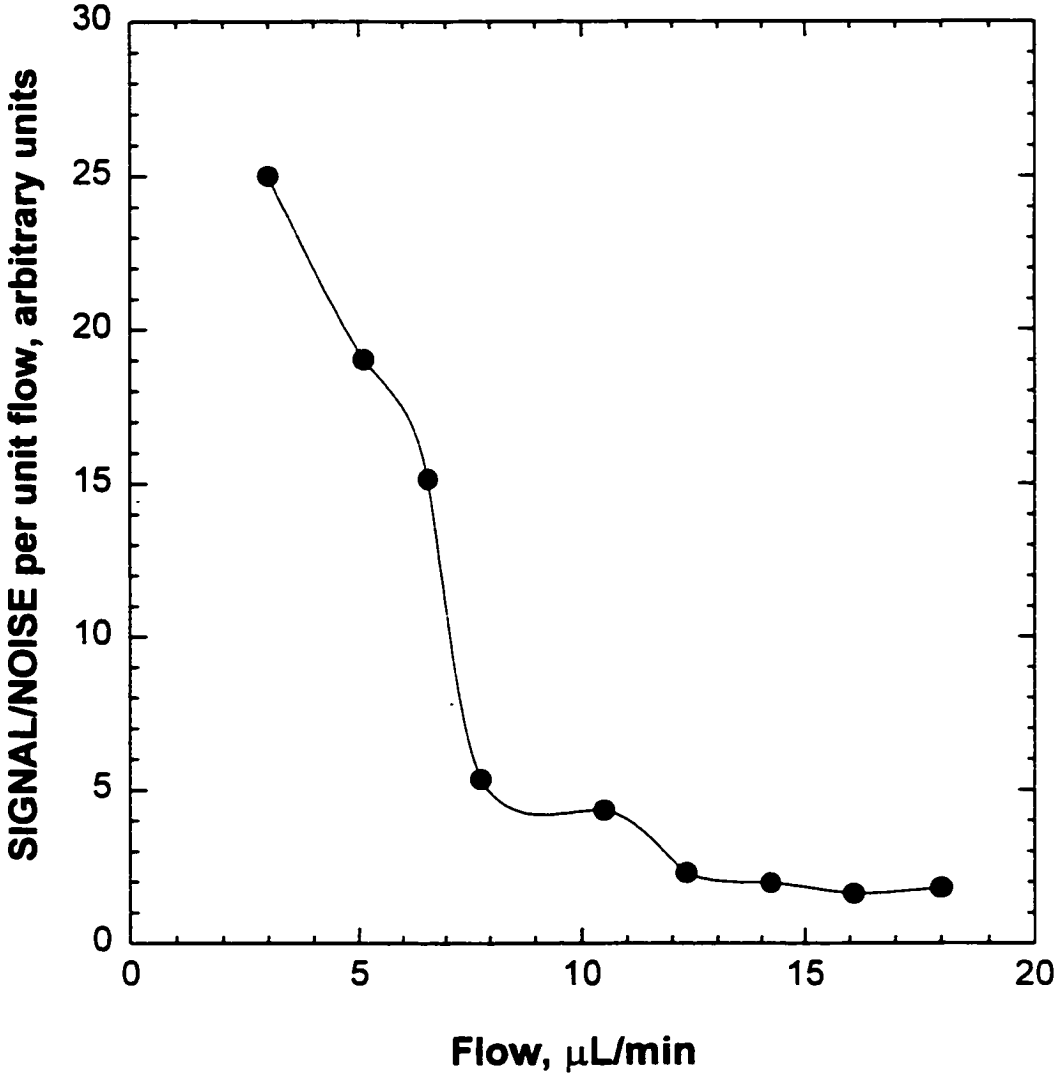

Figure 5.19 The effect of sample flow rates on signal to noise ratio of copper emission.

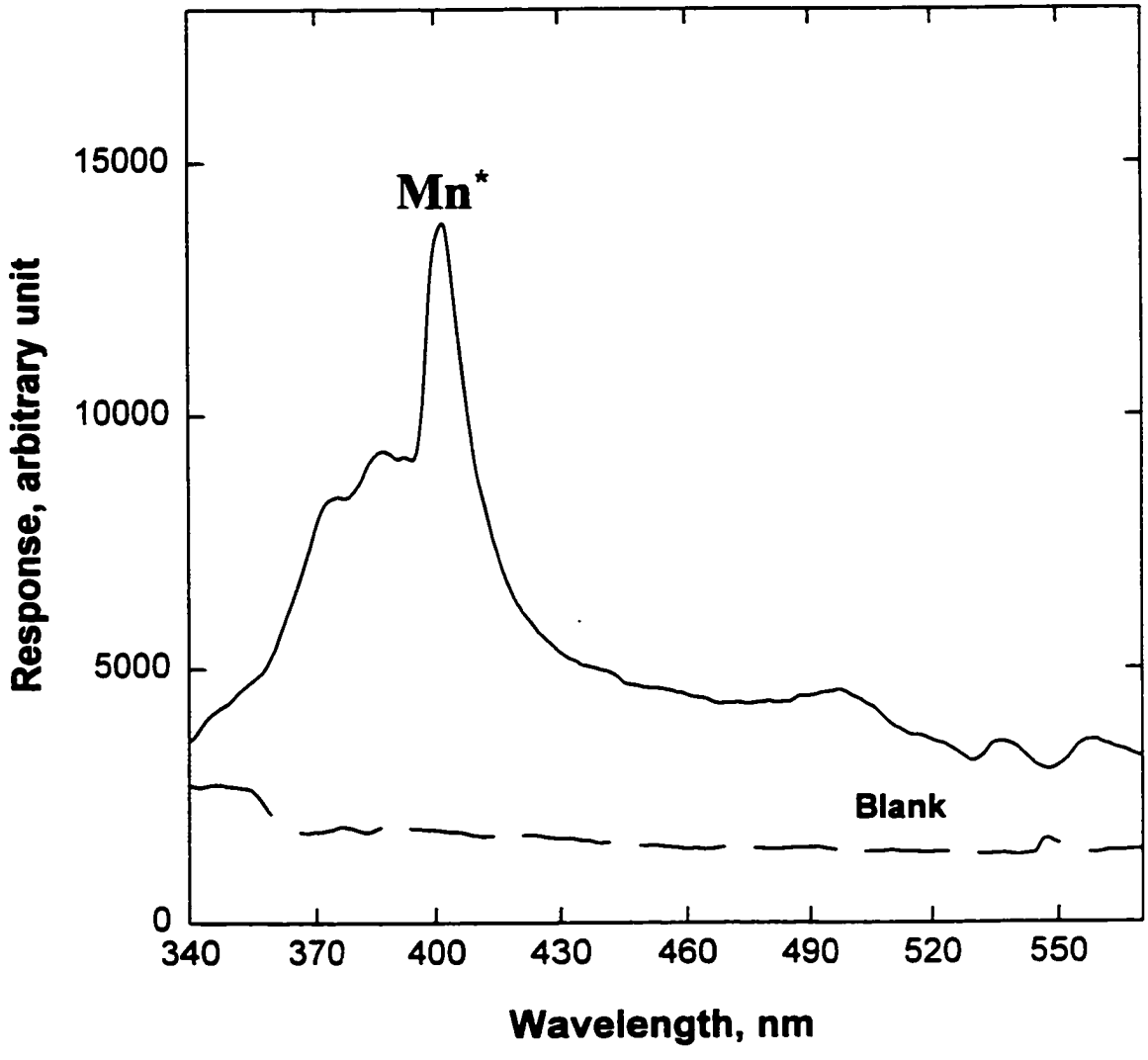

Figure 5.20 Spectrum from manganese chloride in aqueous solution.

strongest lines of atomic manganese, at 403.076 and 403.307 nm (also to the strong line at 403.449) [127]. According to Pearse and Gaydon [125], a system of diffuse bands at 350-400 nm originates from MnOH in an oxy-hydrogen flame containing manganese salts. In the present spectrum, this range of emission is observed, and it might be due to MnOH. The combined 403 nm lines offer the greatest sensitivity in the FPD [127]. The 405 nm interference filter was used to determine the detection limit by considering the peak to peak noise. Figure 5.21 shows the time profile of manganese emission obtained at 405 nm. For $S/N_{p-p}=2$ the detection limit was 1.1 ng Mn/s. The mass detection limit of manganese by using the HEN in ICP is 0.37 µg Mn/L or 0.3 pg Mn/s [27]. The data in Figure 5.22 show the correlation of signal for sodium emission (SDS) and manganese emission. Clearly, noise on the analytical signal (manganese) and noise on the reference signal are well correlated. As stated earlier, SDS not only decreases the surface tension of the solution, but it can also be used as an internal standard to reduce the correlated noise on the signal.

5.3.3.4 SILVER

The spectra of silver nitrate and sodium nitrate (blank) in aqueous solution are shown in Figure 5.23. Silver showed its characteristic line at 328 nm. Thus, silver produces an emission response in this small hydrogen-rich type flame for electrospray sample introduction.

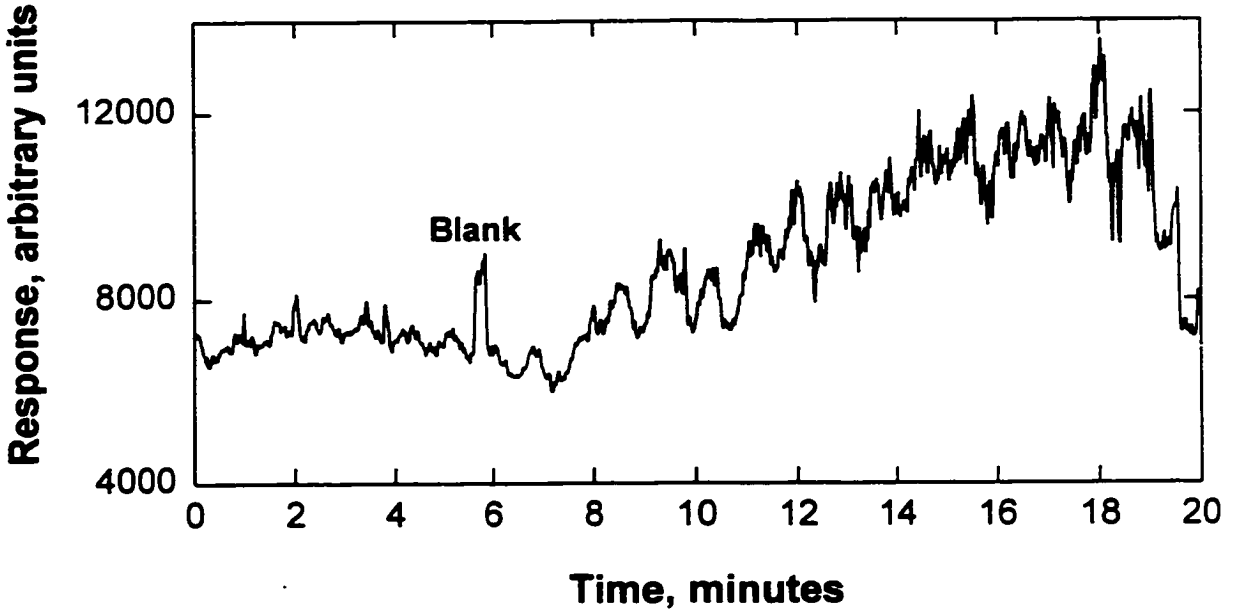

Figure 5.21 Emission at 405 nm (interference filter) from an aqueous solution of manganese chloride. Sample flow rate: 3.1 ng Mn/s.

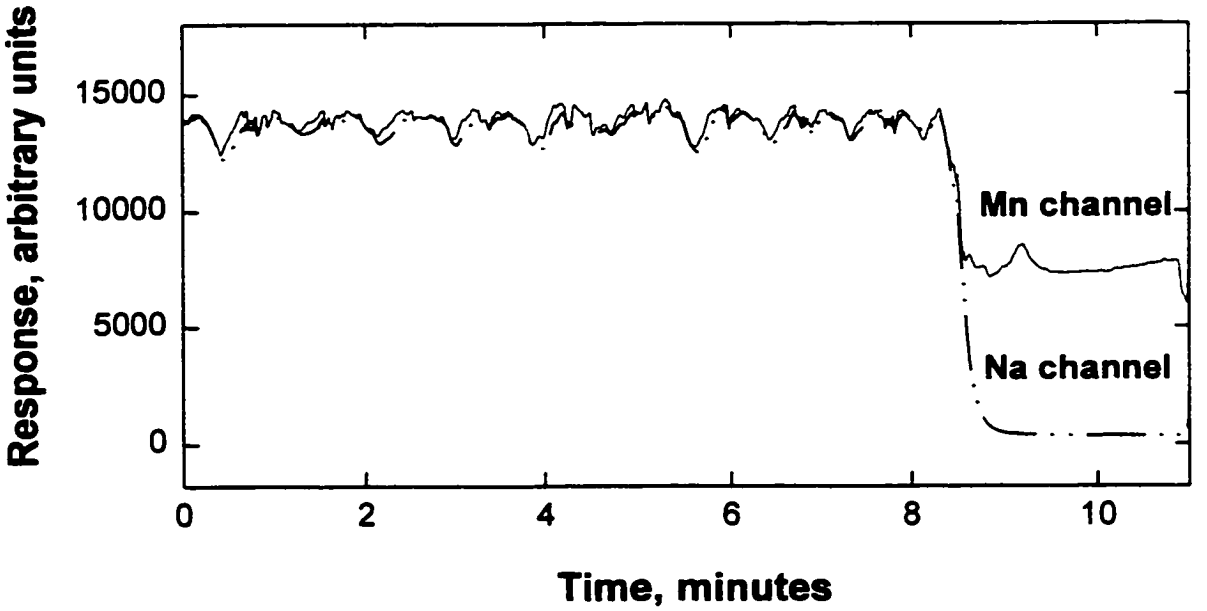

Figure 5.22 Mn channel: Emission at 405 nm from solution of manganese chloride. PMT type and voltage: R-374 and 600 V; Sample flow rate: 11.9 Mn/s. Na channel: Emission at 600 nm (WB interference filter) from solution of sodium dodecyl sulphate. PMT type and voltage: R-268 and 445 V; Sample flow rate: 19.5 ng Na/s; Hydrogen: 130 mL/min; Air: 176 mL/min; Nitrogen: 330 mL/min; Voltage: 4400 V.

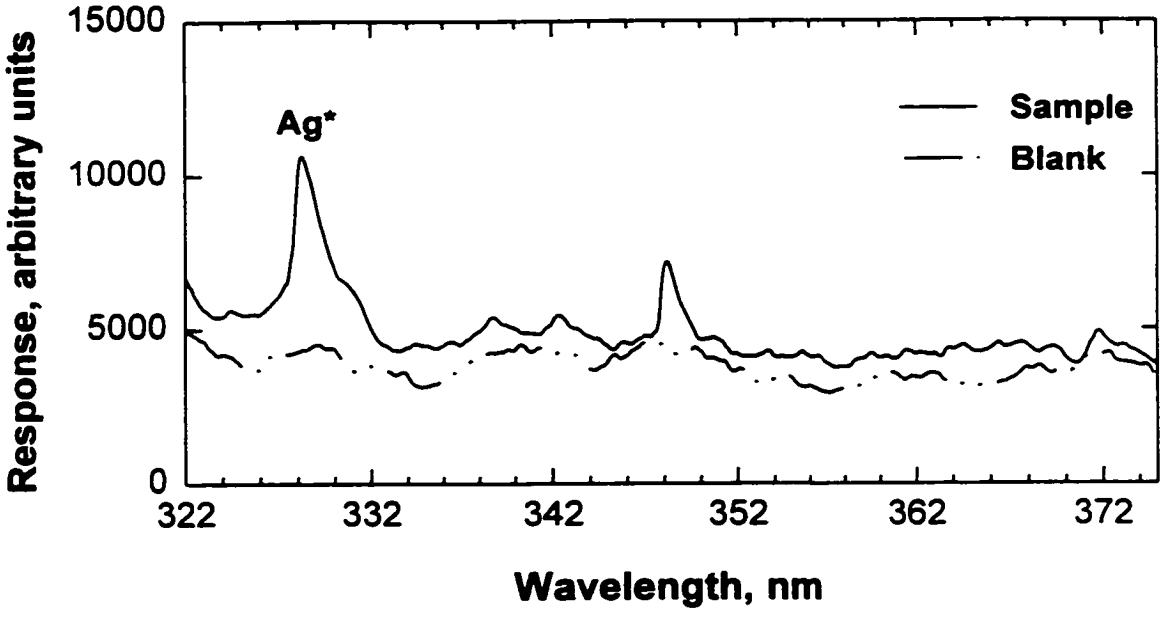

Figure 5.23 Spectrum from silver nitrate in aqueous solution.

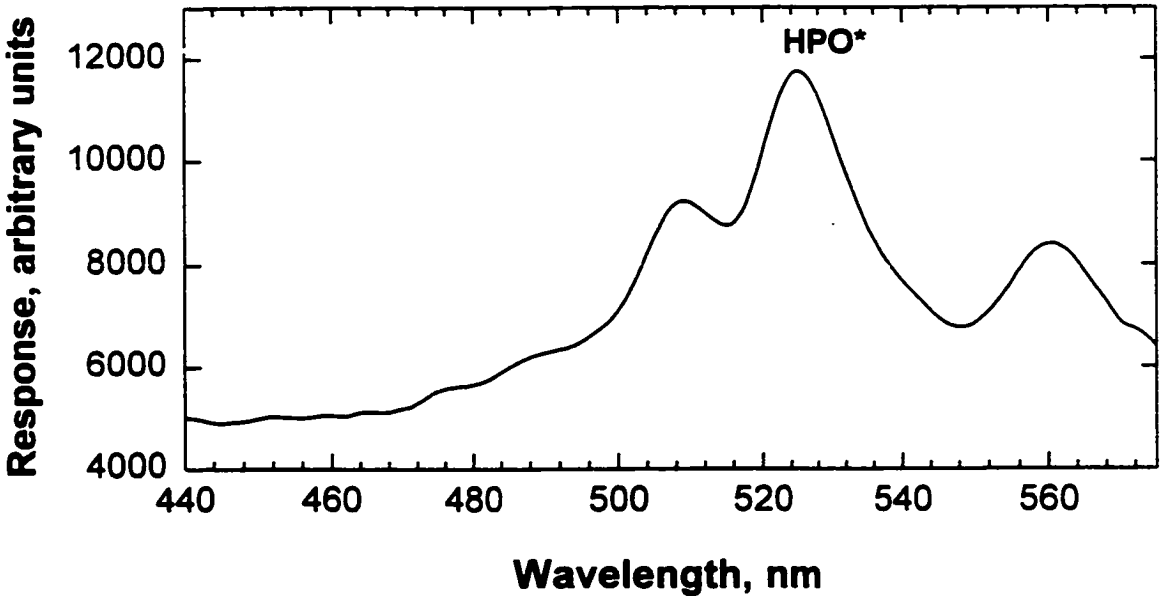

Figure 5.24 Emission obtained from disodium hydrogen phosphate in aqueous solution.

5.3.3.5 PHOSPHORUS

The spectrum of phosphorus from disodium hydrogen phosphate is shown Figure 5.24. This spectrum appeared at a relatively high hydrogen flow rate.

5.3.3.6 CADMIUM

Figure 5.25 shows the first and second order of the cadmium emission lines at 326.1 nm and 652.2 nm respectively. The monochromator was set at 326.1 nm to record the emission time profile illustrated in Figure 5.26. The detection limit was 7.2 ng Cd/s for a S/N_{p-p} of 2.

5.3.3.7 INDIUM

Indium chloride in aqueous solution (SDS) was introduced into the flame and the spectrum shown in Figure 5.27 was obtained. Two indium lines at 410 and 451 nm appeared in the spectrum. Based on the indium chloride spectrum [168], the 355.6 nm band may be present. However, the 359.9 nm indium chloride band was not apparent. The detection limit of indium was determined by using a combination of two filters (cut-off at 500 nm and cut-on at 345 nm). In these conditions, the detection limit was 17.7 ng In/s for S/N_{p-p} of 2.

5.3.3.8 SCANDIUM

Spectra of scandium in nitric acid (2%) solution and a blank solution (2% nitric acid) are shown in Figure 5.28. According to Alkemade and Herrmann [126],

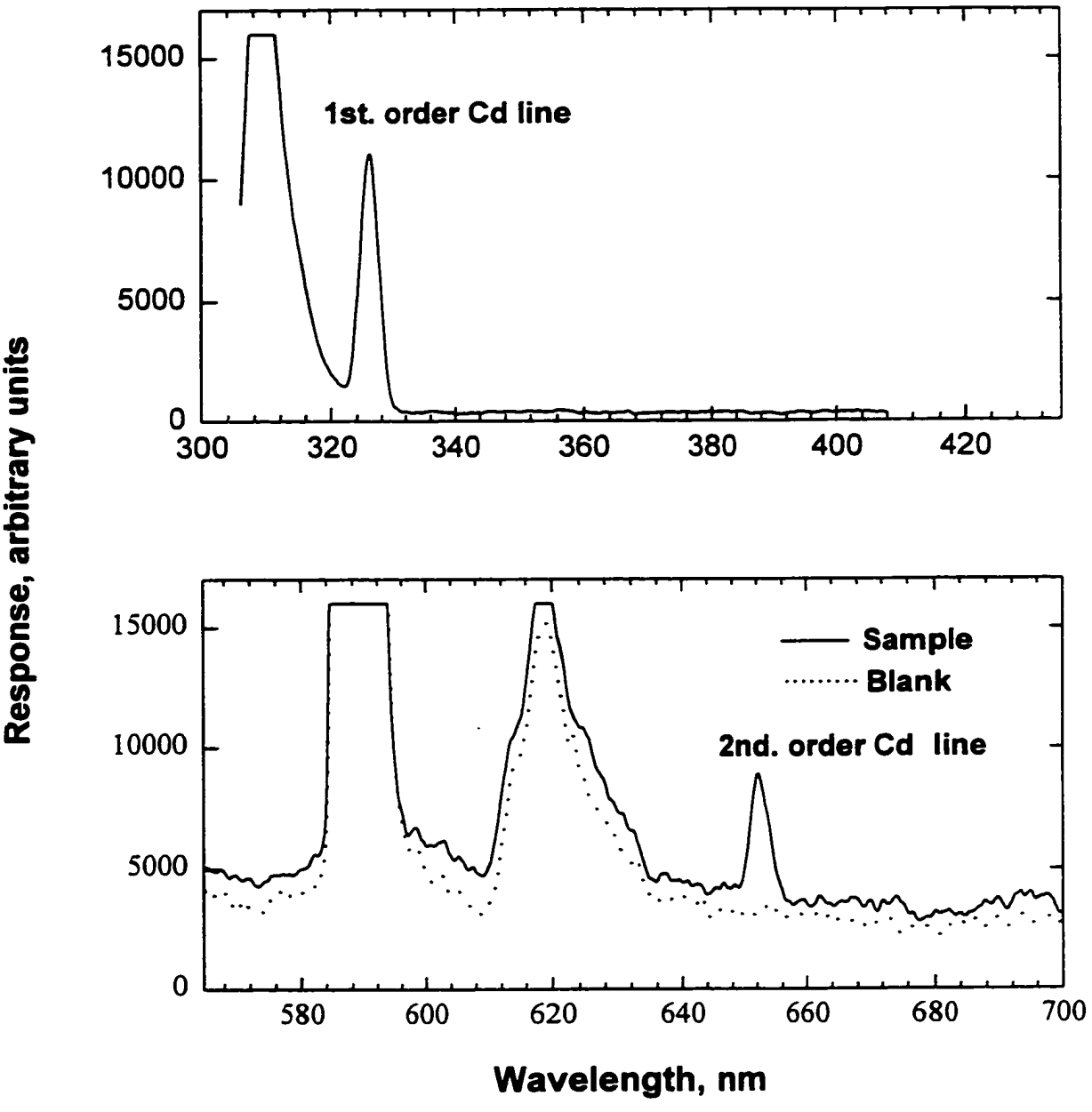

Figure 5.25 Spectrum from cadmium chloride in aqueous solution.

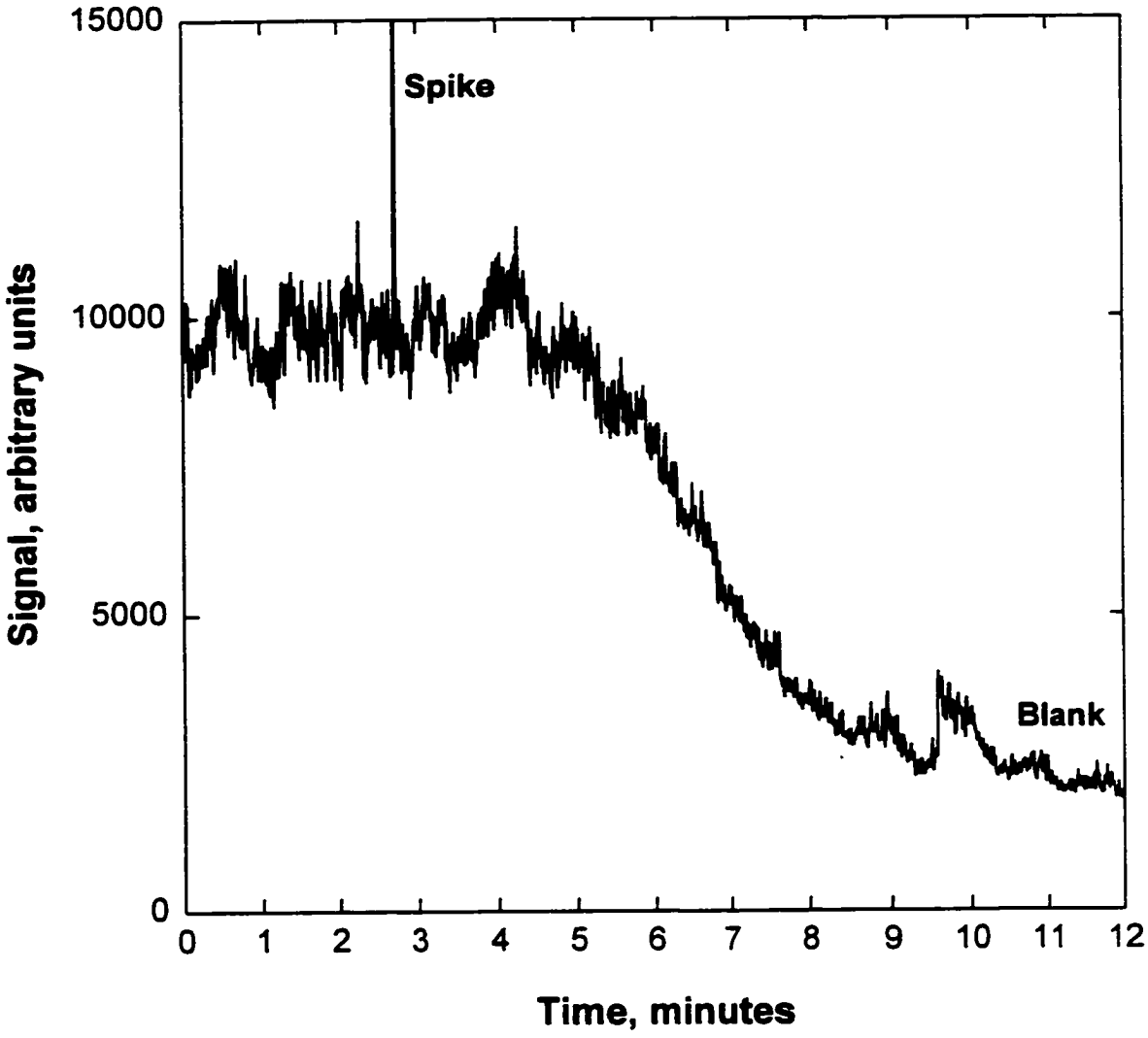

Figure 5.26 Emission at 326.1 nm from an aqueous solution of cadmium chloride.

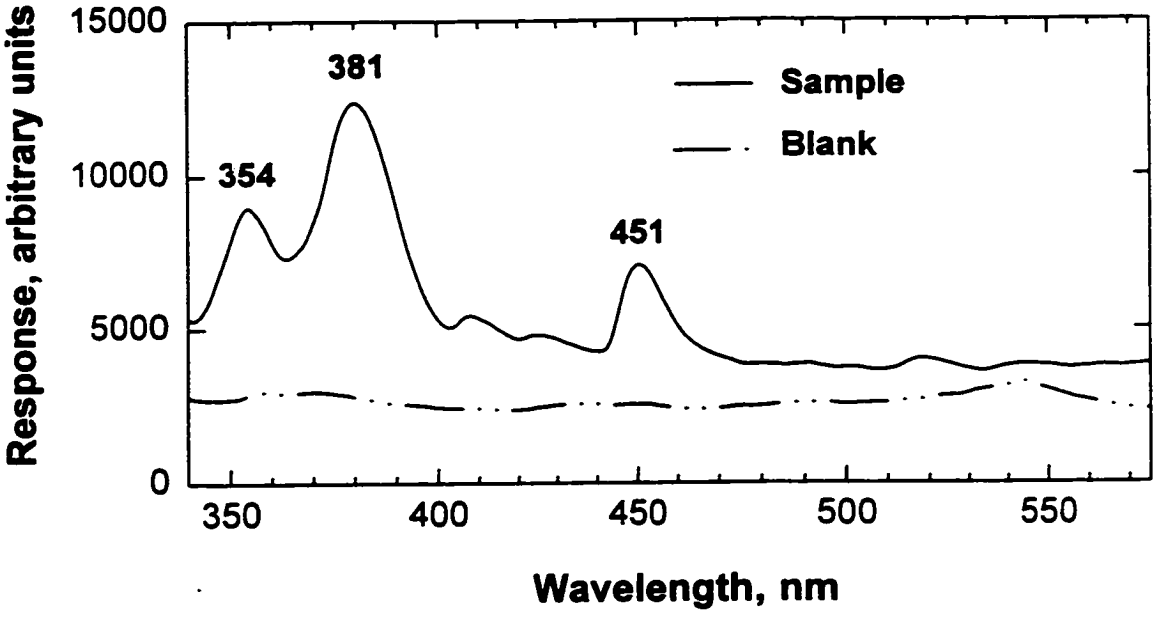

Figure 5.27 Spectrum from indium chloride in aqueous solution.

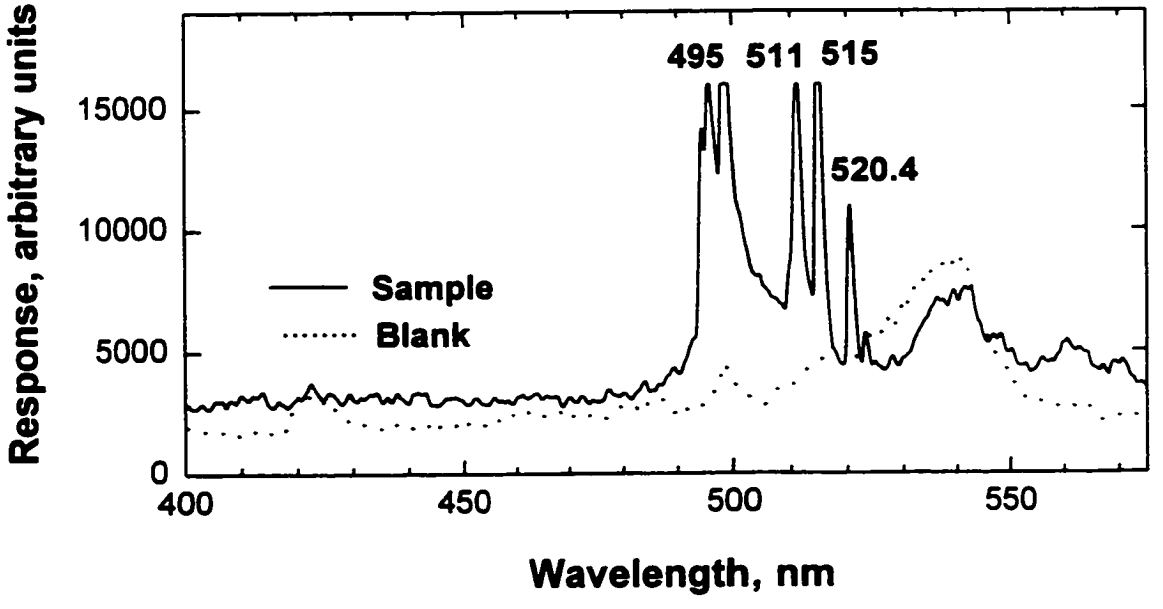

Figure 5.28 Emission obtained from scandium in 2% nitric acid solution.

scandium emissions (lines/bands) in oxy-hydrogen flames appear at 509.7 nm and 517.1 nm and 520.9 nm for nonaqueous solvent. These lines/bands arise from ScO and Sc (520.9). The features in Figure 5.20 correspond to these wavelengths.

5.3.3.9 MAGNESIUM

The magnesium spectrum is shown in Figure 5.29. Based on Pearse and Gaydon [125], magnesium oxide has a complex system of bands in the region 364-396 nm with heads degraded in both directions. Some, but not all, of these bands are due to a transition of MgO. For the same flame, MgOH exhibits two groups of diffuse bands around 370-383 nm [125]. The present spectrum shows emissions at these wavelengths; they are likely to belong to MgO and MgOH.

5.3.3.10 BARIUM

According to Pearse and Gaydon [125], when barium salts are introduced into a flame, BaO emission bands are observed. These bands are illustrated in Figure 5.30 at 570, 549, 534, 508, 485 nm. Therefore, the spectrum probably arises from BaO emissions.

5.3.3.11 SELENIUM

The spectrum of selenium dioxide in aqueous solution was determined and was found to be similar to the sulphur spectrum in Figure 5.9. The spectrum of

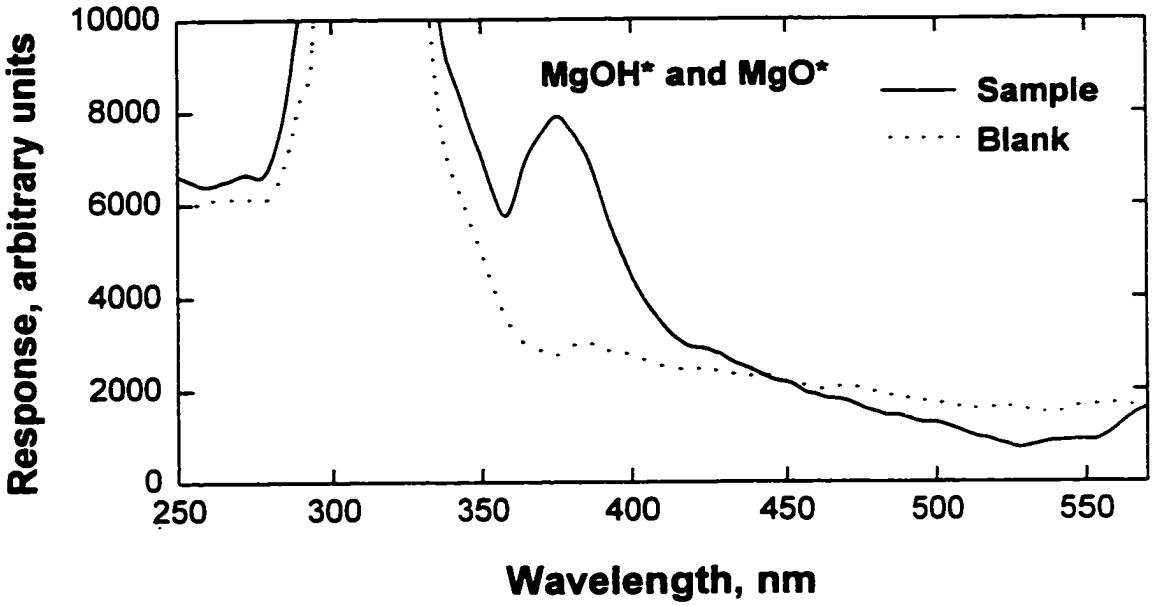

Figure 5.29 Emission obtained from magnesium chloride in aqueous solution.

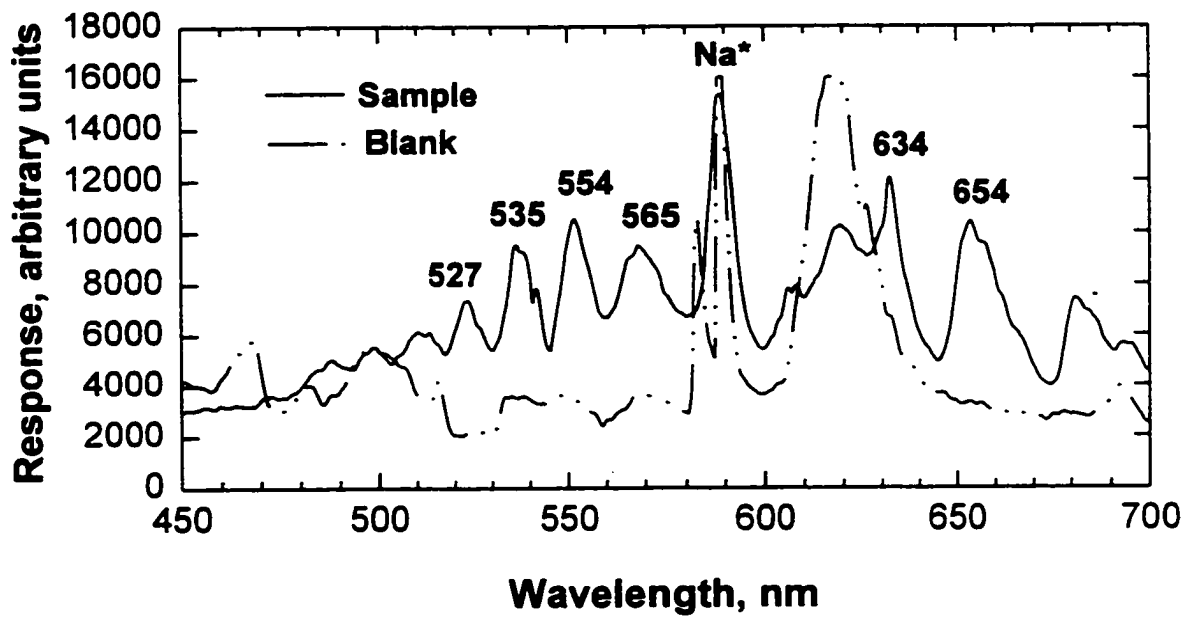

Figure 5.30 Molecular band emission from barium chloride in aqueous solution.

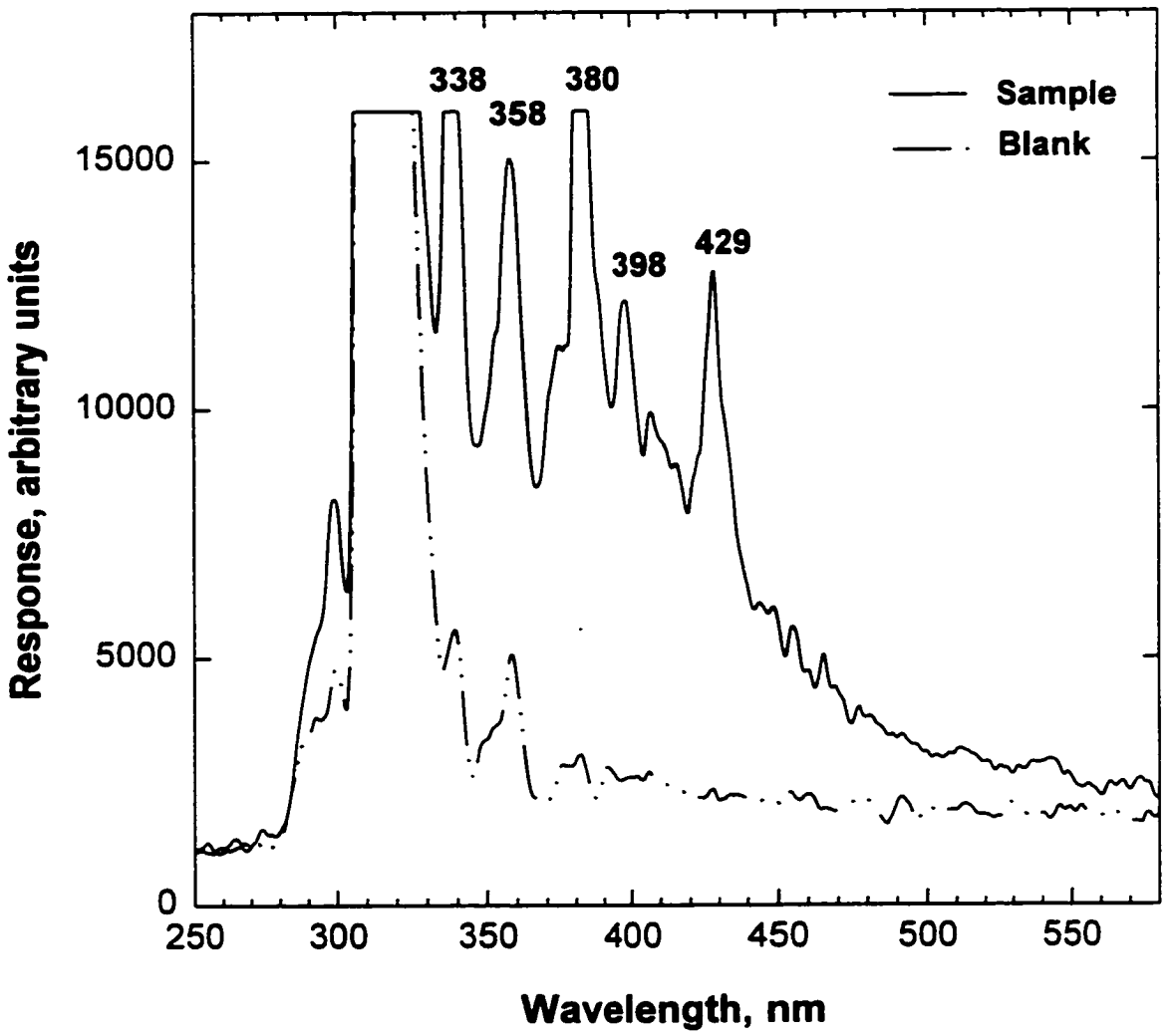

Figure 5.31 Emission spectrum from selenium oxychloride in aqueous solution.

selenium oxychloride in aqueous solution was also determined and is shown in Figure 5.31. In the FPD, Se_2 band emissions occur between 460 nm and 562 nm [169,170]. The spectrum shown differs from that of Se_2. Asundi and coworkers [171] recorded bands of the SeO spectrum, some of which occur at: 339.48, 357.65, 367.77, 372.52, 376.81, 382.28, 385.75, 390.75, 394.98 and 399.72 nm. A number of these bands (338, 358, 398) appear in Figure 5.24 and the spectrum might therefore originate from SeO emissions.

5.3.3.12 BORON

The boron spectrum from boric acid in the oxy-hydrogen flame has been recorded [172]. The spectrum shown in Figure 5.32 includes bands at 471.5, 493, 495, 518 and 547.6 nm. Based on Pearse and Gaydon [125], narrow emission bands are observed in an arc or flame when boric acid is introduced. Maxima at 639, 620, 603, 580, 545, 518, 493, 471, 452 nm arise from BO_2. The BO bands are usually present as well. A boron spectrum [45] is a mixture of molecular band emissions of BO (from transition of $A^2\Pi \longrightarrow X^2\Sigma^+$) and BO_2 (from transition of $A^2\Pi_u \longrightarrow A^2\Pi_g$). A 546 nm peak wavelength interface filter has been used to measure boron hydrides using the FPD [173].

5.3.3.13 ARSENIC

The continuum spectrum shown in Figure 5.33 is due to the introduction of arsenic pentoxide into the flame. Some continuum spectra for arsenic with a

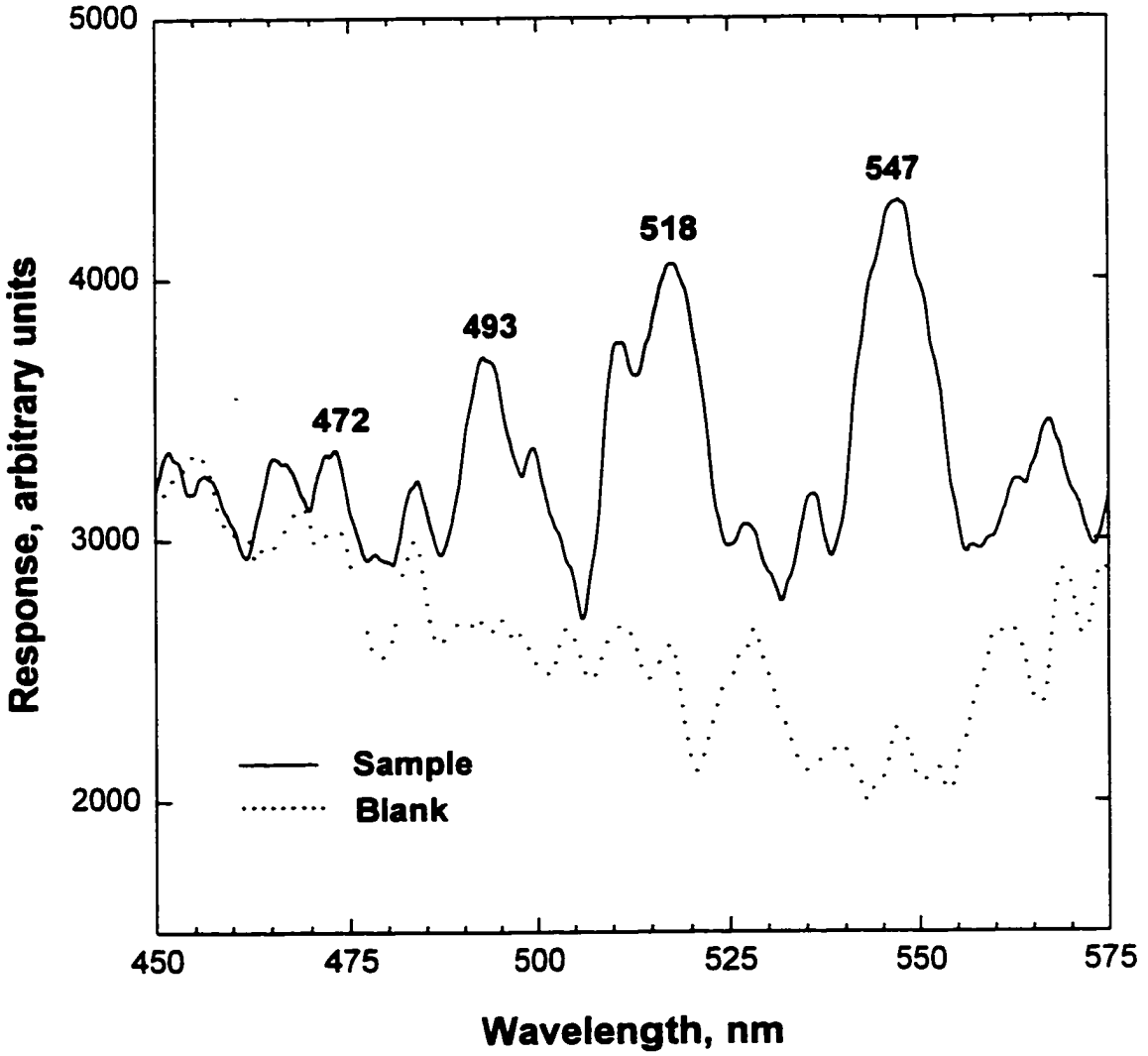

Figure 5.32 Molecular band emission obtained from boric acid in aqueous solution.

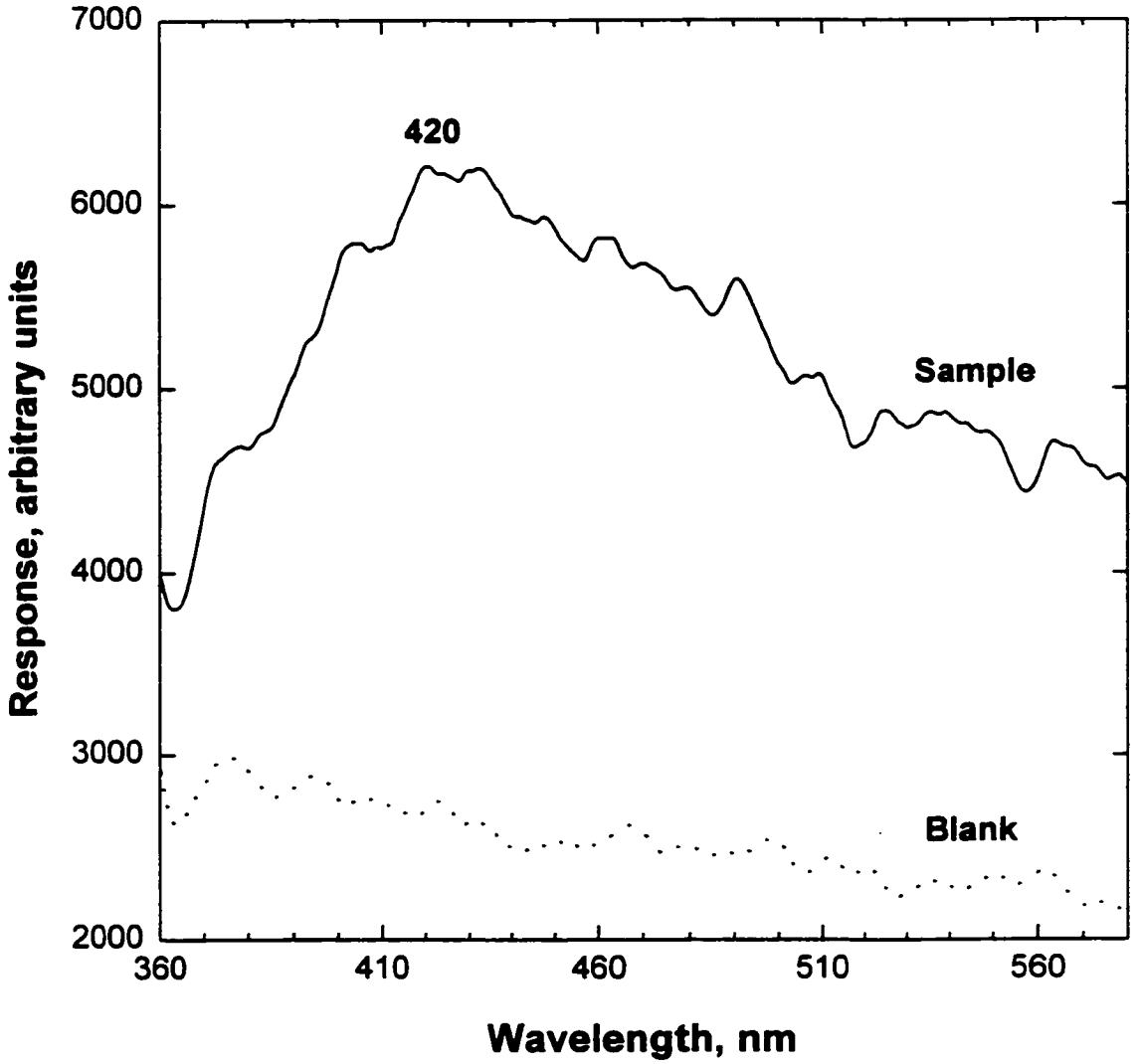

Figure 5.33 Continuum spectrum from arsenic acid (arsenic pentoxide) aqueous solution.

maximum at 460 nm or 500 nm (analytical flame spectroscopy) have been previously reported [172]. The emitting species is believed to be AsO [174]. Aue and Sun [45] reported an arsenic spectrum by introducing triphenyl arsine into the FPD and the spectrum was a continuum with maximum around 550 nm. The As spectrum in Figure 5.26 is a continuum with maximum emission at 420 nm.

5.3.3.14 NICKEL

The spectra of nickel chloride in aqueous solution, with SDS used as a surfactant, and the blank are shown in Figure 5.34. Nickelocene as a volatile compound has shown response in GC-FPD, but no emitter was identified [46]. The atomic line of nickel appears at 352.4 nm. Several systems of NiO occur between about 500 and 750 nm [125]. The spectrum between 350 and 470 nm probably belongs to NiCl because these features were not observed in a nickel acetate scan. Under conditions listed for Figure 5.34, it is difficult to assign each molecular band emission to a particular molecule. However, NiCl, NiO and NiH should be considered as candidates for producing much of the emission in the visible region of the spectrum. The detection limit of nickel was determined, using a 540 nm interference filter with a 9 nm bandpass, as 1.4 ng Ni/s for S/N_{p-p} of 2. The mass detection limit of nickel, by using the HEN in ICP, is 1.7 pg Ni/s [27].

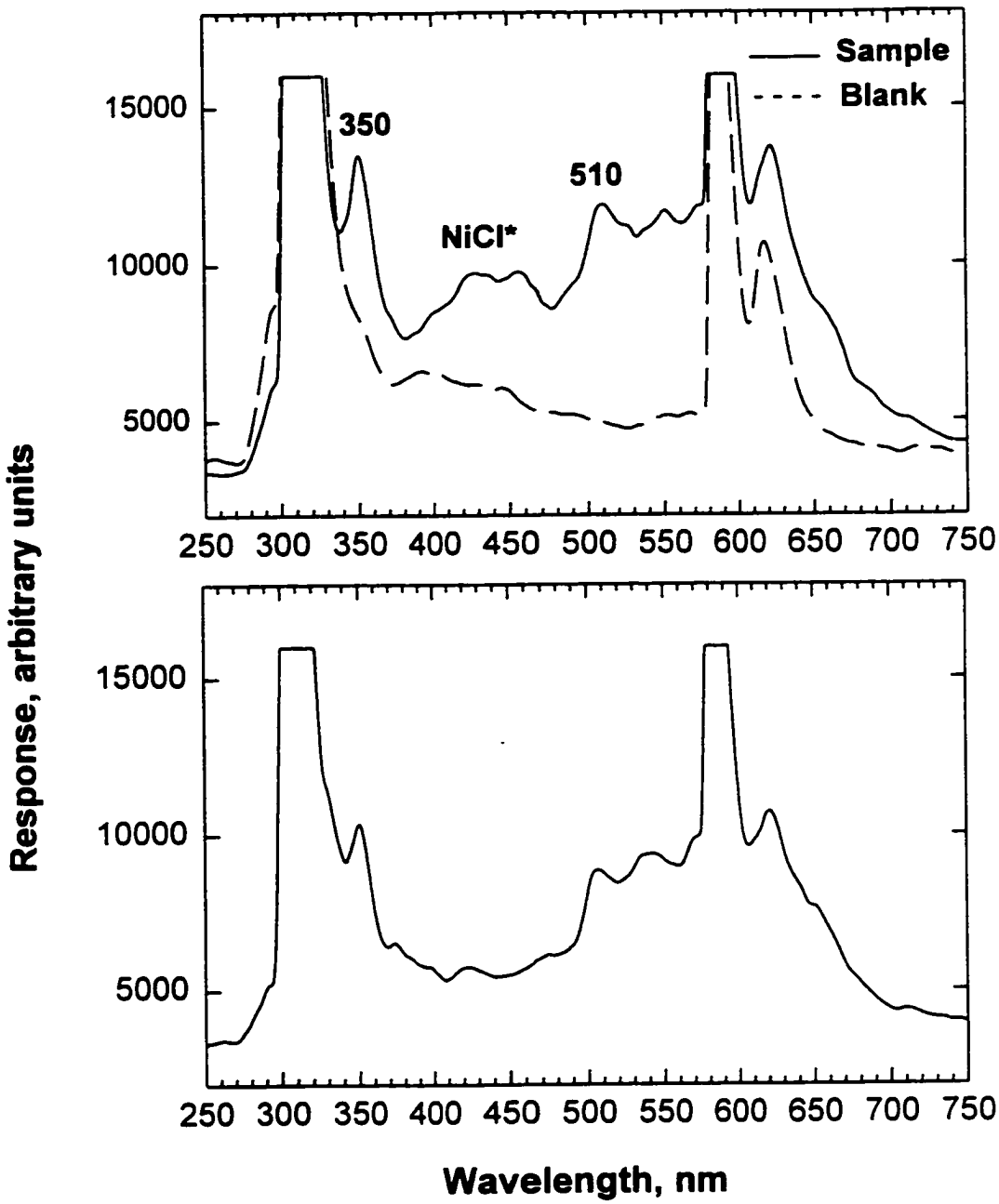

Figure 5.34 Comparison of spectra of nickel chloride (top) and nickel acetate (bottom) at the same conditions.

5.3.4 PHOSPHORUS AND SULPHUR ANALYSIS IN THE BIOLOGICAL SAMPLES.

5.3.4.1 PHOSPHORUS

The application of the electrospray-FPD was demonstrated for the determination of phosphorus in nucleotides such as AMP. The analysis of phosphorus is important in biological samples such as deoxyribonucleic acid (DNA), ribonucleic acid (RNA) and phospholipids [163]. Spectra of phosphorus by introducing deoxyribonucleic acid (degraded free acid from herring sperm) and from lecithin (phosphatidyl choline) as nonvolatile phosphorus compounds are shown in Figures 5.35 and 5.36. The detection limit of phosphorus for lecithin is 2.3 ng P/s. The detection limit of phosphorus for lecithin is larger than the detection limit of phosphorus for AMP. In order to confirm that electrospray-FPD does not have any clogging problems, lecithin was introduced for fifty minutes. The recorded signal is shown in Figure 5.37, with the smoothed data (1201 and 2401 point moving averages) shown in the bottom two frames.

5.3.4.2 SULPHUR

The spectrum obtained by introducing unfractionated bovine bile (ox gall powder) is shown in Figure 5.38. Bile is a complex mixture of different compounds such as bile acid, bile pigment and cholesterol [175]. The spectrum was obtained by the direct introduction into the flame without surfactant because the bile salts and acids are natural surfactants. Figure 5.38 shows the sulphur spectrum accompanied by spectral interferences from components in the bile. Components

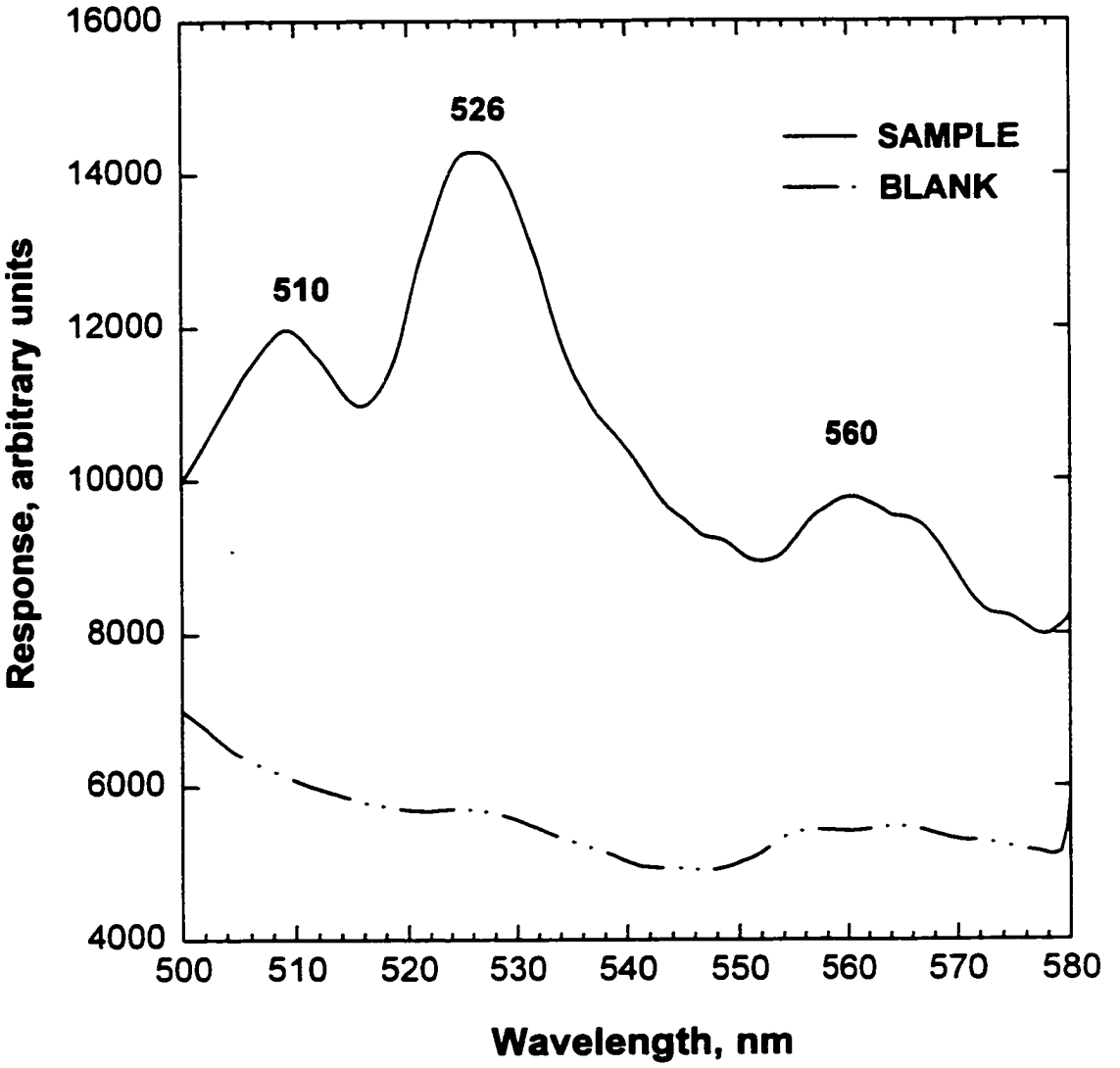

Figure 5.35 Spectrum from deoxyribonucleic acid (DNA degraded free acid from Herring sperm in aqueous solution) (modified by adding sodium dodecyl sulphate). Hydrogen: 250 mL/min; Air: 250 mL/min; Nitrogen: 350 mL/min; Voltage: 5350 V; 1/8 meter grating monochromator with R-1104 PMT; Slits: 0.7mm; Solution concentration: 0.25 % w/v (original sample); Solution flow rate: 12 μL/min.

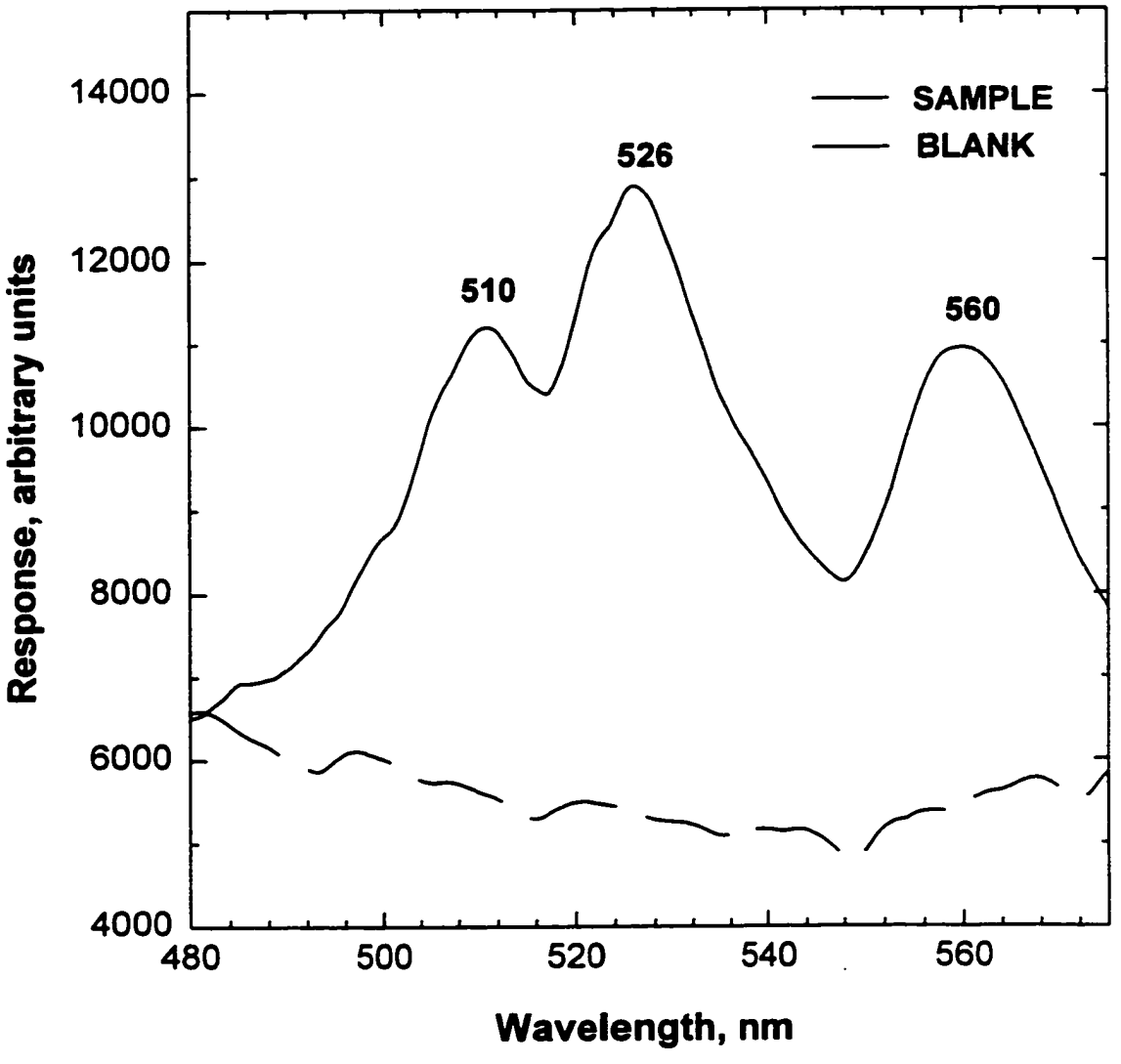

Figure 5.36 Spectrum from lecithin (phosphatidyl choline) in aqueous solution (modified by adding sodium dodecyl sulphate). Hydrogen: 250 mL/min; Air: 190 mL/min; Nitrogen: 350 mL/min; Voltage: 4000 V; 1/8 meter grating monochromator with R-1104 PMT; Slits: 0.7mm; Sample flow rate: 35 ng P/s.

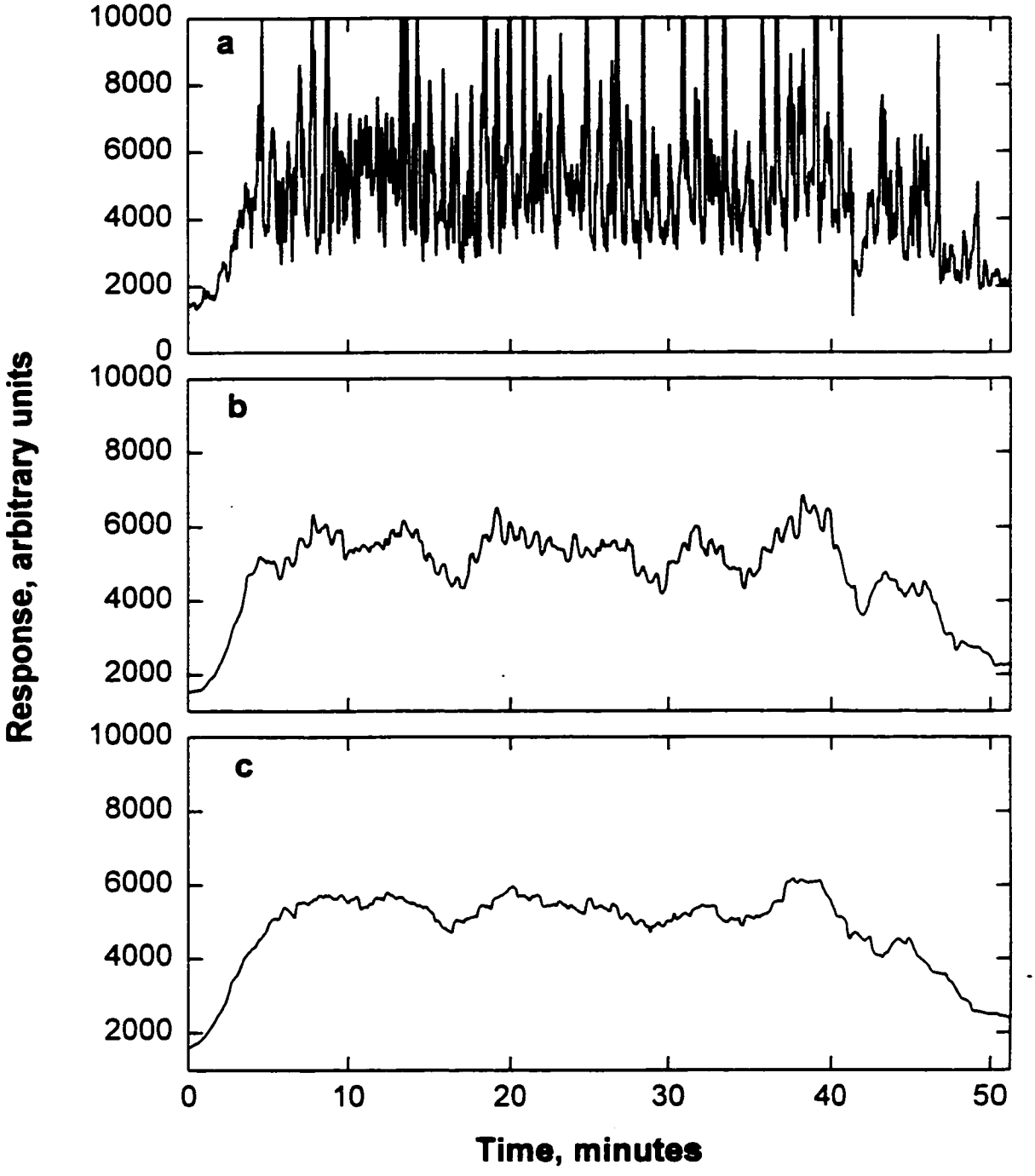

Figure 5.37 Emission at 524 nm (interference filter) from an aqueous solution of lecithin. Experimental conditions are the same as Figure 5.36 except sample flow rate: 22ng P/s. a. Original data. b and c are smoothed data with 1201 point and 2401 point moving average filters.

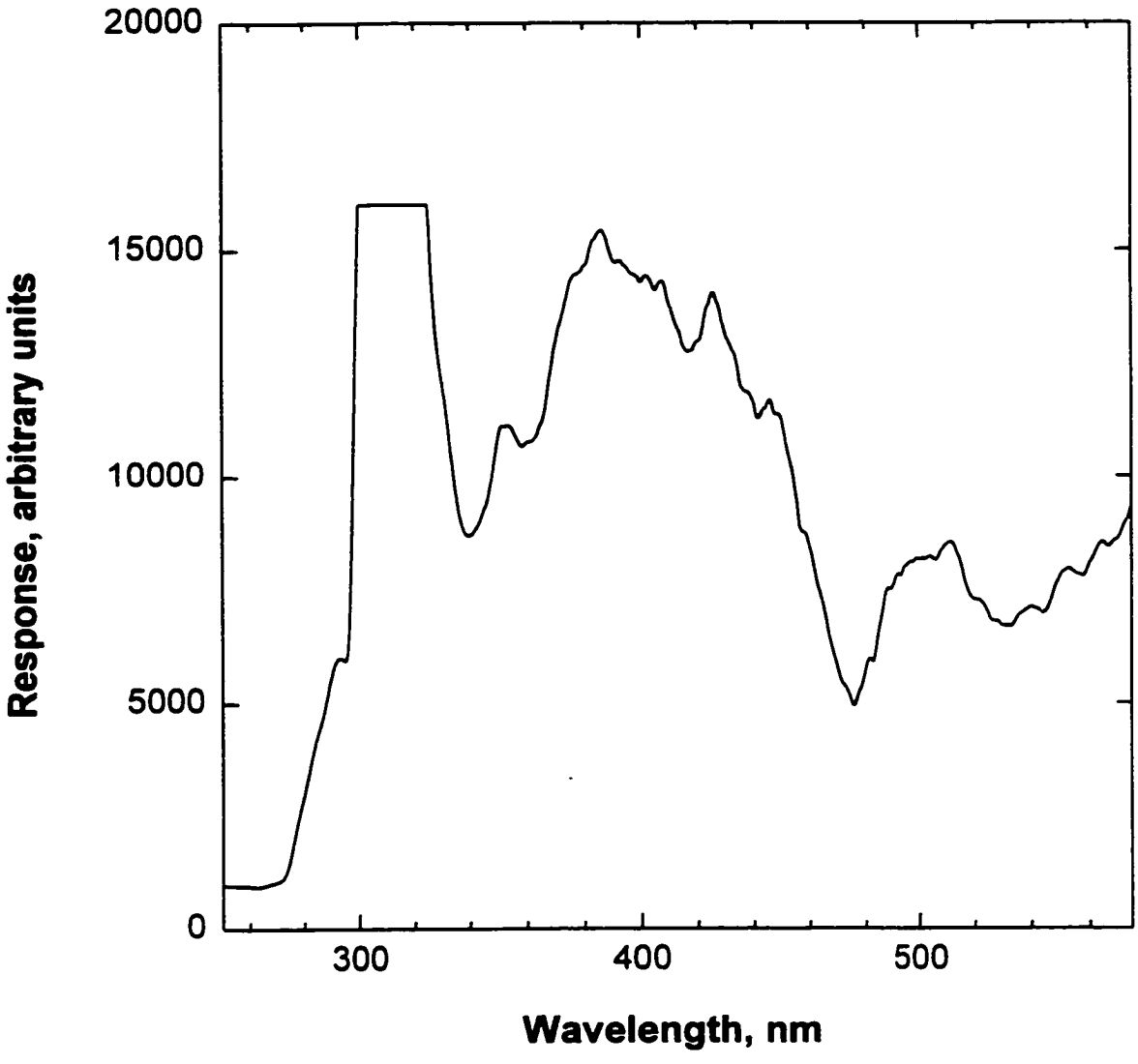

Figure 5.38 Spectrum of bile from bovine (ox gall powder) unfractionated in aqueous solution. Hydrogen: 250 mL/min; Air: 220 mL/min; Nitrogen: 330 mL/min; Voltage: 4800 V; 1/8 meter grating monochromator with R-1104 PMT; Slits: 0.5 mm; Solution concentration: 1% w/v; Solution flow rate: 12 μL/min.

of the unfractionated bile were unknown and the analysis of biological compounds with no information on the sample matrices is of limited utility. Therefore, the application of electrospray-FPD for the determination of the sulphur in biological samples was examined using glutathione (reduced γ-L-glutamyl-L-cysteinyl-glycine) as an example. There are also other techniques for the determination of glutathione [176]. Recently, Orwar and associates [177] used 2,3 naphthalenedicarboxaldehyde (NDA) as a selective fluorogenic label for glutathione to form a highly fluorescent derivative. The authors used laser-induced fluorescence as a detector in capillary electrophoresis. Electrospray-FPD is a direct and sensitive technique for sulphur determination which responds directly to the sulphur. The sulphur spectrum obtained by introducing glutathione in aqueous solution (modified by adding polyoxyethylene sorbitan) is shown in Figure 5.39. The signal recorded by introducing aqueous glutathione solution into the flame and monitoring sulphur emission with a 370 nm band pass filter (80 nm band pass) is shown in Figure 5.40. The bottom two frames of Figure 5.40 show the smoothed data from two moving average filters. The experimental conditions and calibration curve are described in the following sections.

5.3.4.2.1 Experimental conditions

The experimental conditions used to obtain the calibration curve were: Hydrogen: 310 mL/min; Air: 165 mL/min; Nitrogen: 270 mL/min; Voltage: 4500 V; Optical filters: a 370 nm band pass filter (80 nm bandpass) and a

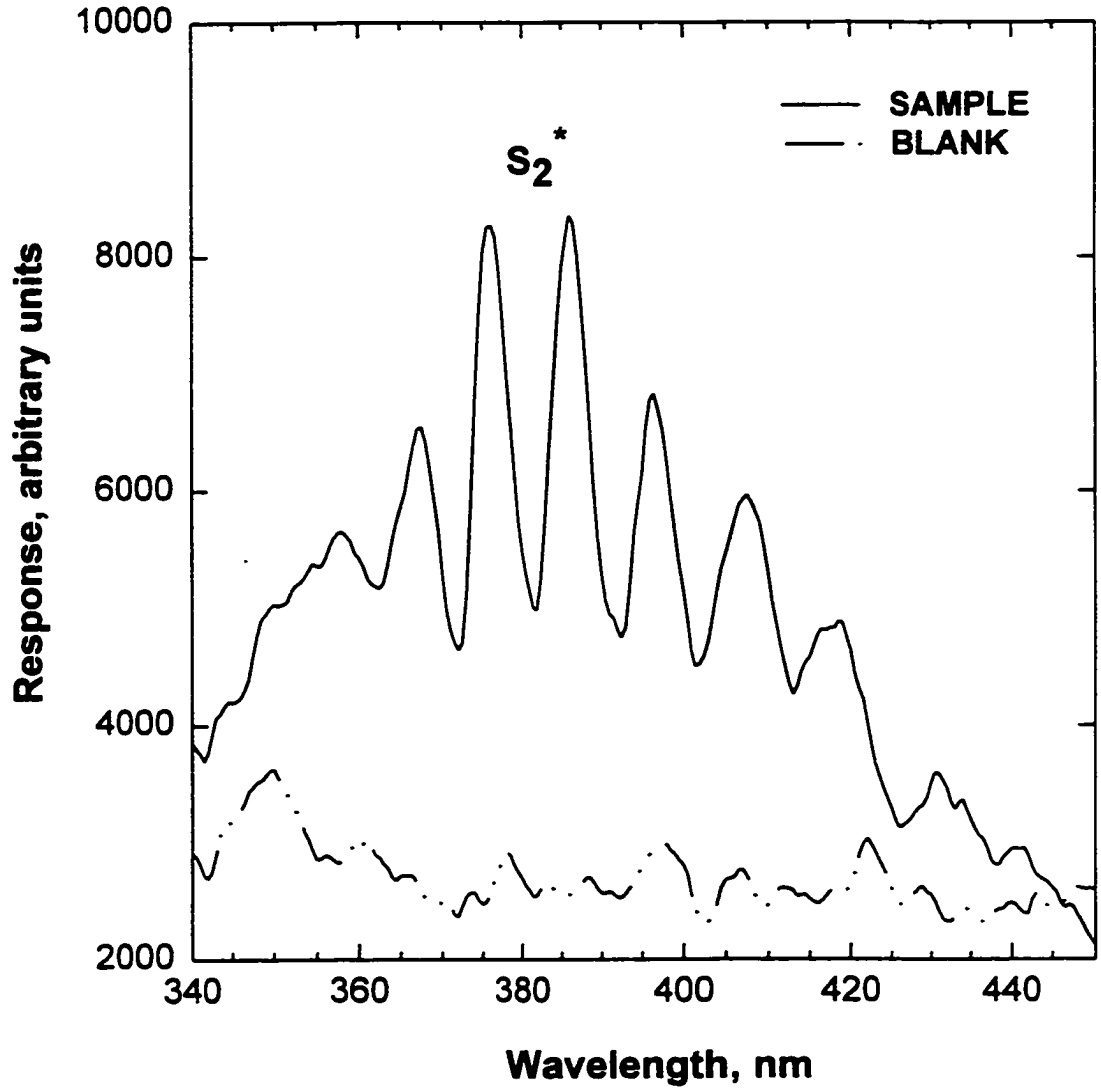

Figure 5.39 Spectrum from glutathione (reduced γ-L-glutamyl-L-cysteinyl-glycine) in aqueous solution (modified by adding polyoxyethylene sorbitan). Hydrogen: 320 mL/min; Air: 200 mL/min; Nitrogen: 330 mL/min; Voltage: 5200 V; 1/8 meter grating monochromator with R-1104 PMT; Slits: 0.5 mm; Solution flow rate: 70 ng S/s.

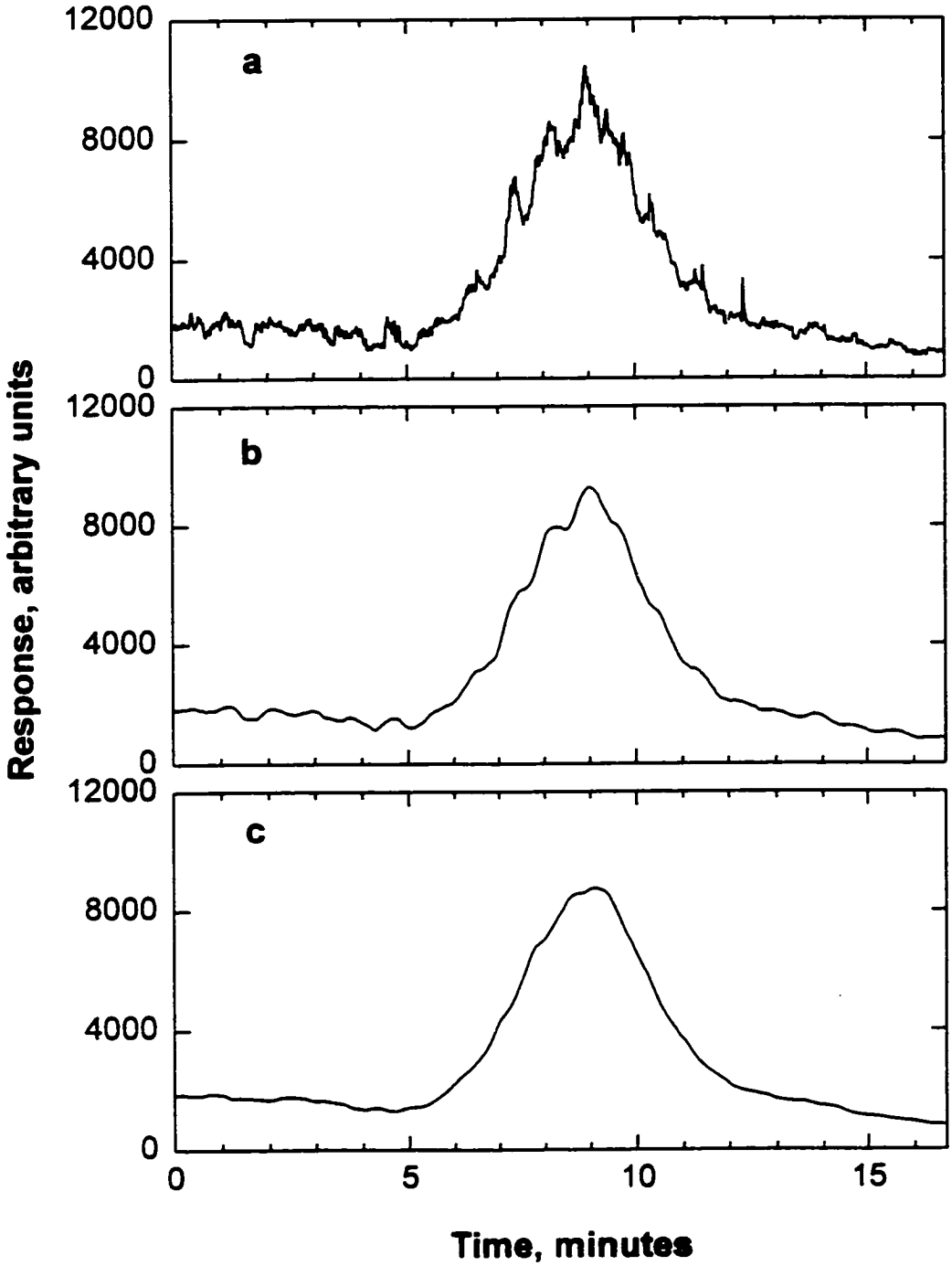

Figure 5.40 Emission at 370 nm (band pass filter) from an aqueous solution of reduced glutathione. Experimental conditions are the same as Figure 5.39 except sample flow rate: 14 ng S/s. a. Original data. b and c are smoothed data with 301 point and 601 point moving average filters.

405 nm interference filter (9 nm bandpass); PMT type and voltage: R-268 and 500 V for both channels; Sample flow rate: 11.4 µL/min; Time constant of the analog filter: 1.8 seconds.

5.3.4.2.2 Calibration curve

The calibration curve is shown in Figure 5.41. The detection limit is 1 ng S/s when a 405 nm interference filter was used. This detection limit can be compared with other selective and sensitive elemental detectors to evaluate the potential of the electrospray-FPD for the sulphur determination. The detection limit of sulphur using thermochemical-HPLC-FPD for CS_2, as an example, is 2.25 ng S/s [61]. ICP and ICP-MS are other elemental detectors that can be compared with electrospray-FPD. The most sensitive line for sulphur emission by ICP is 180.73 nm [178]. Therefore the oxygen, which can absorb sulphur emission, must be excluded in the optical path and in the monochromator. The detection limit is 1000-3000 ng S/mL or 23-70 ng S/s [178]. The detection limit is improved by using HPLC-DIN-ICP, and is 164 ng S/mL or 287 pg S/s [23]. The best detection limit for sulphur is obtained by ICP-MS, in spite of requiring the measurement of the ^{34}S isotope (4.2% abundance) [163]. There is a serious spectral interference from O_2^+ at m/z = 32 for the most abundant sulphur isotope (^{32}S) [164]. The detection limit of sulphur for the amino acids cysteine and methionine by using this method is 150 ng S/mL or 3 ng S/s based on $S/\sigma = 3$. The mass detection limits of the electrospray-FPD, HPLC-DIN-ICP, and ICP-MS (in this case) for sulphur analysis are comparable.

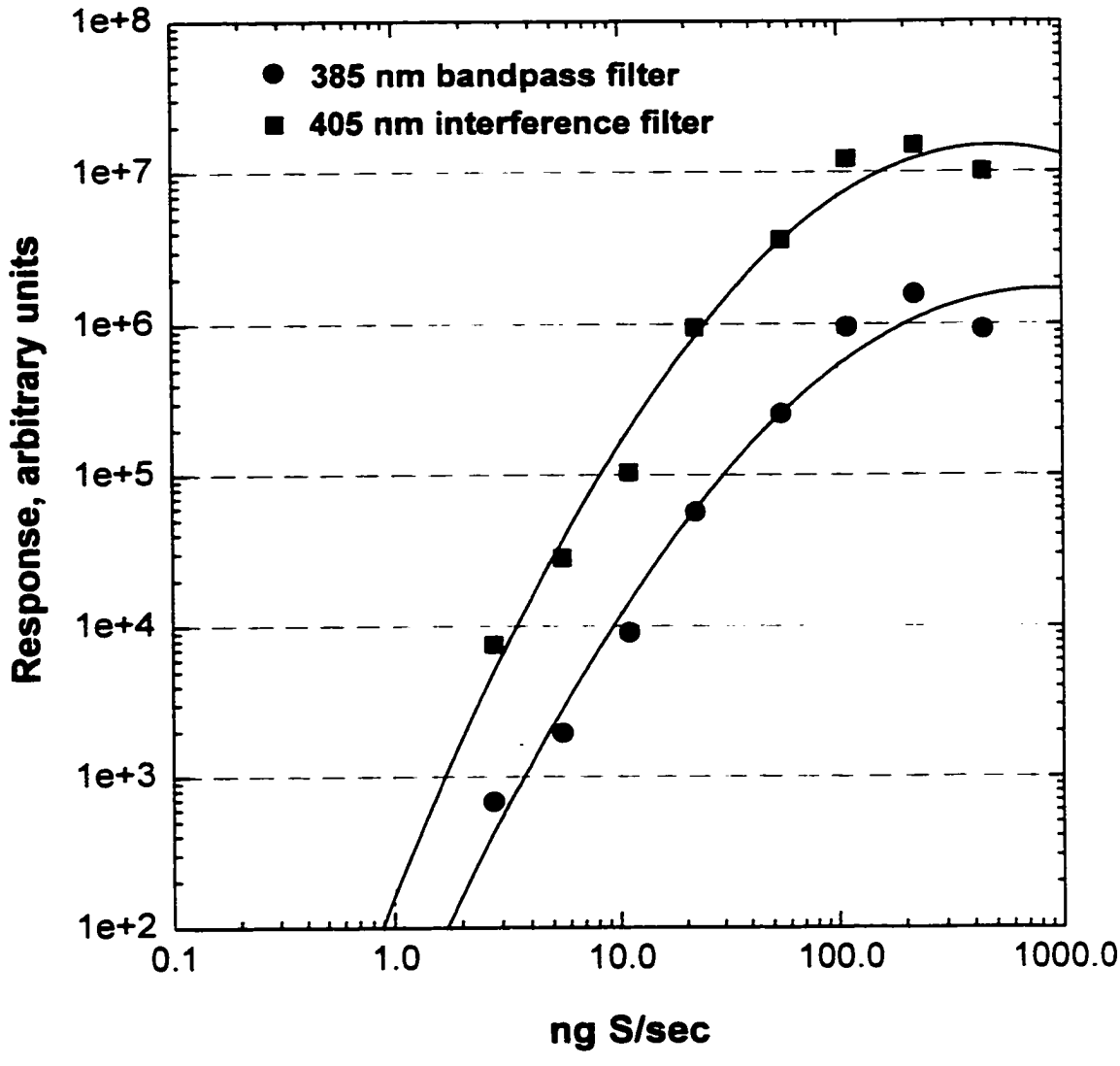

Figure 5.41 Calibration data for reduced glutathione. Experimental conditions are in the text.

5.4 CONCLUSIONS

1. The electrospray-FPD was used as an interface to introduce metal or nonmetal ionic or neutral compounds into the small hydrogen-rich flame that is the source of emission arising from chemiluminescent reactions. Spectra of selected elements from different groups of the periodic table were determined and mass detection limits of some elements demonstrated the potential of the electrospray-FPD as a successful interface.
2. The application of the electrospray-FPD for phosphorus analysis in biological samples was confirmed by obtaining phosphorus spectra for DNA and lecithin, as well as the calibration curve and detection limit for adenosine 5'-monophosphate. The spectrum, calibration curve and detection limit of glutathione were obtained as an example of sulphur analysis in biological samples.
3. Copper and phosphorus showed higher signal to noise ratios at lower sample flow rates. Therefore, the detection limits can be improved by using lower flow rates.
4. The electrospray-FPD was found capable of operating for hours with aqueous solutions (modified by SDS) without any clogging problems.
5. The optical and the electrical signals were obtained simultaneously by applying voltage across the flame and were observed to have a high degree of correlation.
6. At high voltage, (ca. 5000 V), the NSP appeared strongly with the flame.

Chapter 6

CONCLUSIONS AND FUTURE WORK

6.1 CONCLUSIONS

The prime objective of this research was to devise an efficient and sensitive method for introducing very small volumes of flow-carried aqueous solutions directly into the flame of a suitably modified flame photometric detector (FPD).

1. In the initial approach, an attempt was made to project liquid layers of nanometer thickness in cylindrical form into the flame, by letting fast gas streams converge over the sharp edge of a transport capillary. The developed device performed adequately for short periods of time, but suffered from flicker noise (droplet formation) and plugging. However, it greatly helped to to define and finally solve the temperature problems inherent in the direct introduction of liquids to the FPD flame.
2. To accommodate various liquid inputs and allow multi-signal operations, a six-port FPD was constructed. Four ports served as optical (and/or visual) observation channels, the fifth was used to carry exhaust and provide electrical polarization and monitoring. The device offered separate heated and cooled regions and, once assembled, performed fully to expectations: it could be used in many different modes and for all planned experiments of this study. Thus it represented the first prototype of a simple, yet highly efficient multi-channel

instrument on which various kinds of chemiluminescent phenomena can be studied in the future.

3. For the above-mentioned thin-film introduction system, and for the later-used electrospray (ES) source, multiple optimizations were conducted for several typical analytes, several types of flames, the peculiar conditions of a flame of small size and low temperature receiving a direct liquid input, and the noise characteristics of the various arrangements. Not surprisingly, the optimum conditions of the liquid-supplied FPD differed greatly from those of the conventional (i.e. gas-supplied) FPD.
4. An ES introduction source was constructed and, after much optimization, proved successful. It represents, to the author's knowledge, the first source of its kind that, while introducing high concentrations of non-volatile solutes directly into the FPD flame, is not subject to plugging of the capillary, and that is able to accept uninterrupted, heavy analyte concentrations over extended periods of time (hours). The typical operating range of the new ES source is 1-10 μL/min, but lower and higher flows can still be used.
5. The optimization of this new source also involved varying the composition of the electrosprayed solvent. Experiments were conducted with various organic polar liquids as well as with water-based solutions. Both could be successfully run with the FPD, although organic liquids produced optical quenching (this effect, which is due to hydrocarbonaceous fragments in the flame, parallels the behaviour of the conventional, gas-phase FPD). Typical additives to the

aqueous phase included formic and other acids, hydrophilic polymers, and, most importantly, various types of neutral and anionic surfactants. Some of the latter greatly improved performance, i.e. they promoted the smooth introduction of liquid flow with no (or a minimum of) flicker noise attending.

6. The new ES source was characterized by using the classical noise power spectrum (the Fourier transform) as a diagnostic and quantitative tool. Under baseline conditions, noise proved to be almost purely fundamental, i.e. it equalled the square root of the PMT's photoelectron generation rate. High analyte loads - similar to an effect known from the conventional FPD - generated 1/f noise and sometimes also cyclical interference noise.
7. Dual-channel operation with subtractive or ratio-based algorithms removed much of the correlated noise; yet, the improvement in terms of detection limits rarely exceeded a factor of two. Similar behaviour can be expected for other analytes.
8. Because of the biological importance of sulphur and phosphorus, and their excellent sensitivity in the conventional FPD, the capabilities of the new ES-FPD instrument were mostly characterized by using these two elements. With non-volatile analytes - some of which were important biochemicals such as glutathione and adenosine monophosphate - detection limits for sulphur and phosphorus ranged around 1 ng/s. Thus the ES-FPD should serve well as detector for a wide range of biochemicals, after separation by such methods as micro-column HPLC or capillary electrophoresis.

9. The main advantages of the new ES-FPD unit are its simplicity and excellent performance with extremely small samples, and its high sensitivity and selectivity for certain elements such as sulphur and phosphorus. This analytical combination is difficult if not impossible to obtain from classical flame or plasma systems. On the other hand, analytical methodologies other than the ES-FPD should be used when the sample is large and highly diluted, or when a greater number of elements need to be determined.

10. A limited survey was carried out on a variety of other analyte elements in some ionic form. The ionic form was chosen - over, where available, the organometallic form - because it is the non-volatility of the solute that represents the major problem in liquid introduction (and that precludes conventional GC-FPD operation). As could be expected of a detector that relies mainly on chemical (as opposed to thermal) excitation, the response to various elements was highly selective. The detection limits for some of the better responding analytes ranged from 0.6 ng/s for Cu to 20 ng/s for In.
The luminescence from a variety of elements - the common alkali and earth alkali metals as well as Sc, S, P, Mn, Ni, Cu, B, Se, and As - was strong enough to obtain clear spectra. These spectra included some well-known molecular bands and atomic lines, but also revealed a significant number of emitters of unknown origin. It is suggested that, beyond analytical utility, the ES-FPD can serve as a novel source for basic spectrochemical studies, particularly as regards molecular bands and continua.

11. The electrical current of the ES-FPD correlated with both sample introduction and, when present, flicker noise. The ES-FPD could consequently be used as a combined optical-electrical sensor, to both analytical and mechanistic ends. At the same time, optical spectra clearly documented the presence of the second positive system of dinitrogen. Metastable nitrogen - cf. the high-power nitrogen plasmas of the literature - could hence be conceivably used to boost excitation efficiency and modify analyte selectivity.

6.2 Future Work

The seeds of future work in this new ES-FPD area are already contained in the "Conclusions" above:

1. The ES-FPD source needs to be coupled to flow-compatible separation systems such as capillary electrophoresis, micro-column ion chromatography, etc. These "hyphenated" future instruments could then be used to meet biochemical needs such as analyses of extremely limited samples, e.g. of the protoplasm from just a few cells.
2. With the knowledge gained on the ES source, the thin-film introduction approach (see 6.1.1 above) should be given a second chance to show its mettle. Obviously, success would come to this approach only with better control of source dimensions and operating conditions. However, a successful thin-film source remains theoretically more promising than electrospray (nm vs. um liquid

thickness); it is also experimentally simpler and does not require high voltage.

3. The literature of the conventional FPD includes several previously unreported band systems and continua. These are of obvious spectrochemical interest. The conventional FPD is, however, restricted to gaseous inputs. The development of the new ES-FPD has removed this restriction - and any species capable of dissolution can now be introduced into this low-temperature chemiluminescent flame source. A much extended survey of spectrochemically interesting analytes is therefore called for.
4. As discussed in paragraph 6.1.11 above, the ES-FPD responds both electrically and optically to analytes. This dual-channel response needs to be explored both for its mechanistic inferences and its potential analytical utility. Also, the ES-FPD can easily produce metastable dinitrogen, a species that is capable of efficient energy transfer and has been repeatedly used in this manner to promote excitation in plasma systems. The additional excitation and likely different selectivity of nitrogen metastables should therefore be investigated with a view to improving analytical performance.
5. The physical construction and flow regimes of the ES source,and the particular solvent compositions developed for smooth solution transfer, might well be applicable to some of the other analytical methodologies that currently rely on electrospray as a means of introducing liquid samples.

REFERENCES

1. R. P. W. Scott, Liquid Chromatography Detectors, J. Chrom. Library 33, 2nd edition, Elsevier, Amsterdam (1986).
2. D. A. Skoog and J. J. Leary, Principles of Instrumental Analysis, 4th. edition, Saunders College Publishing, Florida (1992).
3. V. L. McGuffin and M. Novotny, Anal. Chem. 53, 946 (1981).
4. S. Greenfield and A. Montaser, in Inductively Coupled Plasma in Analytical Atomic Spectrometry, 2nd edn., Edited by A. Montaser and D. W. Golightly, VCH, New York, 1992.
5. A. Gustavsson, in Inductively Coupled Plasma in Analytical Atomic Spectrometry, 2nd edn., Edited by A. Montaser and D. W. Golightly, VCH, New York, 1992.
6. P. C. Uden, J. Chromatogr. 703, 393 (1995).
7. B. L. Sharp, J. Anal. Atom. Spectrom. 3, 613 and 939 (1988).
8. R. F. Browner and A. W. Boorn, Anal. Chem. 56, 875A (1984).
9. J. C. Ivaldi, J. Vollmer, and W. Slavin, Spectrochim. Acta 46B, 1063 (1991).
10. L. R. Layman and F. E. Lichte, Anal. Chem. 54, 638 (1982).
11. M. A. Tarr, G. Zhu, and R. F. Browner, Appl. Spectrosc. 45, 1424 (1991).
12. R. H. Clifford, P. Sohal, H. Liu, and A. Montaser, Spectrochim. Acta 47B, 1107 (1992).
13. R. H. Clifford, P. Sohal, H. Liu, and A. Montaser, Spectrochim. Acta 48B,

1221 (1993).

14. J. A. Olivares and R. S. Houk, Anal. Chem. 58, 20 (1986).

15. D. D. Smith and R. F. Browner, Anal. Chem. 54, 533 (1982).

16. J. F. Kamicky, L. T. Zitelli, and S. Vanderwal, Anal. Chem. 59, 327 (1987).

17. M. A. Tarr, G. Zhu, and R. F. Browner J. Anal. Atom. Spectrom. 7, 813 (1992).

18. M. A. Tarr, G. Zhu, and R. F. Browner, Anal. Chem. 65, 1689 (1993).

19. M. Ibrahim, W. Nisamaneepong, D. L. Hass, and J. A. Caruso, Spectrochim. Acta 40B, 367 (1985).

20. N. Sagliano and R. A. Hartwick, J. Chromatogr. Sci. 24, 506 (1986).

21. J. M. Carey, F. A. Byrdy, and J. A. Caruso, J. Chromatogr. Sci. 31, 330 (1993).

22. D. T. Heitkemper, K. A. Wolnik, F. L. Fricke, and J. A. Caruso, in Inductively Coupled Plasma in Analytical Atomic Spectrometry, 2nd edn., Edited by A. Montaser and D. W. Golightly, VCH, New York, 1992.

23. K. E. Lafreniere, V. A. Fassel, and D. E. Eckels, Anal. Chem. 59, 879 (1987).

24. D. R. Wiederin, F. G. Smith and R. S. Houk, Anal. Chem. 63, 219 (1991).

25. K. E. Lawrence, G. W. Rice, and V. A. Fassel, Anal. Chem. 56, 289 (1984).

26. H. Tan, B. A. Meinhard, and J. E. Meinhard, Recent Investigations of Meinhard Concentric Nebulizers, Presented at the 19th Annual Meeting of the Federation of Analytical Chemistry and Spectroscopy Societies,

Philadelphia, PA, September 1992.

27. J. W. Olesik, J. A. Kinzer, and B. Harkleroad, Anal. Chem. 66, 2022 (1994).
28. H. Liu and A. Montaser, Anal. Chem. 66, 3233 (1994).
29. S. A. Pergantis, E. M. Heithmar and T. A. Hinners, Anal. Chem. 67, 4350 (1995).
30. J. A. Koropchak and M. Veber, CRC Crit. Rev. Anal. Chem. 23, 113 (1992).
31. M. L. Vestal and G. J. Fergusson, Anal. Chem. 57, 2373 (1985).
32 J. A. Koropchak, M. Veber, and J. Heries, Spectrochim. Acta 47B, 825 (1992).
33. N. Jakubowski, I. Feldmann, D. Stuewer, and H. Berndt, Spectrochim. Acta 47B, 119 (1992).
34. S. K. Luo and H. Berndt, Spectrochim. Acta 49B, 485 (1994).
35. R. F. Browner, 1996 Winter Conference on Plasma Spectrochemistry (Fort Lauderdale), Abstracts Book, P. 41, IL1.
36. J. B. French, B. Etkin, and R. Jong, Anal. Chem. 66, 685 (1994).
37. J. W. Olesik and S. E. Hobbs, Anal. Chem. 66, 3371 (1994).
38. T. Z. Torok, Z. Anal. Chem. 119, 120 (1940).
39. D. N. Bernhart, W.B. Chess, and D. Roy, Anal. Chem. 33, 395 (1951).
40. W. A. Dippel, C. F. Bricker, and N. H. Furman, Anal. Chem. 26, 553 (1954).
41. D. W. Brite, Anal. Chem. 27, 1815 (1955).
42. A. Davis, F. J. Dinan, E. J. Labbet, J. D. Chazin, and L. E. Tufts, Anal. Chem. 36, 1066 (1964).

43. R. K. Skogerboe, A.S. Gravatt, and G. H. Morrison, Anal. Chem. 39, 1602 (1967).

44. S. S. Brody and J. E. Chaney, J. Gas Chromatogr. 4, 42 (1966).

45. W. A. Aue, X. Y. Sun, and B. Millier, J. Chromatogr. 606, 731 (1992).

46. X. Y. Sun, B. Millier, and W. A. Aue, Can. J. Chem. 70, 1129 (1992).

47. W. A. Aue, B. Millier, and X. Y. Sun, Can. J. Chem. 70, 1143 (1992).

48. A. Syty and J. A. Dean, Appl. Optics 7, 1331 (1968).

49. P. T. Gilbert, Analytical Flame Spectroscopy, Ed. by R.Mavrodineanu, MacMillan, London, 1970.

50. R. M. Dagnall, K. C. Thompson, and T. S. West, Analyst 93, 72 (1968).

51. K. M. Aldous, R. M. Dagnall, and T. S. West, Analyst 95, 417 (1970).

52. W. N. Elliot and R. A. Moslyn, Analyst 96, 452 (1971).

53. W. N. Elliot, C. Heathcote, and R. A. Moslyn, Talanta 19, 359 (1972).

54. R. P. W. Scott, Contemporary Liquid Chromatography, Wiley, New York, 1976.

55. H. Veening, P. P. H. Tock, J. C. Kraak, and H. Poppe, J. Chromatogr. 352, 345 (1986).

56. B. G. Julin, H. W. Vandenborn, and J. J. Kirkland, J. Chromatogr. 112, 443 (1975).

57. T. L. Chester, Anal. Chem. 52, 638 (1980).

58. T. L. Chester, Anal. Chem. 52, 1621 (1980).

59. P. L. Patterson, R. L. Howe, and A. Abushumays, Anal. Chem. 50, 339

(1978).

60. P. L. Patterson, Anal. Chem. 50, 345 (1978).

61. J. Bernard, T. Nicodemo, N. N. Barthakur, and J. S. Blais, Analyst 119, 1475 (1994).

62. J. S. Blais, G. M. Momplaiser, and W. D. Marshall, Anal. Chem. 62, 1161 (1990).

63. J. S. Blais, D. Huyhues, G. M. Momplaiser, and W. D. Marshall, J. Anal. Atom. Spectrom. 6, 225 (1991).

64. V. L.McGuffin and M. Novotny, J. Chromatogr. 218, 179 (1981).

65. J. M. Miller, Chromatography: Concepts and Contrasts, Wiley, New York, 1988.

66. C. E. Kientz and A. Verweij, Intern. J. Environ. Anal. Chem. 30, 255 (1987).

67. C. E. Kientz, A. Verweij, and H. L. Boter, J. Chromatogr. 467, 385 (1989).

68. T. Sugiyama, Y. Suzuki, and T. Takeuchi, J. Chromatogr. 80, 61 (1973).

69. A. G. Ewing, R. A. Wallingford, and T. M. Olefirowicz, Anal. Chem. 61, 292A (1989).

70. C. E. Sanger, C. E.Kientz, and U. A. Brinkman , J. Chromatogr. 673, 299 (1994).

71. W. A. Aue and X. Y. Sun, J. Chromatogr. 641, 291 (1993).

72. S. K. Chowdhury and B. T. Chait, Anal. Chem. 63, 1660 (1991).

73. G. M. Bose Recherches sur le cause et sur veritable theorie del-electricite wittenberg, 1745.

74. J. Zeleny, J. Phys. Rev. 10, 1 (1917).

75. V. G. Drozin, J. Colloid. Sci. 10, 158 (1955).

76. M. Dole, L. L. Mack, R. L. Hines, R. C. Mobley, L. D. Ferguson and M. B. Alice, J. Chem. Phys. 49, 2240 (1968).

77. L. L. Mack, P. Kralik, A. Rheude, and M. Dole, J. Chem. Phys. 52, 4977 (1970).

78. M. Yamashita and J. B. Fenn, J. Phys. Chem. 88, 4451 (1984).

79. M. Yamashita and J. B. Fenn, J. Phys. Chem. 88, 4671 (1984).

80. L. Voress, Anal. Chem. 66, 481A (1994).

81. R. D. Smith, J. A. Loo, C. G. Edmonds, C. J. Barinaga, and H. R. Udseth, Anal. Chem. 62, 882 (1990).

82. B. Thomson, Direct Ion Emission From Liquids Techniques and Processes, Sciex, Toronto,Ontario, Canada, Note No. 15288.

83. S. A. Hofstadler, R. Bakhtiar, and R. D. Smith, J. Chem. Educ. 73, A82 (1996).

84. P. Kebarle and L. Tang, Anal. Chem. 65, 972A (1993).

85. J. V. Iribarne and B. A. Thomson, J. Chem Phys. 64, 2287 (1976).

86. B. A. Thomson and J. V. Iribarne, J. Chem Phys. 71, 4451 (1979).

87. J. B. Fenn, M. Mann, C. K. Meng, S. F. Wong, and C. M. Whitehouse, Science 246, 64 (1989).

88. F. W. Rollgen, E. Bramer-wegen, and L. Butfering, J. Phys. Colloq. 48, 253 (1987).

89. G. L. Schmelzeiser-Redeker, L. Butfering and F. W. Rollgen, Int. J. Mass Spectrom. and Ion Process 90, 139 (1989).

90. A. T. Blades Jayaweera, M. G. Ikonomou, and P. Kebarle, Int. J. Mass Spectrom. and Ion Process 101, 325 (1990).

91. A. T. Blades, P. Jayaweera, M. G. Ikonomou, and P. Kebarle, Int. J. Mass Spectrom. and Ion Process 102, 251 (1990).

92. A. T. Blades, P. Jayaweera, M. G. Ikonomou, and P. Kebarle, J. Chem. Phys. 92, 5900 (1990).

93. L. Tang and P. Kebarle, Anal. Chem. 65, 3654 (1993).

94. G. R. Agnes and G. Horlick, Appl. Spectrosc. 46, 401 (1992).

95. G. R. Agnes and G. Horlick, Appl. Spectrosc. 48, 649 (1994).

96. G. R. Agnes and G. Horlick, Appl. Spectrosc. 48, 655 (1994).

97. I. I. Stewart and G. Horlick, Anal. Chem. 66, 3983 (1994).

98. G. R. Agnes and G. Horlick, Appl. Spectrosc. 49, 324 (1995).

99. J. P. Chervet, M. Ursem, and J. P. Salzmann, Anal. Chem. 68, 1507 (1996).

100. M. Novotny, Anal. Chem. 53, 1294A (1981).

101. Q. Lu, S. M. Bird, and R. M. Barnes, Anal. Chem. 67, 2949 (1995).

102. H. J. Ache, Fresenius J. Anal. Chem. 355, 467 (1996).

103. J. S. Crain and J. T. Kiely, J. Anal. Atom. Spectrom. 11, 525 (1996).

104. K. E. Lafreniere, V. A. Fassel, and D. E. Eckels, Anal. Chem. 59, 879

(1987).

105. M. R. Emmett and R. M. Caprioli, J. Am. Soc. Mass Spectrom. 5, 605 (1994).

106. M. Wilm and M. Mann, Anal. Chem. 68, 1 (1996).

107. D. C. Gale and R. D. Smith, Rapid Commun. Mass Spectrom. 7, 1017 (1993).

108. G. A. Valaskovic, N. L. Kelleher, D. P. Little, D. J. Aaserud, and F. W. Mclafferty, Anal. Chem. 67 3802 (1995).

109. J. B. Willis, Spectrochim. Acta 23A, 811 (1967).

110. S. D. Olsen and A. Strasheim, Spectrochim. Acta 38B, 973 (1983).

111. J. A. Koropchak and H. Aryamanya-Mugisha, J. Anal. Atom. Spectrom. 4, 291 (1989).

112. R. H. Clifford, H. Tan, H. Liu, A. Montaser, F. Zarrin, and P. B. Keady, Spectrochim. Acta 48B, 1221 (1993).

113. G. M. H. Meesters, P. H. W. Vercoulen, J. C. M. Marijnissen, and B. Scarlett, J. Aerosol Sci. 23, 37 (1992).

114. J. F. Banks, J. S. Shen, C. M. Whitehouse, and J. B. Fenn, Anal. Chem. 66, 406 (1994).

115. C. N. Davies, in Fundamentals of Aerosol Science; Edited by D. T. Shaw, Wiley, New York, 1978.

116. K. S. Chowdhury and B. T. Chait, Anal. Chem. 63, 1660 (1991).

117. D. P. H. Smith, IEEE Trans. Ind. Appl. IA-22, 527 (1986).

118. A. P. Bruins, T. R. Covey, and J. Henion, Anal. Chem. 59, 2642 (1987).

119. R. Gotz, J. W. Elgersma, J. C. Kraak, and H. Poppe, Spectrochim. Acta 49B, 761 (1994).

120. L. B. Loeb, A. F. Kip, G. G. Hudson, and W. H. Bennett, Phys. Rev. 60, 714 (1941).

121. L. G. Christophorou, Adv. in Electronics and Electron Phys. 46, 55 (1978).

122. M. G. Ikonomou, A. T. Blades, and P. Kebarle, J. Am. Soc. Mass Spectrom. 2, 497 (1991).

123. B. Millier, X. Y. Sun, and W. A. Aue, J. Chromatogr. 675, 155 (1994).

124. H. Singh, B. Millier, and W. A. Aue, J. Chromatogr. 724, 255 (1996).

125. R. W. B. Pearse and A. G. Gaydon, The Identification Of Molecular Spectra, 3th. edn., Chapman and Hall Ltd, London (1963).

126. C. T. J. Alkemade and R. Herrmann, Fundamentals of Analytical Flame Spectroscopy, Adam Hilger, Bristol, 1979.

127. W. A. Aue, B. Millier, and X. Y. Sun, Anal. Chem. 62, 2453 (1990).

128. C. G. James and T. M. Sugden, Nature 175, 333 (1955).

129. E. Pungor and A. J. Hegedus, Mikrochim. Acta 1, 87 (1960).

130. D. Binkley and R. Dessy, J. Chem. Educ. 56, 148 (1979).

131. J. D. Winefordner, R. Avni, T. L. Chester, J. J. Fitzgerald, L. P. Hart, D. J. Johnson and F. V. Plankey, Spectrochim. Acta 31B, 1 (1976).

132. G. L. Walden, J. N. Bower, S. Nikdel, D. L. Bolton, and J. D. Winefordner, Spectrochim. Acta 35B, 535 (1980).

133. C. L. Erikson, M. J. Lysaght, and J. B. Callis, Anal. Chem. 64, 1155A (1992).

134. M. P. Goudzwaard and M. T. C. Deollebregt, Spectrochim. Acta 45B, 887 (1990).

135. X. Y. Sun, H. Singh, B. Millier, C. H. Warren, and W. A. Aue, J. Chromatogr. 687, 259 (1994).

136. H. Singh and W. A. Aue, J. Chromatogr. 724, 251 (1996).

137. C. A. Monnig and G. M. Hieftje, Appl. Spectrosc. 43, 742 (1989).

138. E. D. Salin and G. Horlick, Anal. Chem. 52, 1578 (1980).

139. A. Montaser, R. H. Clifford, S. A. Sinex, and S. G. Capar, J. Anal. Atom. Spectrom. 4, 499 (1989).

140. G. M. Hieftje, Anal. Chem. 44, 69A and 81A (1972).

141. C. G. Enke and T. A. Nieman, Anal. Chem. 48, 705A (1976).

142. K. Busch and M. A. Busch, Multielement Detection System for Spectrochemical Analysis, Wiley, Toronto, 1990.

143. M. Marinkovic and T. J. Vickers, Anal. Chem. 42 1613 (1970).

144. C. T. J. Alkemade, W. Snelleman, G. D. Boutilier, and J. D. Winefordner, Spectrochim. Acta 35B, 261 (1980).

145. P. Geladi and B. R. Kowalski, Anal. Chim. Acta 185, 1 (1986).

146. Data transfer program written by P. D. Wentzell 1994.

147. S. A. Myers and D. H. Tracy, Spectrochim. Acta 38B, 1227 (1983).

148. H. H. Ku, J. Res. Bur. Stand. 70C, 263 (1966).

149. J. M. Mermet and J. C. Ivaldi, J. Anal. Atom. Spectrom. 8, 795 (1993).

150. P. Mukerjee and K. J. Mysels, Critical Micelle Concentrations of Aqueous Surfactant Systems. NSRDS-NBS 36, Nat. Bur. Stand. USA 1971.

151. A. N. Wright and C. A. Winkler, Active Nitrogen, Academic Press, New York (1968).

152. W. B. Dodge and R. O. Allen, Anal. Chem. 53, 1279 (1981).

153. G. N. Hays, C. J. Tracy, A. R. Demonchy, and H. J. Oskam, Chem. Phys. Lett. 14, 352 (1972).

154. D. H. Stedman and D. W. Setser, J. Chem. Phys. 50, 2256 (1969).

155. A. Y. M. Ung, Chem. Phys. Lett. 32, 193 (1975).

156. J. Berkowitz, W. A. Chupka, and G. B. Kistiakowski, J. Chem. Phys. 25, 457 (1956).

157. W. L. Borst and S. L. Chang, J. Chem. Phys. 59, 5830 (1973).

158. L. Herman, G. Lucas, and R. Herman, Spectrochim. Acta 11, 325 (1957).

159. A. P. D'Silva, G. W. Rice, and V. A. Fassel, Appl. Spectrosc. 34, 578 (1980).

160. Y. Z. Tang and W. A. Aue, Mikrochim. Acta 11, 29 (1987).

161. D. R. Heine, M. B. Denton, and T. D. Schlabach, Anal. Chem. 54, 81 (1982).

162. K. Yoshida, H. Haraguchi, and K. Fuwa, Anal. Chem. 55, 1009 (1983).

163. S. J. Jiang and R. S. Houk, Spectrochim. Acta 43B, 405 (1988).

164. Y. Shaho and G. Horlick, Appl. Spectrosc. 45, 143 (1991).

165. G. M. Hieftje, J. Anal. Atom. Spectrom. 11, 613 (1996).

166. G. Horlick and Y. Shao, in Inductively Coupled Plasma in Analytical Atomic Spectrometry, 2nd edn., Edited by A. Montaser and D. W. Golightly, VCH, New York, 1992.

167. H. Singh and W. A. Aue, J. Chromatogr. 724, 251 (1996).

168. P. T. Gilbert, Anal. Chem. 38, 1920 (1966).

169. C. G. Flinn and W. A. Aue, J. Chromatogr. 153, 49 (1978).

170. W. A. Aue and C. G. Flinn, J.Chromatogr. 158, 161 (1978).

171. R. K. Asundi, M. J. Khan and R. Samuel, Proceedings of the Royal Society, 157A, 28 (1963).

172. P. T. Gilbert, Analytical Flame Spectroscopy, Edited by Mavrodineanu, MacMillan, London (1964).

173. E .J. Sowinski and I. H. Suffet, Anal. Chem. 46, 1218 (1974).

174. S. Kapila and C. R. Vogt, J. Chromatogr. Sci 17, 327 (1979).

175. J. I. Routh, Introduction to Biochemistry 2nd. edn., W. B. Saunders, Philadelphia, 1978.

176. A. Fontana, and C. Toniolo, Chemistry of the thiol group, Edited by S. Patai, Wiley, Chichester 1974.

177. O. Orwar, H. A. Fishman, N. E. Ziu, R. H. Scheller, and R. N. Zare, Anal. Chem. 67, 4261 (1995).

178. K. Yoshida, T. Hasegawa, and H. Haraguchi, Anal. Chem. 55, 2106 (1983).

IMAGE EVALUATION
TEST TARGET (QA-3)

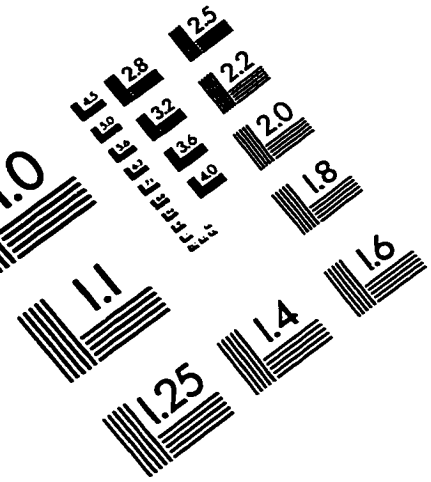

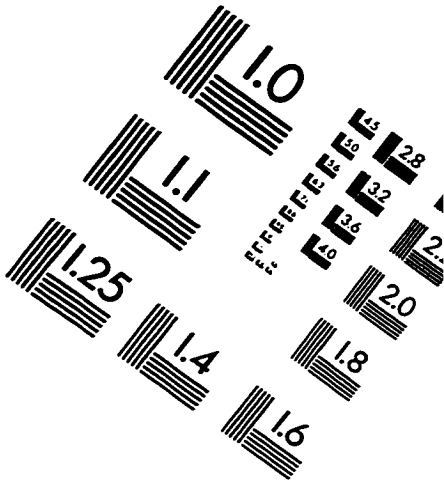

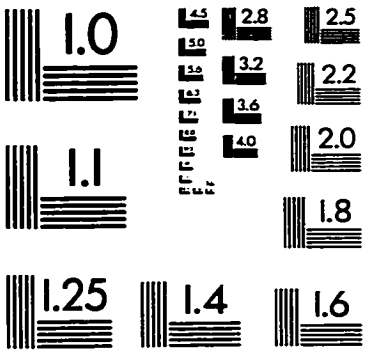

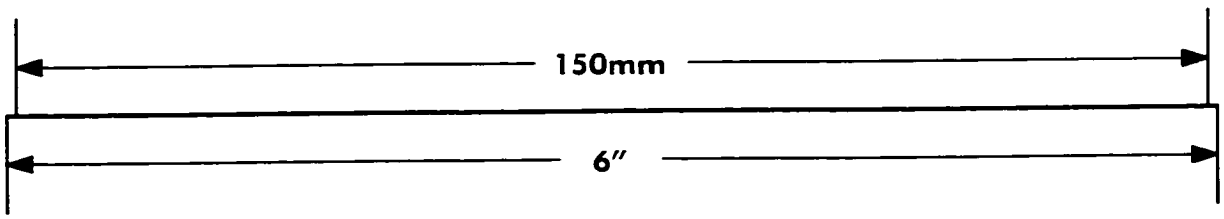

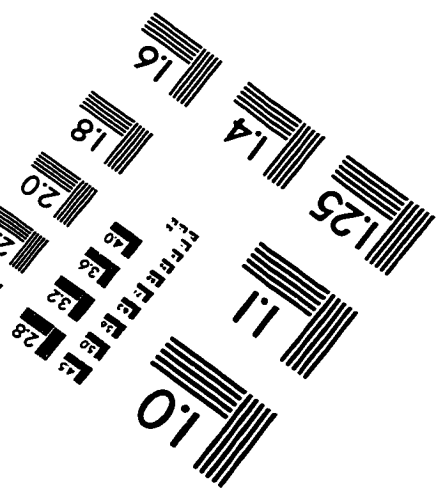

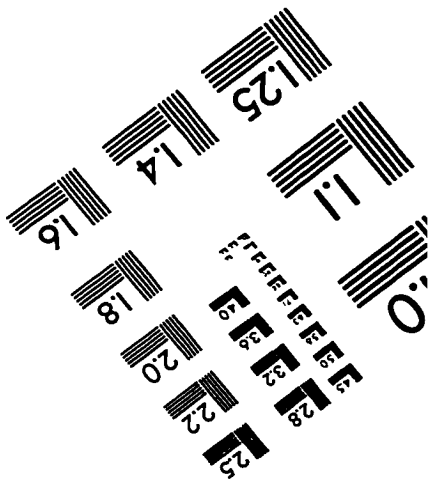

APPLIED IMAGE, Inc
1653 East Main Street
Rochester, NY 14609 USA
Phone: 716/482-0300
Fax: 716/288-5989